Doping a topological quantum spin liquid: slow holes in the Kitaev honeycomb model

Gábor B. Halász

St John's College

University of Oxford

A thesis submitted for the degree of

Doctor of Philosophy

Trinity Term 2015

Abstract

We present a controlled microscopic study of hole dynamics in both a gapped and a gapless quantum spin liquid. Our approach is complementary to previous phenomenological works on lightly doped quantum spin liquids as we introduce mobile holes into the ground state of the exactly solvable Kitaev honeycomb model.

In the spatially anisotropic (Abelian) gapped phase of the model, we address the properties of a single hole [its internal degrees of freedom as well as its hopping properties], a pair of holes [their absolute and relative particle statistics as well as their interactions], and the collective state for a finite density of holes. Our main result is that the holes in the doped model possess internal degrees of freedom as they can bind the fractional excitations of the undoped model and that the resulting composite holes with different excitations bound are distinct fractional particles with fundamentally different single-particle properties and different experimental signatures in the multi-particle ground state at finite doping. For example, some hole types are free to hop in two dimensions, while others are confined to hop in one dimension only. Also, distinct hole types have different particle statistics and, in particular, some of them exhibit non-trivial (anyonic) relative statistics. At finite doping, the respective hopping dimensionalities manifest themselves in an electrical conductivity that is either approximately isotropic or extremely anisotropic.

In the gapless phase of the model, we consider a single hole and address the possibility of a coherent quasiparticle description. Our main result is that a mobile hole has a finite quasiparticle weight which vanishes in the stationary limit. Although this result is obtained in terms of an approximate variational state, we argue that it is also applicable for the exact ground state of the doped model.

Acknowledgements

First of all, I am immensely grateful to my supervisor John Chalker for his patient and insightful guidance. I have learned a lot from working with him over the last four years about not only condensed matter physics but also science in general. His wisdom, dedication, and conscientiousness will continue to be an inspiration for me.

Second, I am greatly indebted to Roderich Moessner who was a collaborator in most of the work presented here. Being like an additional supervisor to me, he opened my eyes to a lot of interesting ideas and suggested many fruitful directions to consider.

Third, I also thank Fiona Burnell, Leonid Glazman, Bertrand Halperin, Johannes Knolle, Dmitry Kovrizhin, Chris Laumann, and Steve Simon for enlightening discussions in relation to this work. Further thanks go to my colleagues at Oxford for providing a great environment, the department administrators for helping in everyday matters and, last but not least, my family and my friends for their never-ending support.

The work presented in this thesis is based on a single published paper [Phys. Rev. B **90**, 035145 (2014)] and an additional manuscript currently in preparation. My work has been supported by the EPSRC under Grant No. EP/I032487/1, and by the Helmholtz Virtual Institute "New States of Matter and Their Excitations".

Contents

Chapter 1

Introduction

The physics of strongly-correlated electrons is at the forefront of research in both theoretical and experimental quantum condensed matter physics. Although the perturbative single-electron framework of Fermi liquid theory is surprisingly successful at describing a broad range of physical phenomena, there is also a rich variety of more exotic phases beyond Fermi liquid theory, in which strong correlations between electrons play a fundamental role. Examples of such strongly-correlated phases include Mott insulators, high-temperature (cuprate) superconductors, quantum spin liquids, and fractional quantum Hall phases. Unlike in Fermi liquids, where the ground state of the interacting system is adiabatically connected to that of the non-interacting one, and the excitations are electron-like quasiparticles that only differ from electrons in renormalized properties such as an effective mass, the ground states of strongly-correlated phases are fundamentally distinct from those of their non-interacting counterparts, and their excitations are collective degrees of freedom exhibiting exotic behavior such as fractionalization. Due to the emergent nature of these excitations and their distinctness from electrons, it is often challenging to detect them via standard experimental techniques designed for measuring single-electron properties and, from a theoretical point of view, it is typically impossible to identify them from a Hamiltonian given in terms of the (original) electronic degrees of freedom. Instead, one requires physical intuition and/or numerical methods to guess the emergent excitations and construct an effective theory in terms of an appropriate language that correctly captures the essential physics.

1.1 Mott insulators and related phases

Mott insulators were among the first strongly-correlated phases to be discovered, and they continue to be of outstanding interest more than half a century later [1, 2]. In the early days of quantum physics, the distinction between metals and insulators was understood in terms of the single-electron picture of band theory. According to this theory, an electronic system must be a metal if it has at least one partially-filled band while it must be an insulator if all its bands are either completely filled or completely empty. However, it was noticed already in the 1930s that certain transition-metal oxides such as NiO are insulators despite the presence of a partially-filled d-electron band. In the following decades, an intense research effort led by Peierls and Mott revealed that the insulating behavior in these transition-metal oxides is due to the strong Coulomb repulsion between electrons occupying the same atomic orbital. To distinguish them from conventional band insulators, these strongly-correlated insulators are called Mott insulators. By varying experimental control parameters such as the bandwidth or the band filling, a quantum phase transition was also demonstrated between a metallic phase and a Mott insulator phase (see Fig. 1.1), and this metal-insulator transition driven by strong correlations became the subject of intense theoretical study. Since the late 1980s, the interest in Mott insulators has been revived by the discovery of other strongly-correlated phases, such as high-temperature superconductors and quantum spin liquids, which can be thought of as derivatives of Mott insulators [3].

1.1.1 Hubbard, Heisenberg, and t-J models

The Hubbard model is a surprisingly versatile toy model in condensed matter physics, which captures the transition between the single-electron limit and the strongly-correlated limit [4]. Based on a simple tight-binding model with localized (Wannier) orbitals at the atomic sites l and a hopping amplitude $-t$ between neighboring sites l and l', this model contains an additional on-site repulsion energy U that penalizes

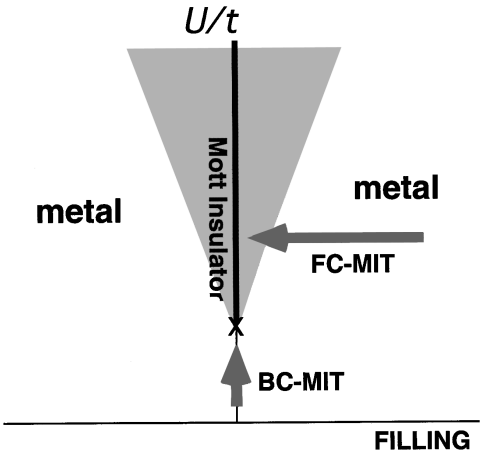

Figure 1.1: (Picture taken from Ref. [2].) Schematic phase diagram of the Hubbard model as a function of the dimensionless ratio U/t and the filling fraction around the central case of half filling. The Mott insulator phase is marked by a thick line, the anomalous metallic phase is marked by gray shading, while the conventional metallic phase occupies the rest of the phase diagram. Two different routes for the metal-insulator transition (MIT) are also indicated: the bandwidth-controlled MIT (BC-MIT) and the filling-controlled MIT (FC-MIT).

double occupation. The Hamiltonian of the Hubbard model takes the form

$$H_{\mathrm{Hub}} = -t \sum_{\langle l,l' \rangle} \sum_{\sigma} \left[\mathbf{c}^{\dagger}_{l,\sigma} \mathbf{c}_{l',\sigma} + \mathrm{H.c.} \right] + U \sum_{l} \mathbf{n}_{l,\uparrow} \mathbf{n}_{l,\downarrow}, \tag{1.1}$$

where $\mathbf{c}^{(\dagger)}_{l,\sigma}$ are standard fermionic creation and annihilation operators for an electron with spin σ at site l, and $\mathbf{n}_{l,\sigma} \equiv \mathbf{c}^{\dagger}_{l,\sigma} \mathbf{c}_{l,\sigma}$ is the corresponding number operator. Despite its apparent simplicity, the Hubbard model captures a broad range of physical phenomena including (anti)ferromagnetism, superconductivity, and the metal-insulator transition described above. Its analytic study is also surprisingly challenging: in one dimension, an exact solution is available by means of a Bethe ansatz [5, 6], but in two or three dimensions, one must resort to approximate methods.

Arguably, the Hubbard model is one of the most important models in condensed matter physics, and certain aspects of its phase diagram are still not properly understood. Even at zero temperature, its phase diagram is extremely rich as it is a function of two crucial parameters: the dimensionless ratio U/t and the filling fraction of the atomic sites (see Fig. 1.1). In the weak-coupling limit of $U \ll t$, the Hamiltonian is dominated by the hopping term $\propto t$, and one essentially recovers the underly-

ing tight-binding model without the on-site repulsion. The resulting single-electron states are then occupied up to a Fermi level, and the ground state is a Fermi liquid exhibiting conventional metallic behavior. In the strong-coupling limit of $U \gg t$, the Hamiltonian is dominated by the on-site repulsion term $\propto U$, and the behavior of the system depends sensitively on the filling fraction. In the important case of half filling, when there is one electron per atomic site, each site is occupied by exactly one electron to avoid double occupation. The electrons are then unable to hop between neighboring sites due to the energy penalty $\sim U$, and the ground state is a Mott insulator exhibiting strong electronic correlations. In the proximity of half filling, when the additional electrons or holes are free to hop without an energy penalty $\sim U$, the ground state is an anomalous metal exhibiting strong fluctuations and a significantly enhanced effective mass. In accordance with the experimental results, a quantum phase transition between the Mott insulator phase and the conventional or the anomalous metallic phase can be achieved by varying the dimensionless ratio U/t or the filling fraction, respectively (see Fig. 1.1).

When the Hubbard model is at half filling in the strong-coupling limit, the low-energy states of the model all have exactly one electron at each atomic site. Since the only remaining degrees of freedom are the electron spins, the low-energy behavior of the resulting Mott insulator is accurately described in terms of an effective spin model. The effective couplings between nearby spins are obtained from perturbation theory by considering second-order hopping processes through high-energy intermediate states in which at least one site is double occupied. In the case of a Hubbard model with full spin-rotation symmetry [see Eq. (1.1)], the effective spin model is the antiferromagnetic Heisenberg model, and the corresponding Hamiltonian becomes

$$H_{\text{Heis}} = J \sum_{\langle l,l' \rangle} \left[\mathbf{S}_l \cdot \mathbf{S}_{l'} - \frac{1}{4} \right], \tag{1.2}$$

where $\mathbf{S}_l \equiv \sigma_l/2$ is the spin of the electron at site l, and $J = 4t^2/U$ is the effective coupling strength from second-order perturbation theory in t/U. This connection between the Hubbard model and the Heisenberg model sheds light on the experimentally observed link between Mott insulators and (anti)ferromagnetism. Indeed,

the stereotypical Mott insulator NiO is found to be antiferromagnetically ordered at sufficiently low temperatures.

When the strong-coupling limit of the Hubbard model is tuned away from half filling via electron or hole doping, the additional electrons or holes are free to hop between neighboring sites. The low-energy behavior of the resulting doped Mott insulator is effectively captured by the t-J model [7], which contains a hopping term $\propto t$ similar to the one in Eq. (1.1) and a coupling term $\propto J$ similar to the one in Eq. (1.2). In the case of hole doping, its Hamiltonian is given by

$$\begin{aligned} H_{t-J} &= -t \sum_{\langle l,l' \rangle} \sum_{\sigma} \left[(1 - \mathbf{n}_{l,-\sigma}) \, \mathbf{c}^{\dagger}_{l,\sigma} \mathbf{c}_{l',\sigma} \, (1 - \mathbf{n}_{l',-\sigma}) + \text{H.c.} \right] \\ &\quad + J \sum_{\langle l,l' \rangle} \left[\mathbf{S}_l \cdot \mathbf{S}_{l'} - \frac{\mathbf{n}_l \mathbf{n}_{l'}}{4} \right], \end{aligned} \tag{1.3}$$

where $\mathbf{n}_l \equiv \mathbf{n}_{l,\uparrow} + \mathbf{n}_{l,\downarrow}$ is the single-site number operator, and the projectors $1 - \mathbf{n}_{l,-\sigma}$ ensure that double occupation is forbidden both before and after the hopping. It should be remarked that the t-J model does not follow from the Hubbard model in the same way the Heisenberg model does at half filling [8]. In fact, by considering all possible second-order hopping processes, the analogous perturbation theory gives a more general strong-coupling model with appropriate three-site terms $\propto J$ in addition to the two-site Heisenberg terms in Eq. (1.3). Nevertheless, the t-J model is commonly used as a starting point in describing lightly doped Mott insulators because it has been argued that the three-site terms are not important near half filling [9].

1.1.2 Doped Mott insulators and quantum spin liquids

The behavior of a Mott insulator upon doping is arguably one of the most important open questions in the physics of strongly-correlated electrons. Historically, the interest in doped Mott insulators exploded after the discovery of cuprate superconductors [10] due to a well-established hypothesis that high-temperature superconductivity in these exotic materials is in fact governed by the physics of lightly doped Mott insulators [3, 11]. This hypothesis was motivated in part by the typical phase diagram of cuprate superconductors, in which the superconducting phase is in proximity to an

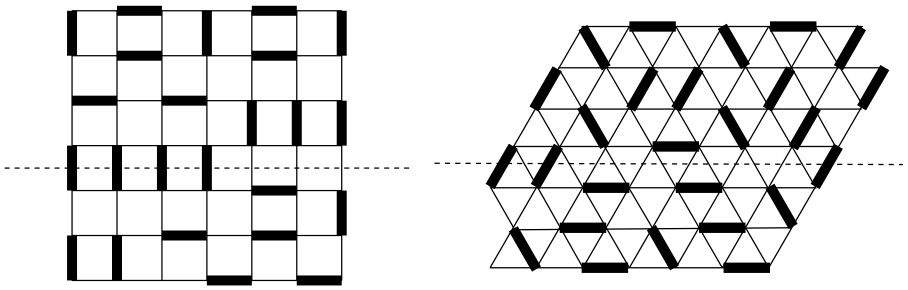

Figure 1.2: (Picture taken from Ref. [21].) Examples of valence bond configurations on the bipartite square lattice (left) and on the non-bipartite triangular lattice (right). Individual valence bonds that correspond to local spin singlets are marked by thick lines, and the topological string that can be used to distinguish topological sectors is marked by a dashed line in each case.

antiferromagnetic one [12]. In the following years, doped magnetic systems received unprecedented attention, and many authors in particular studied hole dynamics in the conventional antiferromagnetic spin state of a Mott insulator. When a hole propagates in a magnetically ordered spin background, it scrambles the spin configuration and leaves behind a string of overturned spins with a finite energy cost per unit length. In the Ising limit, when there are no quantum fluctuations, this string can only be removed if the hole retraces its own path back to the origin, and the hole is therefore confined by an effective linear potential [13, 14]. In the Heisenberg limit, the string can be removed by quantum fluctuations turning back two spins at a time, and the hole is therefore deconfined, but its effective mass is increased significantly due to its interactions with the spin background [15, 16, 17].

These early results on doped magnetic systems indicated that a magnetically ordered spin background has an adverse effect on hole propagation. Moreover, it was recognized that Mott insulators can actually enter a broad range of spin states, some of which are considerably more exotic than the conventional antiferromagnetic state [18]. In particular, Anderson suggested that the parent state of high-temperature superconductivity is an unconventional resonating valence bond (RVB) liquid state with no magnetic order [19, 20]. Schematically, the RVB liquid state is a broad superposition of many valence bond configurations, where each valence bond configuration is a product state of local spin singlets formed along individual valence bonds covering

the lattice (see Fig. 1.2). Anderson's suggestion provided motivation for the study of such unconventional spin states [21], and it was established that the RVB liquid state belongs to the more general class of quantum spin liquids [22, 23, 24].

From a purely theoretical point of view, quantum spin liquids are fractional topological phases. Indeed, they exhibit topological order, a new type of order beyond the Landau paradigm of symmetry breaking, which is characterized by a well-defined ground-state degeneracy and the lack of a corresponding local order parameter [25]. Importantly, the ground-state degeneracy depends on the global topology of the system and is robust against arbitrary local perturbations [26]. In general, the degenerate ground states belong to different topological sectors that are completely indistinguishable by any local measurements and are instead distinguishable by topological strings traversing the entire system. For example, in the case of the RVB liquid, the topological sector is determined by the number of valence bonds crossing the topological string (see Fig. 1.2), although the details of this mapping are crucially different for bipartite and non-bipartite lattices. In the case of a bipartite lattice [22, 23], the sublattice structure provides a self-consistent way of assigning directions to the valence bonds, and the topological sectors are then characterized by an integer ($\mathbb{Z}$) variable: the net valence bond flux crossing the topological string. In the case of a non-bipartite lattice [24], the valence bonds have no directions assigned to them, and the topological sectors are then characterized by an even-or-odd ($\mathbb{Z}_2$) variable: the parity of the number of valence bonds crossing the topological string.

In general, the ground states of topological phases are strongly entangled because they are broad superpositions of many product states in terms of the local variables. Moreover, each topological phase is characterized by a topological entanglement entropy, a subdominant correction to the entanglement entropy, that depends on the topological properties of the ground state and is robust against local perturbations [27, 28]. Importantly, there is also a generic connection between topological phases and emergent gauge theories. For example, in the case of the RVB liquid, one can introduce gauge variables at the bonds of the lattice that are subject to appropriate

gauge constraints at the sites [29]. Once again, there is a crucial difference between bipartite and non-bipartite lattices. For bipartite lattices, the RVB liquid phase corresponds to a $U(1)$ gauge theory with gapless $U(1)$ gauge fields, and its ground state is therefore called a gapless $U(1)$ spin liquid. For non-bipartite lattices, the RVB liquid phase corresponds to a $\mathbb{Z}_2$ gauge theory with gapped $\mathbb{Z}_2$ gauge fields, and its ground state is therefore called a gapped $\mathbb{Z}_2$ spin liquid.

The low-energy excitations of topological phases are fractional in the sense that they carry only a fraction of the inherent electron properties [30, 31]. For example, in the case of the RVB liquid, electrons appear to be split into two constituents, each carrying either only spin or only charge (spin-charge separation), and the corresponding low-energy excitations are neutral spinful fermions (spinons) and charged spinless bosons (holons). In general, a fractional excitation behaves like a topological defect in the sense that it can never be created or annihilated on its own but only together with one or more other fractional excitations. Furthermore, in two dimensions, fractional excitations generally exhibit anyonic statistics. Since the braiding of a particle around an other one is a topologically non-trivial operation in two dimensions, the exchange of two identical particles does not necessarily multiply the quantum state by ± 1 as for bosons or fermions. In the case of Abelian anyons, braiding and exchange operations multiply the quantum state by general complex phase factors, while in the case of non-Abelian anyons, these complex phase factors become (non-commuting) matrices acting on an internal set of quantum states. Importantly, such non-Abelian excitations in gapped topological phases provide a promising direction towards topological quantum computation [32]. The main idea behind this proposal is to encode quantum information into the internal states spanned by the excitations and perform quantum operations by braiding the excitations around one another. The resulting quantum device is believed to be protected against errors by the finite correlation length and the topological nature of the braiding operations.

From a practical point of view, quantum spin liquids typically appear in frustrated magnetic systems, where strong quantum fluctuations suppress magnetic ordering

down to zero temperature [33]. Indeed, some of the most promising experimental quantum spin liquid candidates are geometrically frustrated antiferromagnets based on the kagome lattice [34, 35] or the pyrochlore lattice [36]. Unfortunately, the lack of magnetic order is merely an indirect signature and could also be indicative of ordinary paramagnetic behavior, while the most important direct signatures of topological order, such as the ground-state degeneracy and the topological entanglement entropy, are virtually impossible to measure in an experiment. Because of these complications, a direct experimental detection of a quantum spin liquid remained elusive for more than two decades after Anderson's original suggestion. In a recent experiment, however, signatures of fractional excitations have been detected in the kagome-lattice antiferromagnet herbertsmithite [35]. Since fractional excitations are always created in groups of more than one, their typical signature is a continuum spectrum instead of a clear-cut dispersion relation.

Although realistic frustrated spin models based on the kagome or the pyrochlore lattice are useful in providing guidelines towards experimental realizations, their theoretical study is extremely challenging because one must resort to approximate or numerical techniques in the absence of an exact solution. For example, it took more than a decade to establish that the ground state of the spin-1/2 kagome-lattice antiferromagnetic Heisenberg model is a quantum spin liquid [34], and the precise nature of this quantum spin liquid is still a subject of intense debate [37]. In terms of an alternative direction that is suitable for exact analytic calculations, a breakthrough was achieved by Kiteav. In two seminal publications, he introduced two exactly solvable two-dimensional models with quantum spin liquid ground states: the toric-code model [38] and the Kitaev honeycomb model [39].

1.1.3 Kitaev honeycomb model

The Kitaev honeycomb model is a two-dimensional quantum spin model [39]. Since the model is exactly solvable and features a quantum spin liquid ground state, it provides a convenient playground for studying quantum spin liquids in a setting where

exact analytic calculations are available. Although it is a frustrated spin model, the frustration in its ground state does not arise due to geometric constraints (geometric frustration) as in the kagome-lattice and the pyrochlore-lattice models but because of non-commuting spin coupling terms in its Hamiltonian (exchange frustration). In fact, the Kitaev honeycomb model belongs to the more general class of quantum compass models, in which the spin-rotational symmetry of the spin coupling terms is broken due to spin-orbit coupling [40]. We now provide a brief review of the model and its essential properties, while a more detailed discussion of its technical features is delayed until the next chapter.

The model consists of spin-1/2 degrees of freedom that are located at the sites of a honeycomb lattice and are coupled to their neighbors by Ising interactions. Based on their orientation, there are three types of bonds (x, y, and z) connecting neighboring sites, and correspondingly, there are three types of Ising interactions coupling neighboring spins via three different spin components (σ^x, σ^y, and σ^z). The Hamiltonian of the model takes the form

$$H_{\mathrm{Kit}} = -J_x \sum_{\langle l,l' \rangle \in x} \sigma_l^x \sigma_{l'}^x - J_y \sum_{\langle l,l' \rangle \in y} \sigma_l^y \sigma_{l'}^y - J_z \sum_{\langle l,l' \rangle \in z} \sigma_l^z \sigma_{l'}^z, \tag{1.4}$$

where $J_{x,y,z}$ are the Ising coupling strengths on the x, y, and z bonds, respectively. Since the three Ising terms acting on a given site do not commute with one another, there is exchange frustration in the model that gives rise to strong quantum fluctuations and explains why the ground state is a quantum spin liquid. Furthermore, although the relation $0 \leq J_x \leq J_y \leq J_z = 1$ can always be assumed without loss of generality, the Ising coupling strengths $J_{x,y,z}$ can have different magnitudes, and the model can therefore exhibit a spatial anisotropy. Importantly, the ground state of the model is a fundamentally different kind of quantum spin liquid in the almost isotropic and the strongly anisotropic cases.

The model can be solved exactly by means of a standard procedure [39], which reveals that its elementary excitations are fluxes and fermions (see Sec. 2.1). More precisely, the exact solution maps the quantum spin model in Eq. (1.4) to an emergent $\mathbb{Z}_2$ gauge theory, where the fluxes are (redundantly) represented by static $\mathbb{Z}_2$ gauge

variables, and the fermions are then coupled to these emergent gauge fields. Importantly, the fluxes are always gapped, while the fermions can be gapped or gapless. Indeed, one can distinguish two phases of the model based on its spatial anisotropy: the fermions are gapped in the strongly anisotropic case of $J_z > J_x + J_y$ (gapped phase), while they are gapless in the almost isotropic case of $J_z < J_x + J_y$ (gapless phase). It should be remarked that the model also has an alternative exact solution by means of a Jordan−Wigner transformation, which maps the quantum spin model to a BCS pairing model of spinless fermions [41].

As mentioned above, the two phases of the model have fundamentally distinct ground states. In the gapped phase, the ground state is a $\mathbb{Z}_2$ spin liquid featuring gapped excitations with Abelian anyonic statistics (Abelian gapped phase). Moreover, in the extremely anisotropic limit of $J_{x,y} \ll J_z$, the fluxes have much smaller excitation energies than the fermions (see Sec. 2.2), and the low-energy physics is therefore dominated by the fluxes. If the fermions are then integrated out, the emergent gauge theory of the model reduces to a pure $\mathbb{Z}_2$ gauge theory [42]. Indeed, the gapped phase is equivalent to a triangular-lattice RVB liquid in terms of its topological order. In the gapless phase, the ground state is an algebraic spin liquid featuring gapless fermion excitations at a finite number of Dirac points [43, 44]. However, these Dirac points are protected by time-reversal symmetry, and the model can therefore be driven into a gapped phase by applying an external magnetic field [39]. At leading order in perturbation theory, such an external field is represented by additional three-site terms in Eq. (1.4). Importantly, the model remains exactly solvable in this new gapped phase, and its ground state is again a gapped spin liquid, which is, however, different from the $\mathbb{Z}_2$ spin liquid as it features excitations with non-Abelian anyonic statistics (non-Abelian gapped phase).

In the absence of perturbations, the dynamic spin-spin correlations are extremely short ranged in both the (Abelian) gapped and the gapless phases of the model. To be more precise, they vanish identically unless the two spins are located at neighboring sites [45]. However, since this result is an artifact of the fluxes being static and

localized, the spin-spin correlations are expected to be longer ranged in the presence of a generic perturbation. Indeed, the analogous energy-energy correlations are found to decay exponentially in the gapped phase and algebraically in the gapless phase [46]. From an experimental point of view, the relevant quantity is the dynamic structure factor, which is the Fourier transform of the dynamic spin-spin correlations in both space and time, because it can be measured directly by inelastic neutron scattering. In a recent work, the dynamic structure factor of the model has been calculated exactly, and direct signatures of fractional excitations have been pointed out [47]. In particular, since a spin fractionalizes into a fermion that is either gapped or gapless and a flux that is always gapped, the dynamic structure factor has a finite energy gap for all momenta in both the gapped and the gapless phases.

Ever since the discovery of the model, there has been an intense effort to realize it in an experimental setup, and several viable directions have been proposed. In terms of cold-atom systems, it was argued that the Kitaev honeycomb model can be obtained as an effective spin model of an appropriately engineered Hubbard model in the strong-coupling limit [44, 48]. The main idea is that a spin-dependent hopping amplitude in the Hubbard model of Eq. (1.1) gives rise to spin-anisotropic couplings in the effective spin model of Eq. (1.2). In terms of solid-state materials, the first proposal involved the layered iridium oxides Na_2IrO_3 and Li_2IrO_3, in which the Ir^{4+} ions with $5d^5$ configuration form honeycomb lattices. Due to crystal-field splitting and strong spin-orbit coupling, the low-energy physics of each Ir^{4+} ion is dominated by a Kramers doublet, which can be identified as an effective spin-1/2 degree of freedom [49, 50]. Arising from spin-orbit coupling, these degrees of freedom have both spin and orbital character, and their couplings are therefore strongly anisotropic. In particular, a careful investigation predicts that the low-energy behavior of the layered iridium oxides is captured by the Kitaev−Heisenberg model [49, 51]. For different weights of the Kitaev and the Heisenberg components, this model with Hamiltonian $H_{\mathrm{Kit}} + H_{\mathrm{Heis}}$ has a quantum spin liquid phase and several magnetically ordered phases [52]. So far, however, the quantum spin liquid phase has remained elusive as a finite

ordering temperature was found in all experiments based on these layered iridium oxides [53, 54, 55, 56, 57, 58].

1.1.4 Doping a quantum spin liquid

Following Anderson's suggestion on Mott insulators and their quantum spin liquid states, it is natural to reconsider the problem of doped Mott insulators by studying hole dynamics in a quantum spin liquid instead of an antiferromagnet. In general, holes are expected to be more deconfined in a quantum spin liquid because their propagation is no longer hindered by a magnetically ordered spin background. Nevertheless, there is a highly non-trivial interaction between the holes and the quantum spin liquid background, and understanding a doped quantum spin liquid is therefore a challenging many-body problem.

In the past few decades, many authors have studied doped quantum spin liquids by employing a standard phenomenological treatment that is applicable to doped Mott insulators in general [59]. This treatment is based on a variational approach in terms of an appropriate RVB trial wave function that captures the essential physics of the system. In particular, the magnetic interaction energy can be optimized by encoding ferromagnetic or antiferromagnetic alignment, while the possibility of superconductivity can be incorporated by encoding BCS pairing into the trial wave function. In the absence of doping, the constraint of single occupancy is then enforced by an appropriate (numerical or approximate) projection procedure [60, 61], while in the presence of doping, this projection must be softened, which generally leads to a mean-field theory [59].

In this phenomenological framework, low-energy fractionalization in doped quantum spin liquids is typically captured by a slave-particle (parton) construction, in which electrons are represented by combinations of fractional degrees of freedom such as spinons and holons [42]. Schematically, the electron operators are written as $\mathbf{c}_{l,\sigma} \sim \mathbf{f}_{l,\sigma}\mathbf{b}_l$, where $\mathbf{f}_{l,\sigma}$ and $\mathbf{b}_l$ are appropriate spinon and holon operators, respectively. In the resulting quartic terms, the spinon and the holon operators are then

decoupled via a standard mean-field decomposition that takes the schematic form

$$\mathbf{c}_{l,\sigma}\,\mathbf{c}_{l',\sigma'} \sim \mathbf{f}_{l,\sigma}\,\mathbf{f}_{l',\sigma'}\,\mathbf{b}_{l}\,\mathbf{b}_{l'} \sim \langle \mathbf{f}_{l,\sigma}\,\mathbf{f}_{l',\sigma'}\rangle\,\mathbf{b}_{l}\,\mathbf{b}_{l'} + \mathbf{f}_{l,\sigma}\,\mathbf{f}_{l',\sigma'}\,\langle \mathbf{b}_{l}\,\mathbf{b}_{l'}\rangle. \tag{1.5}$$

The phenomenon of spin-charge separation is naturally captured by this mean-field decomposition as spin is carried by spinons while charge is carried by holons. However, depending on the precise forms of the slave-particle construction and the subsequent mean-field decomposition, several distinct slave-particle mean-field theories can be obtained for the same Hamiltonian. The possible mean-field saddle points are then most efficiently classified in terms of projective symmetry groups [42], while the fluctuations around these mean-field saddle points generally give rise to gauge theories [62]. Importantly, there are an extremely large number of distinct saddle points [63, 64, 65], and it is also challenging to decide which of these saddle points are actually stable [66]. Given a Hamiltonian, it is not immediately clear how to choose the most relevant saddle point, and the construction of a slave-particle mean-field theory is therefore not a fully controlled procedure.

The setting of the Kitaev honeycomb model provides a great opportunity to employ a complementary approach in studying a doped quantum spin liquid. On one hand, the doped Kitaev honeycomb model has been studied extensively in the phenomenological framework of slave-particle mean-field theories [67, 68, 69, 70, 71, 72]. Remarkably, the construction by You *et al.* in Ref. [70] recovers the exact ground-state correlations in the limit of the undoped model, and therefore it provides a reasonably controlled starting point for its discussion of the doped model. On the other hand, even though the undoped Kitaev honeycomb model has a readily available exact solution, a microscopic treatment of the doped Kitaev honeycomb model based on this exact solution seems to be missing from the literature. To the best of our knowledge, the most relevant works in this direction are the those by Willans *et al.* on the magnetic properties of static vacancies in the model [73, 74]. The aim of the present work is to fill in this gap in the literature by providing a controlled microscopic treatment of mobile holes in the Kitaev honeycomb model.

1.2 Thesis summary

In this thesis, we present a controlled microscopic study of mobile holes in a topological quantum spin liquid. Our approach is complementary to previous phenomenological works on doped quantum spin liquids as our starting point is the ground state of the exactly solvable Kitaev honeycomb model [39]. To be more precise, we consider an effective $t-J$ model on the honeycomb lattice, where the Heisenberg coupling terms in Eq. (1.3) are substituted with the Ising coupling terms in Eq. (1.4). The Hamiltonian of this effective $t-J$ model takes the form

$$\begin{aligned} H &= -J_x \sum_{\langle l,l'\rangle \in x} \sigma_l^x \sigma_{l'}^x - J_y \sum_{\langle l,l'\rangle \in y} \sigma_l^y \sigma_{l'}^y - J_z \sum_{\langle l,l'\rangle \in z} \sigma_l^z \sigma_{l'}^z \\ &\quad - t \sum_{\langle l,l'\rangle} \sum_{\sigma} \left[\left(1 - \mathbf{n}_{l,-\sigma}\right) \mathbf{c}_{l,\sigma}^{\dagger} \mathbf{c}_{l',\sigma} \left(1 - \mathbf{n}_{l',-\sigma}\right) + \text{H.c.} \right]. \end{aligned} \tag{1.6}$$

Since the Kitaev honeycomb model remains exactly solvable in the presence of static vacancies or, equivalently, stationary holes [73, 74], we describe the hopping of mobile holes via a quasistationary approach, in which the hopping term $\propto t$ in Eq. (1.6) is treated as a perturbation on top of the remaining terms $\propto J_{x,y,z}$, and the hopping is then characterized by its matrix elements between the exact eigenstates of the model with stationary holes at different positions.

We study both the (Abelian) gapped and the gapless phases of the model. In the gapped phase, our quasistationary approach is exact when the bare hopping amplitude t is much smaller than the energy gap of the bulk excitations. Since a mobile hole in this limit does not generate any bulk excitations, the hopping problem is greatly simplified as we can restrict our attention to the ground states of the model with stationary holes at different positions. We address both the single-particle properties of individual holes and the multi-particle ground state at finite doping. Our main result is that the holes in the doped model possess internal degrees of freedom because they can bind the fractional excitations of the undoped model and that the resulting composite holes with different excitations bound are distinct fractional particles with fundamentally different single-particle properties (see Table 1.1) and

different experimental signatures in the multi-particle ground state. In the gapless phase, our quasistationary approach is no longer exact and, moreover, it is not even clear if a mobile hole has a coherent quasiparticle description because bulk excitations are generated for any bare hopping amplitude $t > 0$. Using an approximate variational approach, we argue that a single mobile hole has a finite quasiparticle weight for any $t > 0$ which vanishes in the stationary limit of $t \to 0$.

In the following, we describe the structure of this thesis and provide an extended summary of our results. The second chapter reviews the undoped Kitaev honeycomb model as background for the new results in the remaining chapters. In Sec. 2.1, we introduce the model and describe its exact solution. It is recalled that the ground state of the model has a topological degeneracy and that the elementary excitations are fractional as they can only be created in pairs. There are two kinds of elementary excitations: fluxes, which are always gapped, and fermions, which are either gapped or gapless, depending on the model parameters. In Sec. 2.2, we restrict our attention to the spatially anisotropic (Abelian) gapped phase of the model, which is characterized by gapped fluxes and gapped fermions. We refer to a simple limiting point in this phase, the isolated dimer limit, where the model consists of infinitesimally coupled spin dimers. Furthermore, we explain the notion of superselection sectors to quantify the fractional nature of isolated excitation clusters.

The third chapter is concerned with the single-particle properties of individual holes in the gapped phase of the model. In Sec. 3.1, we introduce the formalism for describing holes, and discuss how the elementary degrees of freedom (modes) are affected by the presence of n holes. The main result of this section is that each hole in the model has three localized internal modes at much smaller energies than the remaining bulk modes (fluxes and fermions). Excitations in these three internal modes are characterized by three corresponding internal quantum numbers: the flux quantum number $h = \{0, 1\}$, the fermion quantum number $q = \{0, 1\}$, and the plaquette quantum number $p = \{0, 1\}$. The quantum numbers h and q specify the kinds of fractional excitations (fluxes and fermions) bound to the hole. They therefore deter-

Hole type		Interpretation	Superselection sector
$h = 0$	$q = 0$	Bare hole	Trivial (1)
	$q = 1$	Hole + fermion	Combined ($e \times m$)
$h = 1$	$q = 0$	Hole + flux	Electric (e)
	$q = 1$	Hole + flux + fermion	Magnetic (m)

Hole type		Hopping dimensionality	Absolute statistics	Relative statistics
$h = 0$	$q = 0$	2D (free & isotropic)	Fermion	Trivial
	$q = 1$	2D (free & anisotropic)	Boson	Non-trivial
$h = 1$	$q = 0$	1D (confined)	Fermion	Non-trivial
	$q = 1$	1D (confined)	Fermion	Non-trivial

Table 1.1: Summary of the most important hole properties for different combinations of the flux quantum number $h = \{0, 1\}$ and the fermion quantum number $q = \{0, 1\}$: interpretations in terms of elementary excitations bound, superselection sectors of equivalent excitation clusters, generic hopping properties (see details in Fig. 3.6), absolute particle statistics, and relative particle statistics (see details in Table 3.5).

mine its superselection sector via an equivalent excitation cluster (see Table 1.1). The quantum number p is related to the discrete spin-rotation symmetry $\sigma^{x,z} \to -\sigma^{x,z}$. It therefore acts as a spin quantum number and determines the local magnetization around the hole. Since h and q quantify the fractional nature of the hole, they are robust against arbitrary local perturbations of sufficiently small strength. This robustness does not extend to p in general, but it does so in the important special case of a Heisenberg perturbation. We also consider interactions between holes and find an attractive two-hole interaction that is diagonal in h and p but not in q. To ensure that holes do not undergo pair formation or phase separation, we implicitly assume the presence of a sufficiently strong Coulomb repulsion.

In Sec. 3.2, we introduce the formalism for describing hole hopping, and discuss the hopping properties of isolated holes in the model. Our approach is restricted to the regime of slow hopping, where the bulk modes are not excited as the hopping amplitude is much smaller than their energy gap. This section has two main results. First, the internal quantum numbers h, q, and p are all conserved by the hopping. The various hole types with different quantum numbers can therefore be treated as distinct particles. Second, the hopping properties of a hole are unaffected by its

quantum number p but are strikingly affected by its quantum numbers h and q. Since the model is spatially anisotropic in the gapped phase, the two perpendicular dimensions of the lattice are not equivalent. At a generic point of the gapped phase, $h = 0$ holes are free to hop in two dimensions, while $h = 1$ holes are confined to hop in one dimension only (see Table 1.1). Restricting our attention to $h = 0$ holes, the two-dimensional hopping problem of $q = 0$ holes is approximately isotropic, while that of $q = 1$ holes is strongly anisotropic. This difference is amplified in the isolated dimer limit, where $q = 0$ holes remain free to hop in two dimensions, while $q = 1$ holes become confined to hop in one dimension only. We also determine the absolute and the relative particle statistics of the various hole types (see Table 1.1), and provide an intuitive explanation for our results by referring to the fermionic nature of the bare holes and the anyonic nature of the fractional excitations bound to them.

The fourth chapter is concerned with the multi-particle ground state of the gapped phase in the case of finite doping. In Sec. 4.1, we describe the multi-hole state representing a finite density of mobile holes, and determine the ground-state hole quantum numbers h, q, and p that minimize the energy of such a multi-hole state. In the absence of hole interactions, there are two complementary regimes distinguished by the model parameters. In the first regime, all holes in the ground state are fermions with quantum numbers $h = 0$ and $q = 0$. They therefore fill two identical Fermi seas with different quantum numbers $p = \{0, 1\}$. Since these holes are free to hop in two dimensions, the electrical conductivity is approximately isotropic. In the second regime, all holes in the ground state are fermions with quantum numbers $h = 1$. They therefore fill four identical Fermi seas with different quantum numbers $q = \{0, 1\}$ and $p = \{0, 1\}$. Since these holes are confined to hop in one dimension only, the electrical conductivity is extremely anisotropic. The two complementary regimes remain applicable in the presence of hole interactions as both the attractive interaction and the Coulomb repulsion are diagonal in the quantum number h. In the first regime, a mean-field treatment restricted to $h = 0$ holes reveals that there is a critical hole density above which $q = 1$ holes appear. Since these holes are bosons, their coherent

condensation leads to charged superfluid behavior and a spontaneous net magnetization. In the second regime, a mean-field treatment restricted to $h = 1$ holes reveals that scattering between coexisting $q = 0$ holes and $q = 1$ holes facilitates hopping in both dimensions of the lattice. This implies that the conductivity anisotropy becomes weaker as the hole density is increased.

In Sec. 4.2, we qualitatively discuss hole hopping beyond the regime of slow hopping, where the bulk modes are excited as the hopping amplitude is larger than their energy gap. Each hole is then surrounded by a cloud of fluctuating excitations (fluxes and fermions), but the internal quantum numbers h, q, and p are applicable as long as the hole density is sufficiently small so that the excitation clouds around different holes do not merge. However, any hole with quantum numbers other than $h = 0$ and $q = 0$ is unstable against a spontaneous decay into a lower-energy hole with quantum numbers $h = 0$ and $q = 0$. In Sec. 4.3, we compare our results from the exact description with those from the most closely related mean-field treatment in Ref. [70]. By contrasting the respective ground states, we find two main discrepancies between the two approaches. First, the quantum numbers h and q that specify the kinds of fractional excitations bound to the hole are captured in the exact description but ignored in the mean-field treatment. Second, the two approaches predict different particle statistics for holes with quantum numbers $h = 0$ and $q = 0$: they are fermions in the exact description but bosons in the mean-field treatment.

The fifth chapter addresses the possibility of a coherent quasiparticle description for a single mobile hole in the gapless phase of the model. In Sec. 5.1, we introduce the problem by defining the single-hole spectral function and discussing the single-hole eigenstates that are determined by a competition between the potential and the kinetic energies. To simplify our problem, we also refer to a limiting point in the gapless phase, where the model consists of decoupled one-dimensional chains. In Sec. 5.2, we consider the special case of a stationary hole, and calculate the exact low-energy behavior of the single-hole spectral function. The main result of this section is that the spectral function has no delta-function peak and therefore the hole has

a vanishing quasiparticle weight in the stationary limit. In Sec. 5.3, we consider the generic case of a mobile hole, and approximate the actual ground state with a single-parameter variational state that interpolates smoothly between the exact ground state in the stationary limit and that in the absence of the hole. By optimizing both potential and kinetic energies, we obtain the best possible variational state, and repeat our low-energy calculation of the single-hole spectral function. The main result of this section is that the spectral function has a delta-function peak and therefore the hole has a finite quasiparticle weight for a finite hopping amplitude. In Sec. 5.4, we argue that our results for a mobile hole are applicable beyond the variational approach and at a generic point of the gapless phase.

Chapter 2

Kitaev honeycomb model

The aim of this thesis is to provide a controlled microscopic study of mobile holes in an exactly solvable quantum spin liquid: the ground state of the Kitaev honeycomb model. In this chapter, we consider the undoped model, and present a detailed review of its technical features, including the steps of its exact solution. The considerations introduced in this chapter serve as useful starting points towards the new results on the doped model obtained in the remaining chapters.

The structure of this chapter is summarized as follows. In Sec. 2.1, we describe the general features of the model, including its formulation, its exact solution, its ground state, and its elementary excitations. It is verified that the ground state has a topological degeneracy and that the excitations are fractional as they can only be created in pairs. Depending on its parameters, the model has two distinct phases exhibiting a gapped and a gapless excitation spectrum, respectively. In Sec. 2.2, we restrict our attention to the gapped phase of the model, and discuss two additional features that are only applicable in this phase: the isolated dimer limit, a simple limiting point in the gapped phase, where the model breaks down into a set of infinitesimally coupled spin dimers, and the notion of superselection sectors, which can be used to classify the fractional properties of the gapped excitations.

2.1 General properties

2.1.1 Introduction of the model

The Kitaev honeycomb model is an exactly solvable two-dimensional quantum spin model [39]. Each site of the underlying honeycomb lattice supports a spin one-half degree of freedom (particle), and each spin is coupled to its three neighbors by Ising interactions involving the three different spin components. The sites of the bipartite lattice can be divided into two sublattices A and B, while the bonds can be divided into three classes x, y, and z based on their orientations (see Fig. 2.1). If $\alpha_{l,l'} = \{x, y, z\}$ gives the type of the bond connecting two neighboring sites l and l', each site l has three neighbors $\tilde{\alpha}(l)$ with $\tilde{\alpha} = \{x, y, z\}$ such that $\alpha_{l,\tilde{\alpha}(l)} = \tilde{\alpha}$. Using this notation, the Hamiltonian of the model reads as

$$H_\sigma = -\sum_{l\in A} \sum_{\alpha=x,y,z} J_\alpha \sigma_l^\alpha \sigma_{\alpha(l)}^\alpha, \tag{2.1}$$

where σ_l^α are the physical (Pauli) spin operators, and $J_{x,y,z}$ are the Ising coupling strengths on the x, y, and z bonds, respectively. In the following, we assume without loss of generality that $0 \leq J_x \leq J_y \leq J_z = 1$.

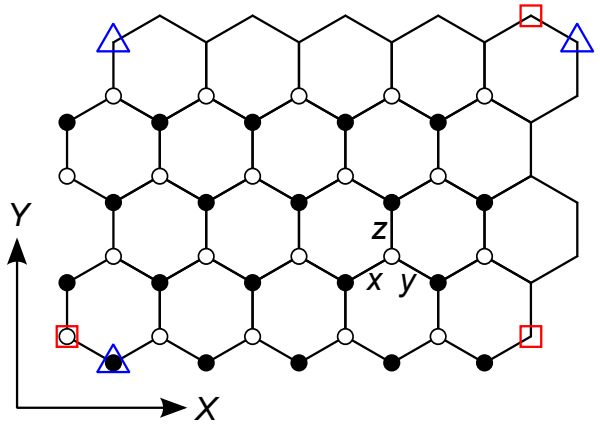

Figure 2.1: Illustration of the honeycomb lattice with dimensions $N_X = 5$ and $N_Y = 4$. Due to the periodic boundary conditions, several sites are identified with each other, such as the three sites marked by red rectangles and the three sites marked by blue triangles. Inequivalent sites in the sublattice A (B) are marked by white (black) dots. Examples of the three bond types (x, y, z) are also indicated.

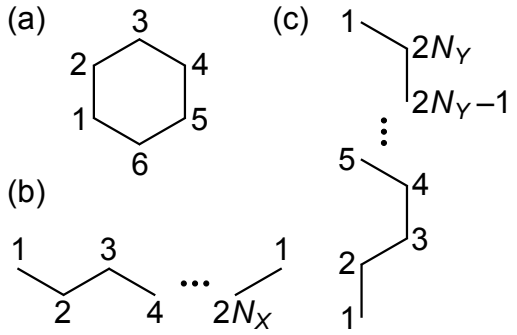

Figure 2.2: Site labeling convention for the generators of the loop operator group: the plaquette operators W_P (a) and the topological operators W_X (b) and W_Y (c).

We consider a lattice with periodic boundary conditions in both the horizontal (X) and the vertical (Y) directions. The $N_X \times N_Y$ lattice has $N \equiv N_X N_Y$ plaquettes, $2N$ sites, and $3N$ bonds (see Fig. 2.1). Based on their relative displacements in the X direction, the horizontal plaquette stripes of the lattice can be divided into two classes, even and odd, such that an even (odd) stripe is neighbored only by odd (even) stripes. We assume that N_Y is even so that periodic boundary conditions are applicable in the Y direction without a stripe mismatch between the top and the bottom of the lattice. Note though that these boundary conditions are specified only for the purpose of completeness and that our main results are in fact independent of the boundary conditions.

2.1.2 Flux degrees of freedom

The Hamiltonian in Eq. (2.1) can be solved exactly by means of a standard procedure [39]. The first step is to notice that there is a commuting non-dynamic observable W_C for each closed loop C of the lattice. For a loop C containing L sites labeled $\{1, 2, \ldots, L\}$, this non-dynamic observable is

$$W_C = \sigma_1^{\alpha_{1,2}} \sigma_2^{\alpha_{1,2}} \sigma_2^{\alpha_{2,3}} \sigma_3^{\alpha_{2,3}} \ldots \sigma_L^{\alpha_{L,1}} \sigma_1^{\alpha_{L,1}}. \tag{2.2}$$

Since the lattice is bipartite, the length L of the loop is always even. We also assume that sites labeled with odd (even) numbers belong to the sublattice A (B).

The loop operators W_C are commuting non-dynamic observables because they commute with each other as well as with the Hamiltonian H_σ. This means that the

different flux sectors characterized by distinct eigenvalues (± 1) of the loop operators can be considered independently. Furthermore, the group spanned by all loop operators is generated by a finite number of $\mathbb{Z}_2$ loop operators: those corresponding to the plaquettes P and the topological strings X and Y going around the lattice in the X and Y directions. Using the site labeling convention in Fig. 2.2, these generating loop operators take the forms

$$\begin{aligned} W_P &= \sigma_1^x \sigma_2^y \sigma_3^z \sigma_4^x \sigma_5^y \sigma_6^z, \\ W_X &= -\sigma_1^z \sigma_2^z \sigma_3^z \ldots \sigma_{2N_X}^z, \\ W_Y &= -\sigma_1^x \sigma_2^y \sigma_3^y \sigma_4^x \sigma_5^x \sigma_6^y \sigma_7^y \sigma_8^x \ldots \sigma_{2N_Y-1}^y \sigma_{2N_Y}^x. \end{aligned} \tag{2.3}$$

Importantly, there are only $N-1$ independent plaquette operators due to the global constraint $\prod_P W_P = 1$. This means that only $N+1$ flux degrees of freedom are found for the original $2N$ spin degrees of freedom and that the remaining $N-1$ degrees of freedom still must be identified. Note also that the excitation energies corresponding to the flux degrees of freedom are discussed in Secs. 2.1.4 and 2.2.1.

2.1.3 Fermion degrees of freedom

To solve the model exactly in each flux sector $\{W_C = \pm 1\}$, four Majorana fermions are introduced at each site l of the lattice: c_l and b_l^α with $\alpha = x, y, z$ [39]. The corresponding operators satisfy the standard anticommutation relations

$$\begin{aligned} &\{b_l^\alpha, b_{l'}^{\alpha'}\} = 2\delta_{ll'}\delta_{\alpha\alpha'}, \qquad && (b_l^\alpha)^2 = 1, \\ &\{c_l, c_{l'}\} = 2\delta_{ll'}, && c_l^2 = 1, \\ &\{b_l^\alpha, c_{l'}\} = 0. \end{aligned} \tag{2.4}$$

The physical spin operators are then expressed in terms of the Majorana fermions as $\sigma_l^\alpha = i b_l^\alpha c_l$. From this expression and the relations in Eq. (2.4), certain properties of the spin operators can be immediately recovered: $[\sigma_l^\alpha, \sigma_{l'}^{\alpha'}] = 0$ for $l \neq l'$, $\{\sigma_l^\alpha, \sigma_l^{\alpha'}\} = 0$ for $\alpha \neq \alpha'$, and $(\sigma_l^\alpha)^2 = 1$.

Since complex fermions are more straightforward to understand than Majorana fermions, it is useful to construct complex fermions by pairing up the Majorana

fermions. Each Majorana fermion b_l^α belongs to an end of a bond, and the standard choice is to pair up the ones that belong to the two ends of the same bond. For each site $l \in A$, three complex bond fermions are then obtained as

$$\chi_l^\alpha = \frac{1}{2}\left[b_l^\alpha - ib_{\alpha(l)}^\alpha\right], \qquad (\chi_l^\alpha)^\dagger = \frac{1}{2}\left[b_l^\alpha + ib_{\alpha(l)}^\alpha\right]. \tag{2.5}$$

Each Majorana fermion c_l belongs to a site, and the standard choice is to pair up the ones that belong to any two sites connected by a z bond. In terms of $c_{l,A} \equiv c_l$ and $c_{l,B} \equiv c_{z(l)}$ that are defined for each site $l \in A$, one complex matter fermion is then obtained for each pair of sites as

$$f_l = \frac{1}{2}\left(c_{l,A} + ic_{l,B}\right), \qquad f_l^\dagger = \frac{1}{2}\left(c_{l,A} - ic_{l,B}\right). \tag{2.6}$$

The state of the bond fermion χ_l^α can be measured with the bond fermion operator $ib_l^\alpha b_{\alpha(l)}^\alpha = 1 - 2(\chi_l^\alpha)^\dagger\chi_l^\alpha$, while the state of the matter fermion f_l can be measured with the matter fermion operator $-ic_{l,A}c_{l,B} = 1 - 2f_l^\dagger f_l$. In particular, we say that a bond (matter) fermion is excited if its bond (matter) fermion operator takes an eigenvalue -1 rather than $+1$.

When expressed in terms of the Majorana fermions, the Hamiltonian in Eq. (2.1) takes the quartic form

$$H_{\hat{u}} = i\sum_{l\in A}\sum_{\alpha=x,y,z} J_\alpha \hat{u}_{l,\alpha(l)} c_l c_{\alpha(l)}, \tag{2.7}$$

where the $3N$ bond fermion operators $\hat{u}_{l,\alpha(l)} \equiv ib_l^\alpha b_{\alpha(l)}^\alpha$ are commuting non-dynamic observables because they commute with each other as well as with the Hamiltonian $H_{\hat{u}}$. This means that the different bond fermion sectors characterized by distinct eigenvalues (± 1) of the bond fermion operators can be considered independently. On the other hand, the Hamiltonian $H_{\hat{u}}$ is quadratic and hence exactly solvable in each bond fermion sector $\{u_{l,\alpha(l)} \equiv \langle\hat{u}_{l,\alpha(l)}\rangle = \pm 1\}$. If the Majorana fermions c_l corresponding to the two sublattices are incorporated into two vectors $c_{A,B}$ with elements $(c_A)_l = c_{l,A}$ and $(c_B)_l = c_{l,B}$, the Hamiltonian in Eq. (2.7) becomes

$$H_u = ic_A^T \cdot M \cdot c_B, \qquad M_{ll'} = u_{l,z(l')} J_{\alpha_{l,z(l')}}, \tag{2.8}$$

where $J_{\alpha_{l,z(l')}} = 0$ if l and $z(l')$ are not neighbors. The matrix M has a singular value decomposition $M = U \cdot S \cdot V^T$, where S is a positive-semidefinite diagonal matrix, while U and V are real orthogonal matrices. We assume in the following that the singular values $S_k \equiv S_{kk}$ are in an increasing order such that $0 \leq S_1 \leq S_2 \leq \ldots \leq S_N$. The orthogonal matrices U and V give a new set of Majorana fermions as

$$\gamma_{k,A} = \sum_{l \in A} U_{lk} c_{l,A}, \qquad \gamma_{k,B} = \sum_{l \in A} V_{lk} c_{l,B}, \tag{2.9}$$

and the corresponding complex matter fermions become

$$\phi_k = \frac{1}{2}\left(\gamma_{k,A} + i\gamma_{k,B}\right), \qquad \phi_k^\dagger = \frac{1}{2}\left(\gamma_{k,A} - i\gamma_{k,B}\right). \tag{2.10}$$

In terms of these new matter fermions ϕ_k, the Hamiltonian in Eq. (2.8) takes the quadratic free-fermion form

$$H_\phi = \sum_{k=1}^{N} S_k \left(2\phi_k^\dagger \phi_k - 1\right). \tag{2.11}$$

The ground-state energy in the given bond fermion sector is then $-\sum_k S_k$, and the elementary excitations are the free matter fermions ϕ_k with excitation energies $2S_k$.

It is important to understand the relation between the commuting non-dynamic observables in the physical spin picture and the Majorana fermion picture: the loop operators and the bond fermion operators, or equivalently, the flux sectors and the bond fermion sectors. When expressed in terms of the Majorana fermions, the loop operators W_C take the form

$$W_C = b_1^{\alpha_{1,2}} b_2^{\alpha_{1,2}} b_2^{\alpha_{2,3}} b_3^{\alpha_{2,3}} \ldots b_L^{\alpha_{L,1}} b_1^{\alpha_{L,1}} = \hat{u}_{1,2}\hat{u}_{3,2}\hat{u}_{3,4}\hat{u}_{5,4}\ldots\hat{u}_{L-1,L}\hat{u}_{1,L}, \tag{2.12}$$

and in particular, the plaquette operators W_P become

$$W_P = \hat{u}_{1,2}\hat{u}_{3,2}\hat{u}_{3,4}\hat{u}_{5,4}\hat{u}_{5,6}\hat{u}_{1,6}. \tag{2.13}$$

These expressions show that the non-dynamic observables in the physical spin picture are uniquely determined by those in the Majorana fermion picture. However, the converse can not be true because there are $3N$ bond fermion operators in the Majorana

fermion picture for only $N+1$ loop operators in the physical spin picture. In fact, there is a gauge transformation $D_l \equiv b_l^x b_l^y b_l^z c_l$ for each site l that flips three bond fermions but does not flip any loops. This means that the bond fermion sectors before and after the gauge transformation correspond to the same flux sector. Since $D \equiv \prod_l D_l$ does not flip any bond fermions, there are $2N-1$ independent gauge transformations D_l, and the discrepancy between the numbers of non-dynamic observables in the two pictures is therefore explained.

The gauge redundancy in the Majorana fermion picture follows from an enlarged Hilbert space with respect to the physical spin picture. In particular, the Hilbert space of a single site is 4 dimensional in the Majorana fermion picture and only 2 dimensional in the physical spin picture. This discrepancy is consistent with the fact that the spin identity $-i\sigma_l^x\sigma_l^y\sigma_l^z \equiv 1$ in the physical spin picture translates into the gauge constraint $D_l = +1$ in the Majorana fermion picture. In fact, all the states in the Majorana fermion picture that are related to each other by gauge transformations D_l are equivalent descriptions of the same state in the physical spin picture. This physical state can be obtained from any of the gauge-related states by a projection onto the subspace with $D_l = +1$ for all l. The corresponding projection operator takes the form

$$\mathcal{P} = \prod_l \left(\frac{1 + D_l}{2} \right) = \mathcal{P}' \left(1 + D \right), \tag{2.14}$$

where $\mathcal{P}'$ contains all terms in $\mathcal{P}$ that flip bond fermions in inequivalent ways [43]. Since $D = (-1)^{N_\chi + N_f}$ when expressed in terms of the bond fermion number $N_\chi \equiv \sum_\alpha \sum_{l \in A} (\chi_l^\alpha)^\dagger \chi_l^\alpha$ and the matter fermion number $N_f \equiv \sum_{l \in A} f_l^\dagger f_l$, any states with odd total fermion number are projected to zero. There is a resulting global constraint for physical states: the total fermion number $N_\chi + N_f$ must be even. In each bond fermion sector with an even (odd) number of excited bond fermions, the number of excited matter fermions also must be even (odd). This means that only $N-1$ matter fermions can be excited independently from each other. The original $2N$ spin degrees of freedom are then fully recovered via the identification of the $2N$ natural degrees of freedom in the model: the $N+1$ fluxes and the $N-1$ fermions.

2.1.4 Ground state and excitations

The exact solution of the model provides a simple procedure for identifying its ground state [39]. Each flux sector can be considered individually and represented with one of its corresponding bond fermion sectors. The ground state in the flux sector is then projected from that in the bond fermion sector (see Sec. 2.1.3), and the overall ground state is the lowest lying of all these individual ground states. Furthermore, it can be shown using translational invariance that the ground state is in the trivial flux sector: the one in which $W_P = +1$ for all plaquettes [75]. The ground-state energy Γ_0 is then $-\sum_k S_k$ as obtained from the matrix M in Eq. (2.8) using the trivial bond fermion sector: the one in which $u_{l,\alpha(l)} = +1$ for all bonds. Note that there are in principle four trivial flux sectors corresponding to the topological eigenvalues $W_{X,Y} = \pm 1$ and that this leads to the existence of four degenerate ground states. However, the topological degrees of freedom are impossible to excite locally, and therefore we neglect them by considering only the trivial topological sector with $W_X = W_Y = +1$. This means that the effective number of degrees of freedom is reduced to $2N - 2$.

It is also revealed by the exact solution that the elementary excitations above the ground state are plaquettes (fluxes) and fermions [39]. We say that a plaquette P is excited (carries a flux) if its plaquette operator W_P takes an eigenvalue -1 rather than $+1$. In the presence of flux excitations, the flux sector can no longer be represented with the trivial bond fermion sector, and the energy $-\sum_k S_k$ is larger than Γ_0. This difference translates into a finite flux excitation energy. Note that fluxes can only be excited pairwise due to the global constraint $\prod_P W_P = 1$. The matter fermion excitations ϕ_k have excitation energies $E_k \equiv 2S_k$, and by considering the distribution of these energies, two distinct phases of the model can be identified. In the gapless phase with $J_z < J_x + J_y$, the smallest excitation energies E_k vanish in the thermodynamic limit. In the gapped phase with $J_z > J_x + J_y$, the excitation energies E_k are all finite in the thermodynamic limit. Note that fermions can only be excited pairwise due to the global constraint that $N_\chi + N_f$ must be even.

2.2 Gapped phase of the model

From this point until the end of the fourth chapter, we restrict our attention to the gapped phase of the Kitaev honeycomb model, where the coupling strengths satisfy $J_x + J_y < J_z$. Since all fluxes and fermions have finite excitation energies, the ground state in this phase is separated from the excited states by a finite energy gap. For simplicity, we measure all energies in units of the largest coupling strength $J_z = 1$ and choose the two smaller coupling strengths $J_{x,y}$ to be equal. The model is then parameterized by the dimensionless coupling strength $J \equiv J_x = J_y < 1/2$.

2.2.1 Isolated dimer limit

When considering the gapped phase, it is useful to start any discussion in the isolated dimer limit of $J = 0$. In this limit, the model separates into N isolated (non-interacting) spin dimers along z bonds [76]. Since the two spins in any dimer are coupled by a ferromagnetic Ising term $-\sigma_l^z \sigma_{z(l)}^z$, they must be either both up or both down in the ground state. However, there is still an exponentially large ground-state degeneracy as each dimer can choose from two configurations. This degeneracy can then be lifted by applying a perturbation theory in the dimensionless coupling strength $J \ll 1$ [74]. At fourth order in J, the projection of the Hamiltonian in Eq. (2.1) onto the degenerate ground-state subspace is

$$\tilde{H}_\sigma = -N - \tilde{C}(N, J) - \frac{J^4}{16} \sum_P W_P. \tag{2.15}$$

The first term is the ground-state energy at $J = 0$ and the remaining terms are the perturbative corrections: the constant term $\tilde{C}(N, J)$ shifts the energy of the entire subspace, while the last term lifts the ground-state degeneracy by specifying the ground-state flux sector. In accordance with Sec. 2.1.4, the actual ground state has $W_P = +1$ for all plaquettes.

It is instructive to write this ground state $|\Omega\rangle$ in terms of both the physical spins and the Majorana fermions. In the physical spin picture, it can be obtained by a projection from any state with $\sigma_l^z \sigma_{z(l)}^z = +1$ for all dimers onto the subspace with

$W_P = +1$ for all plaquettes. For example, by projecting from the all-spins-up state $|\Uparrow\rangle$, the ground state becomes

$$|\Omega\rangle = \prod_P \left(\frac{1 + W_P}{2} \right) |\Uparrow\rangle. \tag{2.16}$$

In the Majorana fermion picture, the trivial flux sector is represented with the trivial bond fermion sector, and the matrix M in Eq. (2.8) is the unit matrix. Since the free matter fermions ϕ_k in Eq. (2.10) are then identical to the original matter fermions f_l in Eq. (2.6), the ground state is the vacuum of the bond fermions and the original matter fermions. Formally, this vacuum state $|0\rangle$ is defined by $\chi_l^\alpha |0\rangle = 0$ and $f_l |0\rangle = 0$ for all l and α. The physical ground state in Eq. (2.16) is then $|\Omega\rangle = \mathcal{P}|0\rangle$.

The excitations above the ground state can be discussed in a similar manner. The flux excitations are obtained by projecting onto a subspace with excited plaquettes $W_P = -1$ in the physical spin picture and by exciting an appropriate set of bond fermions in the Majorana fermion picture. Due to the presence of the gauge transformations D_l, it is possible to represent any flux sector with a bond fermion sector in which only x and y bond fermions are excited. Since the matrix M in Eq. (2.8) does not depend on these bond fermions for $J = 0$, we recover the result in Eq. (2.15) that the flux excitation energies $E_P \sim J^4$ vanish when $J \to 0$. The fermion excitations are obtained by projecting from a state with broken dimers $\sigma_l^z \sigma_{z(l)}^z = -1$ in the physical spin picture and by exciting the corresponding matter fermions in the Majorana fermion picture. Since $u_{l,z(l)} = +1$ for all dimers when only x and y bond fermions are excited, the relation $\sigma_l^z \sigma_{z(l)}^z = \hat{u}_{l,z(l)}(1 - 2 f_l^\dagger f_l)$ shows that excited matter fermions indeed correspond to broken dimers. Furthermore, it follows from both pictures that these fermion excitations all have exactly the same energy $E_f = 2$.

It is a conceptual problem that we require $J > 0$ for a finite plaquette excitation energy but $J = 0$ for the presence of the isolated dimers. In fact, since the localized matter fermions at $J = 0$ all have the same excitation energy, even an infinitesimally small perturbation $J \ll 1$ is enough to delocalize them across the entire lattice and have them form a band of a small width $\Delta E_f \sim J$. This implies that the free (delocalized) matter fermions ϕ_k and the original (localized) matter fermions f_l are

entirely different for any $J > 0$. To obtain the ground state at $J > 0$, the vacuum state $|0\rangle$ is then projected onto the subspace where no free matter fermions ϕ_k are excited. Using this method, the physical ground state takes the form

$$|\Omega\rangle = \mathcal{P} \prod_{k=1}^{N} \left(\phi_k \phi_k^\dagger \right) |0\rangle. \tag{2.17}$$

Although the perturbation mixes the various creation operators, and consequently, the various annihilation operators together, it does not significantly mix the creation operators with the annihilation operators. This implies that the $J > 0$ ground state in Eq. (2.17) is close to the $J = 0$ ground state $\mathcal{P}|0\rangle$ and can be described faithfully in terms of the localized matter fermions. We therefore often simultaneously assume a finite plaquette excitation energy and localized matter fermions, always mentioning when the perturbative interactions between the matter fermions are important.

2.2.2 Global constraints and superselection sectors

The numbers of independent flux and fermion excitations are limited by two essential global constraints. In the physical spin picture, these two constraints can be obtained by noticing that the product of all plaquette operators W_P corresponding to plaquettes in even (η) stripes, or alternatively, plaquettes in odd (μ) stripes is equivalent to the product of all dimer operators $\lambda_l \equiv \sigma_l^z \sigma_{z(l)}^z$. Mathematically, these two relations are

$$\prod_{P \in \eta} W_P = \prod_{P \in \mu} W_P = \prod_{l \in A} \lambda_l. \tag{2.18}$$

Since the W_P and the λ_l are all $\mathbb{Z}_2$ variables, the first equality recovers the global constraint $\prod_P W_P = 1$, while the second equality becomes $\prod_{l \in A} \lambda_l \prod_{P \in \mu} W_P = 1$. In the Majorana fermion picture, the first equality is automatically satisfied because $\hat{u}_{l,\alpha(l)}^2 = 1$ for all bonds. The second equality can be understood by noticing that an excited z bond fermion corresponds to two excited plaquettes that are either both in an even stripe or both in an odd stripe while an excited x or y bond fermion corresponds to one excited plaquette in an even stripe and one excited plaquette in an odd stripe. Since this property translates into $\prod_{P \in \mu} W_P = (-1)^{N_{\chi^x} + N_{\chi^y}}$ and the

relation $\lambda_l = \hat{u}_{l,z(l)}(1 - 2f_l^\dagger f_l)$ implies $\prod_{l\in A}\lambda_l = (-1)^{N_{\chi^z}+N_f}$, the second equality recovers the global constraint that $N_\chi + N_f$ must be even.

There is an alternative formulation of the global constraints given in Eq. (2.18) where one electric (magnetic) charge e (m) is assigned to each excited plaquette in an even (odd) stripe and one from both charges e and m is assigned to each broken dimer. The global constraints in this formulation are that the total numbers of electric charges (N_e) and magnetic charges (N_m) both must be even [39]. In particular, if there are isolated clusters of excitations in the lattice, each of them can be classified into four superselection sectors based on the types of unpaired charges it contains: trivial (1), electric (e), magnetic (m), and combined ($\epsilon \equiv e \times m$). When different clusters are combined, the superselection sector of the combined cluster is given by the fusion rules in Table 2.1. Using this language, the global constraints mean that the combination of all clusters belongs to the trivial superselection sector 1.

	1	e	m	ϵ
1	1	e	m	ϵ
e	e	1	ϵ	m
m	m	ϵ	1	e
ϵ	ϵ	m	e	1

Table 2.1: Fusion rules governing the combination of superselection sectors when different excitation clusters are combined.

The most important property of the superselection sectors is that they are robust against arbitrary local perturbations. Since a local perturbation acts only within one excitation cluster, it could only change the superselection sector of the cluster by also violating at least one global constraint. The superselection sector of an excitation cluster can then only be changed by a non-local perturbation that also changes the superselection sector of a different cluster or creates an additional cluster with a non-trivial superselection sector.

Chapter 3

Individual holes in the gapped phase

In this chapter, we consider the gapped phase of the Kitaev honeycomb model, and aim to characterize the properties of individual mobile holes. We are primarily interested in the internal degrees of freedom possessed by these holes and their manifestations in single-particle behavior such as hopping properties and particle statistics. Since the model remains exactly solvable in the presence of stationary holes [73, 74] and the bulk excitations are not excited by a mobile hole if its bare hopping amplitude is much smaller than the bulk energy gap, the hole propagation can be described by effective hopping amplitudes between the exact ground states of the model with stationary holes at different positions.

The structure of this chapter is summarized as follows. In Sec. 3.1, we introduce the formalism for describing holes in the model, and discuss the internal degrees of freedom possessed by these holes. Our main result is that each hole has three internal quantum numbers: the first two quantum numbers describe binding between the hole and the fractional excitations (fluxes and fermions) of the model, while the third quantum number determines the local magnetization around the hole. Since the first two quantum numbers encode fractional properties, they are robust against local perturbations, but they can be exchanged by holes that are close to one another. In Sec. 3.2, we introduce the formalism for describing hole hopping, and discuss the properties of mobile holes in the model. Our main result is that the different hole

types characterized by different quantum numbers and hence different excitations bound are fundamentally distinct in terms of their hopping properties and particle statistics [77, 78]. For example, some hole types are free to hop in two dimensions, while others are confined to hop in only dimension only.

3.1 Stationary holes

3.1.1 Description of holes

We introduce n holes into the Kitaev honeycomb model by removing the spin one-half particles from n sites of the honeycomb lattice. For the model with $n > 0$ holes, the exact solution in Sec. 2.1 is still applicable, but it must be performed in a different way because there are no Majorana fermions at the hole sites [73, 74]. It is then not clear how to construct complex fermions from the remaining Majorana fermions, and the bond fermion operators, or equivalently, the plaquette operators acting on the hole sites become ill-defined.

To fix this problem, we use an alternative description: the spin one-half particles are not actually removed from the hole sites, but only their Ising couplings with their neighbors are switched off. This way, we obtain 2^n copies of the original model that correspond to the different configurations of the n non-interacting hole spins. Since there are still Majorana fermions at all sites, the bond fermion operators and the plaquette operators remain well-defined. This means that the exact solution can be performed in exactly the same way as in Sec. 2.1. However, there is an additional 2^n-fold degeneracy due to the presence of the non-interacting hole spins, which is unphysical and hence must be discarded.

Formally, we can demand all hole spins to be in the spin-up state: $\sigma_l^z = +1$ for all sites $l \in \Delta$, where Δ is the set of hole sites. To obtain a physical state, we then must use the appropriate projection operator, which takes the form

$$\mathcal{Q}_\Delta = \prod_{l\in\Delta} \left(\frac{1+\sigma_l^z}{2} \right) = \prod_{l\in\Delta} \left(\frac{1+ib_l^z c_l}{2} \right). \tag{3.1}$$

Note that the treatment of the unphysical hole spins is completely analogous to the

treatment of the unphysical Majorana fermions. In the Majorana fermion picture, different states corresponding to the same state in the physical spin picture are related by gauge transformations D_l. We can work in different gauges and then use the projector $\mathcal{P}$ to enforce the constraint $D_l = +1$ at all sites. In the hole spin picture, different states corresponding to the same state in the actual hole picture are related by gauge transformations $\sigma^z_{l\in\Delta}$. We can work in different gauges and then use the projector $\mathcal{Q}_\Delta$ to enforce the constraint $\sigma^z_l = +1$ at all hole sites.

3.1.2 Internal degrees of freedom

We now investigate how the excitations above the ground state as discussed in Sec. 2.1.4 are affected by the introduction of $n > 0$ holes into the model. Since each hole corresponds to one fewer spin degree of freedom and the topological degrees of freedom are neglected, the total number of $\mathbb{Z}_2$ degrees of freedom (modes) is $2N - n - 2$. We restrict our attention to the thermodynamic limit of $N_{X,Y} \to \infty$ and assume that the holes in the model are isolated such that the smallest distance between any two holes is $R \gg 1$.

In the presence of $n > 0$ holes, we distinguish two types of plaquettes: hole plaquettes that contain one hole site each and bulk plaquettes that contain no hole sites. Each hole site $l \in \Delta$ is contained by three plaquettes $P_l^{x,y,z}$ whose corresponding plaquette operators $W_{P_l^{x,y,z}}$ act on the hole site with $\sigma_l^{x,y,z}$, respectively. The number of hole plaquettes is therefore $3n$ and the number of bulk plaquettes is $N - 3n$. From a perturbation theory in $J \ll 1$, there is a finite excitation energy $E_P \sim +J^4$ for bulk plaquettes and no excitation energy for hole plaquettes. However, at each hole site $l \in \Delta$, there is a finite excitation energy $E_Q \sim -J^8$ for the hole loop Q_l surrounding all three hole plaquettes. The negative excitation energy $E_Q < 0$ means that the hole loop operators W_{Q_l} preferentially take eigenvalues -1 in the ground state [73, 74]. More precisely, since the global constraint $\prod_P W_P = 1$ translates into $\prod_{l\in\Delta} W_{Q_l} = 1$ when no bulk plaquettes are excited, the hole loop operator W_{Q_l} is -1 for all hole sites when n is even and for all but one hole sites when n is odd.

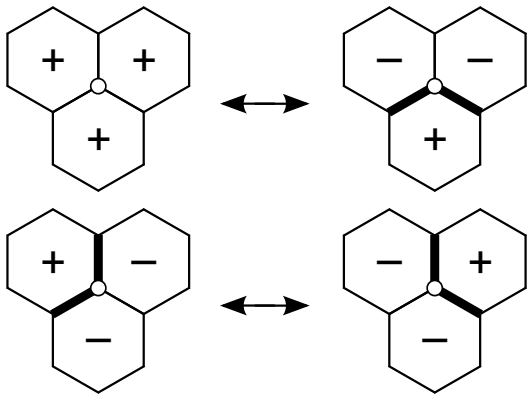

Figure 3.1: Simultaneous gauge transformations D_l and σ_l^z relating the bond fermion sectors around a hole site $l \in \Delta$ (white dot) when there is no flux bound to the hole. Each bond fermion sector is labeled with the excited bond fermions (thick lines) and the corresponding plaquette operator eigenvalues (± 1). Our convention is to consider only the two bond fermion sectors on the left.

Since the hole loop operator is $W_{Q_l} = W_{P_l^x} W_{P_l^y} W_{P_l^z}$ in terms of the individual hole plaquette operators, we say that the hole at site l has a flux bound to it if its hole loop operator W_{Q_l} takes an eigenvalue -1 rather than $+1$. This relation also suggests that each hole has a hole flux mode Q_l with a finite excitation energy and two independent hole plaquette modes $P_l^{x,z}$ with zero excitation energies. In fact, there is one fewer hole plaquette mode due to the presence of the unphysical hole spin: the four plaquette sectors corresponding to $W_{P_l^{x,z}} = \pm 1$ in the hole spin picture are pairwise related by the gauge transformation σ_l^z, and the corresponding bond fermion sectors in the Majorana fermion picture are pairwise related by the gauge transformations D_l and σ_l^z. These gauge transformations are illustrated in Fig. 3.1. In the following, we use the convention in which the two remaining bond fermion sectors are related to each other by the operator $ib_l^x b_l^z$ flipping the x and the z bond fermions around the hole site l. When there is no flux bound to the hole, this means that the two remaining plaquette sectors with $W_{P_l^y} = +1$ are distinguished by $W_{P_l^x} = W_{P_l^z} = \pm 1$. In conclusion, if the model contains $n > 0$ holes, there are $N - 3n$ bulk plaquette (flux) modes with excitation energies $E_P \sim J^4$, there are $n - 1$ hole flux modes with excitation energies $E_Q \sim J^8$, and there are n hole plaquette modes

with zero excitation energies. Note that the number of independent hole flux modes is reduced by 1 due to the global constraint $\prod_P W_P = 1$.

In the presence of $n > 0$ holes, we distinguish two types of fermions: hole fermions and bulk fermions. When $J = 0$, hole fermions are localized at dimers that contain one hole site each, while bulk fermions are localized at dimers that contain no hole sites. Since the bulk dimers have Ising couplings $-\sigma_l^z \sigma_{z(l)}^z$, there is a finite excitation energy $E_f = 2$ for the bulk fermions. However, since the Ising couplings of the hole dimers are switched off, there is no excitation energy for the hole fermions. When $J > 0$, the bulk fermions delocalize across the entire lattice (see Sec. 2.2.1), but the hole fermions remain localized at their holes. More precisely, each hole fermion wave function forms a wedge of opening angle $\pi/3$ around its hole and its amplitude decays exponentially with distance [74]. Since there is one hole fermion for each hole, there are $N-n$ bulk fermion modes with excitation energies $E_f \sim 1$, and there are $n-1$ hole fermion modes with zero excitation energies. Note that the number of independent hole fermion modes is reduced by 1 due to the global constraint that $N_\chi + N_f$ must be even for physical states.

Mode type	Excitation energy	Number of modes	Quantum number	Global constraint
Bulk fermion	~ 1	$N - n$		
Bulk flux	$\sim J^4$	$N - 3n$		
Hole flux	$\sim J^8$	$n - 1$	$h = \{0, 1\}$	$\sum_j h_j = \text{even}$
Hole fermion	0	$n - 1$	$q = \{0, 1\}$	$\sum_j q_j = \text{even}$
Hole plaquette	0	n	$p = \{0, 1\}$	

Table 3.1: Energy hierarchy of independent $\mathbb{Z}_2$ modes in the model with $n > 0$ holes. For the internal modes, the corresponding quantum numbers are also specified along with any global constraints on them.

The independent $\mathbb{Z}_2$ modes of the model with $n > 0$ holes are summarized in Table 3.1. We distinguish two classes of modes depending on their excitation energies and the scaling of their numbers with N and n. The bulk fluxes and the bulk fermions are external (bulk) modes: they have large excitation energies $E \gtrsim J^4$ and their numbers scale with the system size N. These modes are extremely hard to treat

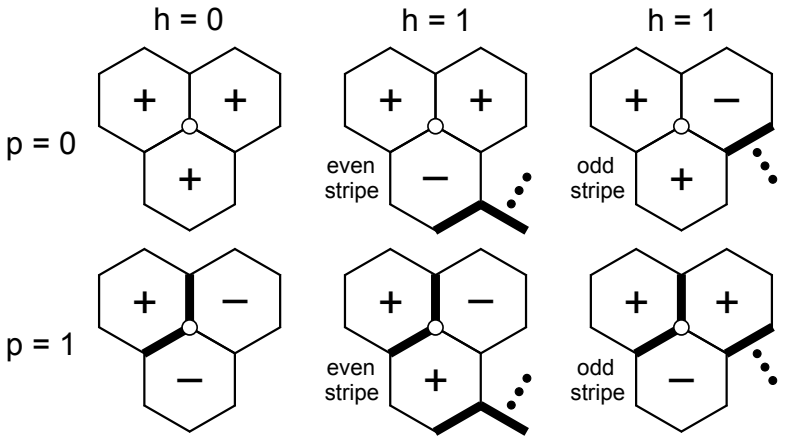

Figure 3.2: Bond fermion sectors around a hole site $l \in \Delta$ (white dot) for different combinations of the flux quantum number $h = \{0, 1\}$ and the plaquette quantum number $p = \{0, 1\}$. Each bond fermion sector is labeled with the excited bond fermions (thick lines) and the corresponding plaquette operator eigenvalues (± 1). For $h = 1$, there are two cases depending on whether P_l^z is in an even stripe or in an odd stripe. The triple dots indicate a string of excited bond fermions connecting two holes with $h = 1$.

in the thermodynamic limit. Conversely, the hole fluxes, the hole fermions, and the hole plaquettes are internal modes: they have small excitation energies $E \lesssim J$[8] and their numbers scale with the hole number n. Since these modes are associated with individual holes, it is straightforward to treat them in the limit when the holes are isolated. Due to the different energy scales of the two classes of modes, we can self-consistently neglect the excitations in the high-energy bulk modes, and concentrate only on the low-energy internal modes.

Each hole in the model has three internal modes, and we characterize these three internal modes with three $\mathbb{Z}_2$ quantum numbers h, q, and p. The flux quantum number is $h = 1$ if the hole has a flux bound to it and $h = 0$ otherwise. The fermion quantum number is $q = 1$ if the corresponding hole fermion is excited and $q = 0$ otherwise. The meaning of the plaquette quantum number p depends on the flux quantum number: if $h = 0$, then $p = 0$ means no hole plaquette excitations and $p = 1$ means two hole plaquette excitations in two neighboring stripes, while if $h = 1$, then $p = 0$ means one hole plaquette excitation in an even stripe and $p = 1$ means one hole plaquette excitation in an odd stripe. The corresponding bond fermion sectors are

shown in Fig. 3.2. Importantly, the distinction between even and odd stripes ensures that N_χ is always even. In the case of n holes labeled $j = \{1, 2, \ldots, n\}$, there are $3n$ internal modes characterized by $3n$ quantum numbers h_j, q_j, and p_j. Since fluxes and fermions can only be excited pairwise, the quantum numbers h_j and q_j are not fully independent from each other. In particular, the global constraint $\prod_P W_P = 1$ translates into $\sum_j h_j = $ even, while the global constraint that $N_\chi + N_f$ is even, or equivalently, that N_f is even translates into $\sum_j q_j = $ even. The various formulations of these two global constraints are presented in Table 3.2.

	Flux constraint	Fermion constraint
Physical spins	$\prod_P W_P = 1$	$\prod_{l\in A} \lambda_l \prod_{P\in\mu} W_P = 1$
Majorana fermions	Automatically satisfied	$N_\chi + N_f = $ even
E / M charges	$N_e + N_m = $ even	$N_m = $ even
Quantum numbers	$\sum_j h_j = $ even	$\sum_j q_j = $ even

Table 3.2: Formulations of the two essential global constraints in terms of the physical spins, the Majorana fermions, the electric / magnetic charges, and the internal quantum numbers.

We are now ready to write down the ground states $|\Omega^{\Delta}_{h,q,p}\rangle$ that correspond to the different values of the internal quantum quantum numbers. Using the method of Sec. 2.2.1, each ground state is obtained from the vacuum state $|0\rangle$ by a projection onto an appropriate subspace. Formally, the physical ground state for $n > 0$ holes at sites $\Delta = \{l_j\}$ with quantum numbers $h \equiv \{h_j\}$, $q \equiv \{q_j\}$, and $p \equiv \{p_j\}$ reads as

$$|\Omega^{\Delta}_{h,q,p}\rangle = \mathcal{Q}_\Delta \mathcal{P} \mathcal{F}_{q;h} \mathcal{B}_p \mathcal{X}_h |0\rangle. \tag{3.2}$$

Before enforcing the gauge constraints with the projection operators $\mathcal{P}$ and $\mathcal{Q}_\Delta$, the vacuum state $|0\rangle$ is acted upon by several operators setting the bond fermion and the matter fermion sectors. The first operator $\mathcal{X}_h$ is responsible for binding fluxes to all holes with $h_j = 1$. Mathematically, $\mathcal{X}_h$ is an appropriate product of $(\chi^\alpha_l)^\dagger$ operators along a set of strings connecting the holes with $h_j = 1$ pairwise. Note that the global constraint $\sum_j h_j = $ even ensures that the holes with $h_j = 1$ can always be paired up. Importantly, we choose $\mathcal{X}_h$ such that it does not excite any z bond fermions and creates the excited plaquette in an even stripe for each hole (see Fig. 3.2). In this

case, $\mathcal{X}_h$ is a product of an even number of $(\chi_l^\alpha)^\dagger$ operators, and therefore it excites an even number of bond fermions. The remaining two operators in Eq. (3.2) are

$$\begin{aligned} \mathcal{B}_p &= \prod_{j=1}^{n} \left(i b_{l_j}^x b_{l_j}^z \right)^{p_j}, \\ \mathcal{F}_{q;h} &= \prod_{k=n+1}^{N} \left(\phi_k \phi_k^\dagger \right) \prod_{j=1}^{n} \left(\phi_j^{1-q_j} \phi_j^\dagger \phi_j^{q_j} \right) \prod_{j=1}^{n} \left[f_{\tilde{z}(l_j)}^\dagger \right]^{q_j}, \end{aligned} \tag{3.3}$$

where $\tilde{z}(l) = l$ if $l \in A$ and $\tilde{z}(l) = z(l)$ if $l \in B$. The operator $\mathcal{B}_p$ sets the bond fermion sector by flipping an even number of bond fermions around the hole sites, while the operator $\mathcal{F}_{q;h}$ projects onto one of the ground states in the given bond fermion sector. The original matter fermions $f_{\tilde{z}(l_j)}^\dagger$ are required only to ensure that $\mathcal{F}_{q;h}$ does not project to zero in the isolated dimer limit. The free matter fermions ϕ_k are obtained from the matrix M in Eq. (2.8): there are n hole fermions ϕ_k with $1 \leq k \leq n$ that have zero energies and $N - n$ bulk fermions ϕ_k with $n + 1 \leq k \leq N$ that have finite energies $E_f \sim 1$. We label the hole fermions consistently such that the hole fermion ϕ_j is localized around the hole site l_j. Note that the matrix M is in general a function of the bond fermions excited by $\mathcal{X}_h$, and therefore $\mathcal{F}_{q;h}$ depends on the flux quantum numbers h_j via the free matter fermions ϕ_k. On the other hand, the bond fermions flipped by $\mathcal{B}_p$ correspond to bonds with switched-off interactions, and therefore $\mathcal{F}_{q;h}$ does not depend on the plaquette quantum numbers p_j.

Hole type		Superselection sector
$h = 0$	$q = 0$	Trivial (1)
	$q = 1$	Combined ($e \times m$)
$h = 1$	$q = 0$	Electric (e)
	$q = 1$	Magnetic (m)

Table 3.3: Superselection sectors of holes with flux quantum numbers $h = \{0, 1\}$ and fermion quantum numbers $q = \{0, 1\}$.

It is useful to interpret the internal quantum numbers in the isolated dimer limit. In this limit, the free matter fermions ϕ_k are identical to the original matter fermions f_l, and therefore the second operator in Eq. (3.3) takes the simplified form $\mathcal{F}_q \equiv$

$\mathcal{F}_{q;h} = \prod_{j=1}^{n} [f^{\dagger}_{\tilde{z}(l_j)}]^{q_j}$. Note that the matrix M is no longer a function of the x and y bond fermions excited by $\mathcal{X}_h$, and therefore $\mathcal{F}_q$ becomes independent of the flux quantum numbers h_j. For a single isolated hole at site l with quantum numbers h, q, and p, the hole dimer operator is then $\lambda_l = \sigma^z_l \sigma^z_{z(l)} = (-1)^{q+p}$. Since the product of the hole plaquette operators is $\prod_{P_l \in \eta} W_P = (-1)^{h+p}$ in even stripes and $\prod_{P_l \in \mu} W_P = (-1)^p$ in odd stripes, we conclude that the different combinations of the quantum numbers h and q are in one-to-one correspondence with the different superselection sectors that the hole can belong to. This correspondence is presented in Table 3.3. Note that if the bulk modes are not excited, isolated holes can indeed be thought of as isolated excitation clusters with well-defined superselection sectors. Furthermore, since the projection operator $\mathcal{Q}_\Delta$ enforces $\sigma^z_l = +1$ at the hole site l, there is a finite local magnetization $\sigma^z_{z(l)} = (-1)^{q+p}$ at the neighboring site $z(l)$ [74]. This magnetization can be reversed by applying the transformation $\sigma^{x,z} \to -\sigma^{x,z}$ to all spins except the hole spin. On the other hand, such a discrete spin rotation is also a symmetry of the model: it flips the hole plaquettes $P^{x,z}_l$ and changes the sign of the hole dimer operator λ_l. It therefore corresponds to a switch in the plaquette quantum number p only. To summarize, the flux and the fermion quantum numbers determine the superselection sector, while the plaquette quantum number determines the local magnetization around the hole. Importantly, these results are also valid in the case of $J > 0$ when $(-1)^{q+p}$ is equal to the product of dimer operators taken over a sufficiently large region around the hole site l.

3.1.3 Interactions and bound states

We now discuss the interactions between two holes at a finite distance R away from each other. In general, the ground-state energy is given by $\Gamma_0 = -\sum_k S_k$, where the N singular values S_k are obtained from the matrix M in Eq. (2.8). In the limit of $R \to \infty$, there are two vanishing singular values $S_1 = S_2 = 0$ corresponding to the two hole fermions, and the ground-state energy $\Gamma_0(\infty)$ is determined by the sum of the remaining $N - 2$ non-vanishing singular values. When R is finite, the interaction

energy between the two holes is defined as the change in the ground-state energy with respect to that in the $R \to \infty$ limit: $\Delta\Gamma_0 \equiv \Gamma_0(R) - \Gamma_0(\infty)$.

The interaction energy $\Delta\Gamma_0$ has two contributions arising from two distinct interaction mechanisms. First, the sum of the $N-2$ non-vanishing singular values is changed by perturbative terms similar to those in Eq. (2.15). Second, the singular value S_2 also becomes non-vanishing due to a hybridization between the two hole fermions [74]. The first contribution $\Delta\Gamma_0^{(1)}$ is non-zero for both sublattices and all directions, while the second contribution $\Delta\Gamma_0^{(2)}$ is non-zero only if the two holes are in opposite sublattices and their relative direction lies in the wedge of opening angle $\pi/3$ such that each hole fermion wave function has a finite amplitude at the hole site of the other hole (see Fig. 3.3). Importantly, the wedges for the two holes in the opposite sublattices point in opposite directions, and therefore this condition for the relative direction is identical from the point of view of both holes.

Since the two contributions decay as $\Delta\Gamma_0^{(1)} \sim J^{2R}$ and $\Delta\Gamma_0^{(2)} \sim J^R$ with the distance R, the second contribution is the dominant one at large distances. From the lowest-order perturbation theory in $J \ll 1$ around the isolated dimer limit, this contribution takes the general form

$$\Delta\Gamma_0^{(2)} = -\frac{R!}{R_x!R_y!}\, J^R, \tag{3.4}$$

where the string of shortest length $R \equiv R_x + R_y$ connecting the two holes contains R_x bonds of x type and R_y bonds of y type [74]. The first contribution can also be calculated from a perturbation theory in $J \ll 1$, but its general form is more complicated. In particular, $\Delta\Gamma_0^{(1)}$ can take both signs: the largest negative result $\Delta\Gamma_0^{(1)} = -J^2/4$ is found when the two holes are at nearest-neighbor sites connected by an x or a y bond, while the largest positive result $\Delta\Gamma_0^{(1)} = J^2/4$ is found when the two holes are at next-nearest-neighbor sites connected by a z bond and an x or a y bond. The interaction energy $\Delta\Gamma_0 = \Delta\Gamma_0^{(1)} + \Delta\Gamma_0^{(2)}$ is always positive when the two holes are in the same sublattice and always negative when the two holes are in opposite sublattices. The absolute values of these positive and negative interaction energies are plotted in Fig. 3.3.

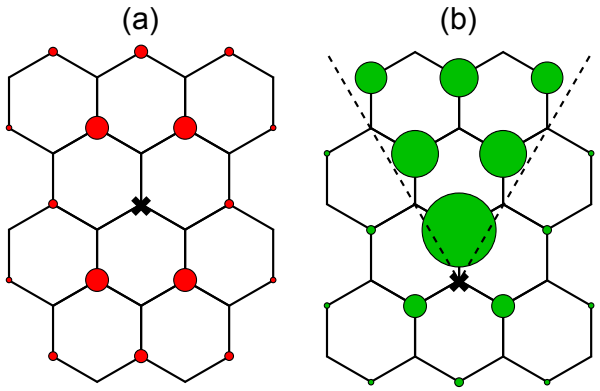

Figure 3.3: Absolute interaction energy $|\Delta\Gamma_0|$ between two holes as a function of their relative position when $J_z = 1.0$ and $J \equiv J_x = J_y = 0.2$. One hole is fixed (black cross) and the other one is moved (red and green dots). Each dot has an area proportional to $\sqrt{|\Delta\Gamma_0|}$. The interaction is either repulsive with $\Delta\Gamma_0 > 0$ (a) or attractive with $\Delta\Gamma_0 < 0$ (b). The wedge of opening angle $\pi/3$ is marked by a dashed line.

Importantly, the first interaction mechanism corresponding to $\Delta\Gamma_0^{(1)}$ is diagonal in the quantum numbers h, q, and p, while the second interaction mechanism corresponding to $\Delta\Gamma_0^{(2)}$ is diagonal only in h and p but not in q. In particular, if we set $h_{1,2} = p_{1,2} = 0$ for simplicity and label the remaining four ground states $|\Omega^{\Delta}_{h,q,p}\rangle$ with the fermion quantum numbers as $|q_1, q_2\rangle \equiv |\Omega_{q_1,q_2}\rangle$, the second interaction has identical matrix elements $\sim J^R$ between the states $|0,0\rangle$ and $|1,1\rangle$, and between the states $|0,1\rangle$ and $|1,0\rangle$. This implies that the eigenstates are in fact $(|0,0\rangle \pm |1,1\rangle)/\sqrt{2}$ and $(|0,1\rangle \pm |1,0\rangle)/\sqrt{2}$. In the strict sense, the fermion quantum numbers q are then no longer valid quantum numbers in the presence of hole interactions. However, since the interaction is exponentially small when the holes are far away from each other, they are still practically valid quantum numbers as they are conserved within an exponentially large timescale $\sim J^{-R}$.

Since the attractive interaction between holes in opposite sublattices is stronger than the repulsive interaction between holes in the same sublattice, the overall interaction between two holes is attractive. The most negative interaction energy $\Delta\Gamma_0 = -1$ is found when the two holes are at nearest-neighbor sites connected by a z bond. In the absence of other interactions, this attraction leads to pair formation, where the holes in the model form bound pairs along z bonds. It is then useful to investigate how these

hole pairs interact with each other. The interaction energy $\Delta\Gamma'_0 \equiv \Gamma'_0(R) - \Gamma'_0(\infty)$ between two hole pairs is completely analogous to that between two single holes. In this case, there are two vanishing singular values for all distances R, and the only contribution to the interaction energy comes from the change in the remaining $N-2$ non-vanishing singular values. From a perturbation theory around the isolated dimer limit, we obtain that the interaction energy between two hole pairs is always negative and decays as $\Delta\Gamma'_0 \sim J^{2R}$ with the distance R. The most negative interaction energy $\Delta\Gamma'_0 = -J^2/4$ is found when two holes from the respective hole pairs are at nearest-neighbor sites connected by an x or a y bond.

In the absence of other interactions, the attraction between hole pairs leads to phase separation, where the holes are all bound together to form a large cluster. However, both single holes and hole pairs are positively charged, and therefore they are also subject to a Coulomb repulsion. Since the attraction between single holes is stronger than that between hole pairs, we can distinguish three complementary regimes in the behavior of the model. If the Coulomb repulsion is weaker than the attraction between hole pairs, the model phase separates. If the Coulomb repulsion is stronger than the attraction between hole pairs but weaker than that between single holes, the elementary particles of the model are hole pairs. If the Coulomb repulsion is stronger than the attraction between single holes, the elementary particles of the model are single holes. In the rest of this thesis, we restrict our attention to single holes and implicitly assume a sufficiently strong Coulomb repulsion such that the model is in the appropriate regime.

3.1.4 Robustness against local perturbations

It is useful to discuss the applicability of the internal quantum numbers when a local perturbation is applied to the model with $n > 0$ holes. We first notice that two arguments are apparently in conflict with each other. On one hand, the quantum numbers q and h are expected to be robust against local perturbations as they are related to the superselection sectors of the model (see Secs. 2.2.2 and 3.1.2). On the

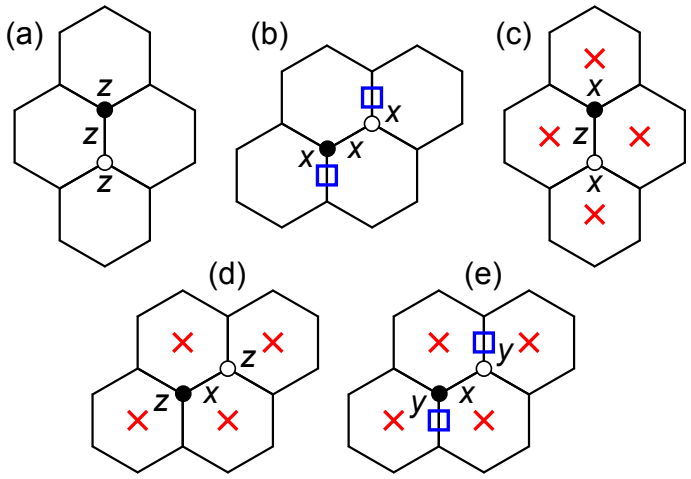

Figure 3.4: Effects of the Heisenberg terms $\sigma_l^z \sigma_{l'=z(l)}^z$ (a), $\sigma_l^x \sigma_{l'=x(l)}^x$ (b), $\sigma_l^x \sigma_{l'=z(l)}^x$ (c), $\sigma_l^z \sigma_{l'=x(l)}^z$ (d), and $\sigma_l^y \sigma_{l'=x(l)}^y$ (e) on the plaquettes and the dimers (fermions) around two neighboring sites l (white dot) and l' (black dot). Flipped plaquettes are marked by red crosses and flipped dimers are marked by blue rectangles.

other hand, the quantum numbers q are not strictly conserved in the presence of hole interactions (see Sec. 3.1.3). Note that the dimensionless coupling strength $J \ll 1$ is a local perturbation in the language of the isolated dimer limit.

The resolution of this apparent conflict is that local perturbations assemble into non-local strings at higher orders of perturbation theory. If two holes (excitation clusters) are connected by such a string, only the combined superselection sector is conserved, while the individual superselection sectors can change. However, when the two holes are at a distance R away from each other, such a string can be assembled only at R-th order of perturbation theory. For a local perturbation of strength δE that creates excitations with energies E_0, the perturbative term responsible for changing the superselection sector is then $\sim (\delta E/E_0)^R$. This means that the superselection sector is conserved within a timescale $\sim (E_0/\delta E)^R$ that is exponentially large when $\delta E \ll E_0$ and $R \gg 1$. Note that the interaction term $\sim J^R$ in Sec. 3.1.3 is recovered as a special case with $\delta E \sim J$ and $E_0 \sim 1$. Since local perturbations excite bulk fluxes with energies $E_P \sim J^4$ and bulk fermions with energies $E_f \sim 1$ in general, we conclude that the quantum numbers h and q are robust against arbitrary local perturbations of strength $\delta E \ll J^4$ as long as the holes are far apart.

It is instructive to examine an explicit example for the conservation of the internal quantum numbers in the presence of a local perturbation. To this end, we perturb the Kitaev honeycomb model with Heisenberg interactions. The contribution of this perturbation to the Hamiltonian reads as

$$\delta H = \delta E \sum_{\langle l,l' \rangle} \left(\sigma_l^x \sigma_{l'}^x + \sigma_l^y \sigma_{l'}^y + \sigma_l^z \sigma_{l'}^z \right), \tag{3.5}$$

where $\langle l, l' \rangle$ indicates a summation over bonds, or equivalently, over pairs of neighboring sites. Based on the type of the bond and the spin components coupled, there are nine types of terms in δH, and these types can be divided into four distinct classes in the isolated dimer limit. The terms $\sigma_l^z \sigma_{z(l)}^z$ only renormalize the coupling strength J_z on the z bonds, and therefore do not flip any plaquettes or dimers (fermions). The terms $\sigma_l^x \sigma_{x(l)}^x$ and $\sigma_l^y \sigma_{y(l)}^y$ correspond to the usual couplings with strengths $J_{x,y}$ on the x and y bonds, and therefore flip no plaquettes but two dimers each. The terms $\sigma_l^x \sigma_{z(l)}^x$, $\sigma_l^y \sigma_{z(l)}^y$, $\sigma_l^z \sigma_{x(l)}^z$, and $\sigma_l^z \sigma_{y(l)}^z$ flip no dimers and four plaquettes each, while the terms $\sigma_l^y \sigma_{x(l)}^y$ and $\sigma_l^x \sigma_{y(l)}^x$ flip two dimers and four plaquettes each. The effects of these types of terms are illustrated in Fig. 3.4. Since the perturbative terms flip either zero or two dimers, the number of broken dimers has a conserved parity, and therefore the parity of $q + p$ does not change either (see Sec. 3.1.2). Since they either flip zero plaquettes or they flip two plaquettes in even stripes and two plaquettes in odd stripes, the numbers of excited plaquettes in even and in odd stripes both have conserved parities, and therefore the parities of $h + p$ and p do not change either. We conclude that the quantum numbers h, q, and p are all conserved in the presence of a Heisenberg perturbation if its strength satisfies $\delta E \ll J^4$ and the holes are far apart.

3.2 Isolated mobile holes

3.2.1 Hopping formalism

We consider a hole hopping model in which the holes introduced into the Kitaev honeycomb model can propagate via nearest-neighbor hopping. Formally, a spin one-half particle at a site l' neighboring an empty hole site l can hop from l' to l with an

amplitude $-t$. We assume that the spin state of the particle is not affected by the hopping. In the hole spin picture, the hopping then exchanges the hole spin at l with the actual spin at l', and this process can be represented by an exchange operator that takes the form

$$\begin{aligned} \mathcal{E}_{l,l'} &= \frac{1}{2}\left(1+\sigma_l^x\sigma_{l'}^x+\sigma_l^y\sigma_{l'}^y+\sigma_l^z\sigma_{l'}^z\right) \\ &= \frac{1}{2}\left(1+b_l^y b_{l'}^y b_l^z b_{l'}^z+b_l^z b_{l'}^z b_l^x b_{l'}^x+b_l^x b_{l'}^x b_l^y b_{l'}^y\right). \end{aligned} \tag{3.6}$$

In the following, we restrict our attention to the regime of slow hopping, where the hopping amplitude is much smaller than the excitation energies of the bulk modes. We can then neglect the excitations in the bulk modes and consider only the ground states $|\Omega_{h,q,p}^{\Delta}\rangle$ corresponding to the internal modes. Since the bulk modes are bulk fluxes with energies $E_P \sim J^4$ and bulk fermions with energies $E_f \sim 1$ in general, the condition of slow hopping becomes $t \ll J^4$.

For simplicity, we restrict our attention to only $n = 2$ isolated holes at sites $l_{1,2}$. However, more holes are assumed to be present in the background so that the quantum numbers $h_{1,2}$ and $q_{1,2}$ can be chosen independently without violating the global constraints. We consider the hopping process in which the hole at site l_1 hops to a neighboring site l_1'. The set of hole sites is $\Delta = \{l_1, l_2\}$ before the hopping and $\Delta' = \{l_1', l_2' \equiv l_2\}$ after the hopping. The ground states corresponding to the hole positions Δ and Δ' take the forms

$$\begin{aligned} |\Omega_{h,q,p}\rangle &\equiv |\Omega_{h,q,p}^{\Delta}\rangle = \mathcal{Q}_{\Delta}\mathcal{P}\mathcal{F}_{q;h}\mathcal{B}_p\mathcal{X}_h|0\rangle, \\ |\bar{\Omega}_{h',q',p'}\rangle &\equiv |\Omega_{h',q',p'}^{\Delta'}\rangle = \mathcal{Q}_{\Delta'}\mathcal{P}\bar{\mathcal{F}}_{q';h'}\bar{\mathcal{B}}_{p'}\bar{\mathcal{X}}_{h'}|0\rangle, \end{aligned} \tag{3.7}$$

where the operators $\bar{\mathcal{X}}_{h'}$, $\bar{\mathcal{B}}_{p'}$, and $\bar{\mathcal{F}}_{q';h'}$ are completely analogous to $\mathcal{X}_h$, $\mathcal{B}_p$, and $\mathcal{F}_{q;h}$ as defined in Sec. 3.1.2. Since different bonds have switched-off interactions before and after the hopping, the operators $\mathcal{F}_{q;h}$ and $\bar{\mathcal{F}}_{q';h'}$ contain different free matter fermions ϕ_k and $\bar{\phi}_k$. By considering the hopping between the respective ground states $|\Omega_{h,q,p}\rangle$ and $|\bar{\Omega}_{h',q',p'}\rangle$, the effective hopping amplitude becomes a finite-dimensional matrix.

The elements of this matrix are given by

$$T_{h,q,p}^{h',q',p'} = -\frac{t\,\langle\bar{\Omega}_{h',q',p'}|\mathcal{E}_{l_1,l_1'}|\Omega_{h,q,p}\rangle}{\sqrt{\langle\bar{\Omega}_{h',q',p'}|\bar{\Omega}_{h',q',p'}\rangle\langle\Omega_{h,q,p}|\Omega_{h,q,p}\rangle}}\,, \tag{3.8}$$

where the ground-state norms in the denominator are required because the ground states $|\Omega_{h,q,p}\rangle$ and $|\bar{\Omega}_{h',q',p'}\rangle$ are not properly normalized in general.

3.2.2 General hopping properties

We notice that the non-trivial terms in the exchange operator $\mathcal{E}_{l_1,l_1'}$ are the Heisenberg terms in Eq. (3.5). It is therefore directly implied by the results in Sec. 3.1.4 that the quantum numbers h, q, and p are all conserved by the hopping. Note that the exchange operator $\mathcal{E}_{l_1,l_1'}$ can in principle change the plaquette (matter fermion) sector in at most two inequivalent ways (see Fig. 3.4). The plaquette (matter fermion) sector after the hopping is then uniquely determined by that before the hopping via the ground-state constraint that no excited plaquettes (matter fermions) are allowed to be left behind. Mathematically, the conservation of the quantum numbers means that the effective hopping matrix is diagonal.

Furthermore, the diagonal hopping matrix elements that differ only in their plaquette quantum numbers p are all identical to each other. Physically, this property follows from the discrete spin-rotation symmetry discussed in Sec. 3.1.2 and the fact that the corresponding transformation switches p. However, it can also be shown explicitly by noticing that $\mathcal{B}_p^\dagger\mathcal{B}_p = 1$ and $\bar{\mathcal{B}}_p^\dagger\mathcal{E}_{l_1,l_1'}\mathcal{B}_p = \mathcal{E}_{l_1,l_1'}$ for all p. We therefore conclude that the effective hopping matrix elements are independent of the plaquette quantum numbers p and take the general form

$$T_{h,q,p}^{h',q',p'} = \delta_{h',h}\delta_{q',q}\delta_{p',p}\,T_{h,q}, \qquad T_{h,q} = -\frac{t\,\langle\bar{\Omega}_{h,q}|\mathcal{E}_{l_1,l_1'}|\Omega_{h,q}\rangle}{\sqrt{\langle\bar{\Omega}_{h,q}|\bar{\Omega}_{h,q}\rangle\langle\Omega_{h,q}|\Omega_{h,q}\rangle}}\,, \tag{3.9}$$

where $|\Omega_{h,q}\rangle \equiv |\Omega_{h,q,p=0}\rangle$ and $|\bar{\Omega}_{h,q}\rangle \equiv |\bar{\Omega}_{h,q,p=0}\rangle$. In the following, we simplify our calculations by considering only these ground states with $p_1 = p_2 = 0$.

Now we derive a formula for the effective hopping matrix element $\tilde{T}_{h,q}$ in the important case when the bond fermion sector (plaquette sector) is conserved by the hopping. This condition is equivalent to $\mathcal{X}_h = \bar{\mathcal{X}}_h$, and it is always satisfied in the

case of trivial flux quantum numbers $h_1 = h_2 = 0$ when $\mathcal{X}_{h=0} = \bar{\mathcal{X}}_{h=0} = 1$. Due to $\langle 0|\mathcal{X}_h^\dagger \mathcal{X}_h|0\rangle = 1$, the ground-state norms in the denominator of Eq. (3.9) become

$$\begin{aligned} \langle \Omega_{h,q}|\Omega_{h,q}\rangle &= \langle 0|\mathcal{X}_h^\dagger \mathcal{F}_{q;h}^\dagger \mathcal{P}\mathcal{Q}_\Delta \mathcal{F}_{q;h}\mathcal{X}_h|0\rangle = \frac{1}{2^{2N+2}}\langle 0|\mathcal{F}_{q;h}^\dagger \mathcal{F}_{q;h}|0\rangle, \\ \langle \bar{\Omega}_{h,q}|\bar{\Omega}_{h,q}\rangle &= \langle 0|\mathcal{X}_h^\dagger \bar{\mathcal{F}}_{q;h}^\dagger \mathcal{P}\mathcal{Q}_{\Delta'} \bar{\mathcal{F}}_{q;h}\mathcal{X}_h|0\rangle = \frac{1}{2^{2N+2}}\langle 0|\bar{\mathcal{F}}_{q;h}^\dagger \bar{\mathcal{F}}_{q;h}|0\rangle. \end{aligned} \tag{3.10}$$

By assuming $l_1 \in A$ without loss of generality, using the property $\sigma_{l_1'}^z \mathcal{E}_{l_1,l_1'} \sigma_{l_1}^z = \mathcal{E}_{l_1,l_1'}$, and keeping only the terms in $\mathcal{E}_{l_1,l_1'}$ that do not change the plaquette sector when $\alpha \equiv \alpha_{l_1,l_1'} = \{x, y, z\}$, the ground-state overlap in the numerator of Eq. (3.9) becomes

$$\begin{aligned} \langle \bar{\Omega}_{h,q}|\mathcal{E}_{l_1,l_1'}|\Omega_{h,q}\rangle &= \langle 0|\mathcal{X}_h^\dagger \bar{\mathcal{F}}_{q;h}^\dagger \mathcal{P}\mathcal{Q}_{\Delta'}\mathcal{E}_{l_1,l_1'}\mathcal{Q}_\Delta \mathcal{F}_{q;h}\mathcal{X}_h|0\rangle \\ &= \frac{1}{8}\langle 0|\mathcal{X}_h^\dagger \bar{\mathcal{F}}_{q;h}^\dagger \mathcal{P}\left(1 + b_{l_1}^\alpha b_{l_1'}^\alpha c_{l_1} c_{l_1'}\right)\mathcal{F}_{q;h}\mathcal{X}_h|0\rangle \\ &= \frac{1}{2^{2N+3}}\langle 0|\mathcal{X}_h^\dagger \bar{\mathcal{F}}_{q;h}^\dagger \left(1 + b_{l_1}^\alpha b_{l_1'}^\alpha c_{l_1} c_{l_1'}\right)\mathcal{F}_{q;h}\mathcal{X}_h|0\rangle \\ &= \frac{1}{2^{2N+3}}\langle 0|\bar{\mathcal{F}}_{q;h}^\dagger \left(1 - i u_{l_1,l_1'} c_{l_1} c_{l_1'}\right)\mathcal{F}_{q;h}|0\rangle. \end{aligned} \tag{3.11}$$

Note that $u_{l_1,l_1'} \equiv \langle 0|\mathcal{X}_h^\dagger \hat{u}_{l_1,l_1'}\mathcal{X}_h|0\rangle$ is determined by the bond fermion sector. Finally, the effective hopping matrix element in the case of a conserved bond fermion sector (plaquette sector) takes the form

$$\tilde{T}_{h,q} = -\frac{t\,\langle 0|\bar{\mathcal{F}}_{q;h}^\dagger \left(1 - i u_{l_1,l_1'} c_{l_1} c_{l_1'}\right)\mathcal{F}_{q;h}|0\rangle}{2\sqrt{\langle 0|\bar{\mathcal{F}}_{q;h}^\dagger \bar{\mathcal{F}}_{q;h}|0\rangle \langle 0|\mathcal{F}_{q;h}^\dagger \mathcal{F}_{q;h}|0\rangle}}. \tag{3.12}$$

Since the operators $\mathcal{F}_{q;h}^{(\dagger)}$ and $\bar{\mathcal{F}}_{q;h}^{(\dagger)}$ are all simple products of matter fermion operators, the vacuum expectation values in Eq. (3.12) can be evaluated using Wick's theorem. The state $|0\rangle$ is the vacuum of the original matter fermions f_l, and the orthogonal matrices U and V are therefore used to express the free matter fermions ϕ_k and $\bar{\phi}_k$ in terms of the original matter fermions f_l.

3.2.3 Hopping in the isolated dimer limit

We now consider the isolated dimer limit ($J = 0$) and evaluate the effective hopping matrix elements explicitly. In this limit, the operators $\mathcal{F}_q \equiv \mathcal{F}_{q;h}$ and $\bar{\mathcal{F}}_q \equiv \bar{\mathcal{F}}_{q;h}$ no longer depend on h and take the simplified forms $\mathcal{F}_q = [f_{\tilde{z}(l_1)}^\dagger]^{q_1}[f_{\tilde{z}(l_2)}^\dagger]^{q_2}$ and $\bar{\mathcal{F}}_q =$

$[f^\dagger_{\tilde{z}(l_1')}]^{q_1}[f^\dagger_{\tilde{z}(l_2)}]^{q_2}$ (see Sec. 3.1.2). The vacuum expectation values in Eq. (3.12) therefore take the respective forms

$$\begin{aligned}
&\langle 0|\mathcal{F}_q^\dagger \mathcal{F}_q|0\rangle = \langle 0|\bar{\mathcal{F}}_q^\dagger \bar{\mathcal{F}}_q|0\rangle = 1, \\
&\langle 0|\bar{\mathcal{F}}^\dagger_{q_1=0}\left(1 - iu_{l_1,l_1'}c_{l_1}c_{l_1'}\right)\mathcal{F}_{q_1=0}|0\rangle = \begin{cases} 2 & (\alpha_{l_1,l_1'} = z) \\ 1 & (\alpha_{l_1,l_1'} = x,y), \end{cases} \\
&\langle 0|\bar{\mathcal{F}}^\dagger_{q_1=1}\left(1 - iu_{l_1,l_1'}c_{l_1}c_{l_1'}\right)\mathcal{F}_{q_1=1}|0\rangle = \begin{cases} 0 & (\alpha_{l_1,l_1'} = z) \\ -u_{l_1,l_1'} & (\alpha_{l_1,l_1'} = x,y), \end{cases}
\end{aligned} \tag{3.13}$$

and the corresponding hopping matrix elements become

$$\begin{aligned}
\tilde{T}_{h,q_1=0} &= \begin{cases} -t & (\alpha_{l_1,l_1'} = z) \\ -t/2 & (\alpha_{l_1,l_1'} = x,y), \end{cases} \\
\tilde{T}_{h,q_1=1} &= \begin{cases} 0 & (\alpha_{l_1,l_1'} = z) \\ u_{l_1,l_1'}\, t/2 & (\alpha_{l_1,l_1'} = x,y). \end{cases}
\end{aligned} \tag{3.14}$$

Note that $u_{l_1,l_1'} = +1$ for $\alpha_{l_1,l_1'} = z$ because $\mathcal{X}_h$ excites only x and y bond fermions. Furthermore, the matrix elements in Eq. (3.14) are independent of the quantum number q_2. Since the two holes are isolated, the hole hopping between l_1 and l_1' is not affected by the other hole at l_2.

It is crucial to emphasize that the matrix elements in Eq. (3.14) are valid only if the bond fermion sector is the same before and after the hopping. However, we demonstrate in the following that the hopping problem for a single isolated hole with quantum numbers $h = \{0,1\}$ and $q = \{0,1\}$ can be constructed by referring to these matrix elements only. The most important steps of the construction are illustrated in Fig. 3.5, while the resulting hopping problems for the different quantum numbers are summarized in Fig. 3.6.

For a hole with no flux bound to it ($h = 0$), the bond fermion sector is always trivial, and the matrix elements in Eq. (3.14) are therefore directly applicable. This means that hopping along x and y bonds is allowed for both values of the quantum number q, while hopping along z bonds is allowed for $q = 0$ but not for $q = 1$. In other words, $q = 0$ holes can hop in both the X and the Y directions, while $q = 1$ holes can hop only in the X direction. Since $u_{l,\alpha(l)} = +1$ for all bonds around an $h = 0$ hole, the hopping problem in the X direction is in fact the same for $q = 0$ and

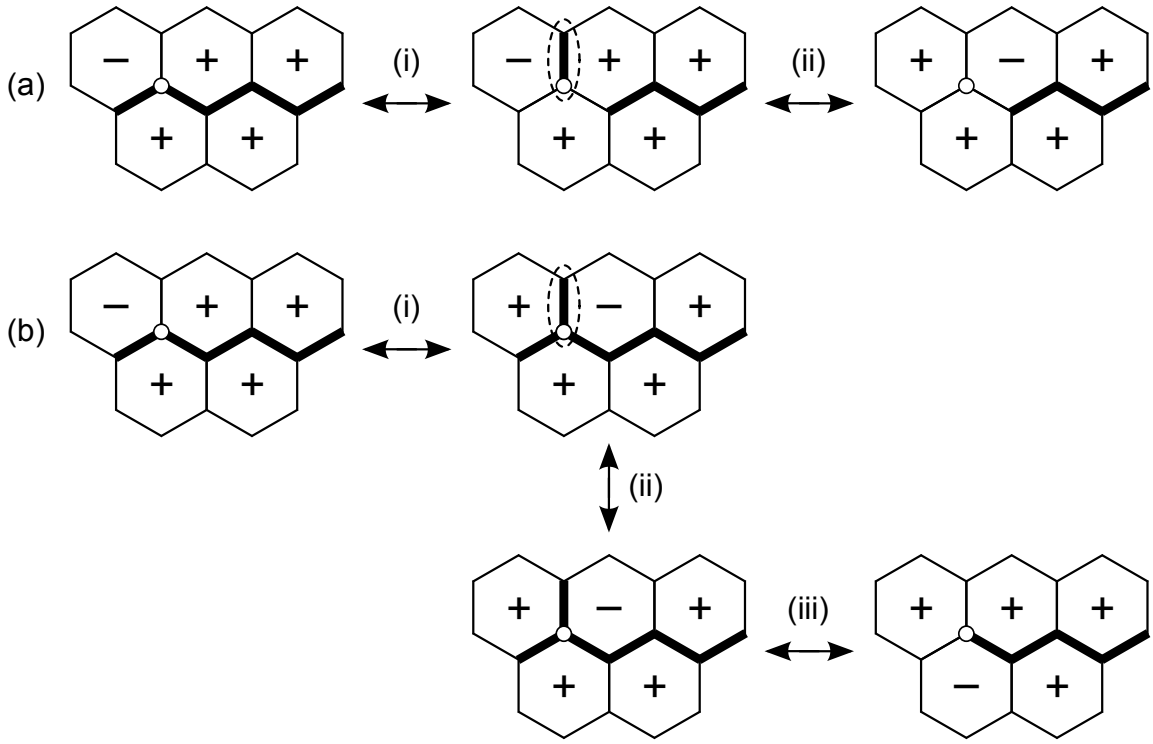

Figure 3.5: Different types of transformations relating bond fermion and matter fermion sectors around a hole site $l \in \Delta$ (white dot) when there is a flux bound to the hole. Each bond fermion sector is labeled with the excited bond fermions (thick lines) and the corresponding plaquette operator eigenvalues (± 1), while each matter fermion sector is labeled with the excited matter fermions (dashed ellipses). (a) Gauge transformations D_l (i) and σ_l^z (ii) for shifting the excited plaquette within a stripe. (b) Transformations σ_l^z (i) [gauge], $c_{\tilde{z}(l)}$ (ii) [q-switch], and $ib_l^x b_l^z$ (iii) [p-switch] for shifting the excited plaquette between neighboring stripes.

$q = 1$. Note that the opposite sign in the matrix element $\tilde{T}_{h,q_1=1}$ is irrelevant because the honeycomb lattice is bipartite.

For a hole with a flux bound to it ($h = 1$), the hopping problem is more complicated because the bond fermion sector depends on the hole position. However, if the hole hops only around the excited plaquette, the bond fermion sector can be chosen to remain the same, and the matrix elements in Eq. (3.14) are therefore applicable. Remember that the excited plaquette is in an even stripe for a $p = 0$ hole (see Fig. 3.2). Furthermore, the excited plaquette can be shifted along its stripe by applying two simultaneous gauge transformations D_l and σ_l^z at the hole site l. After these transformations illustrated in Fig. 3.5(a), the bond fermion and the matter

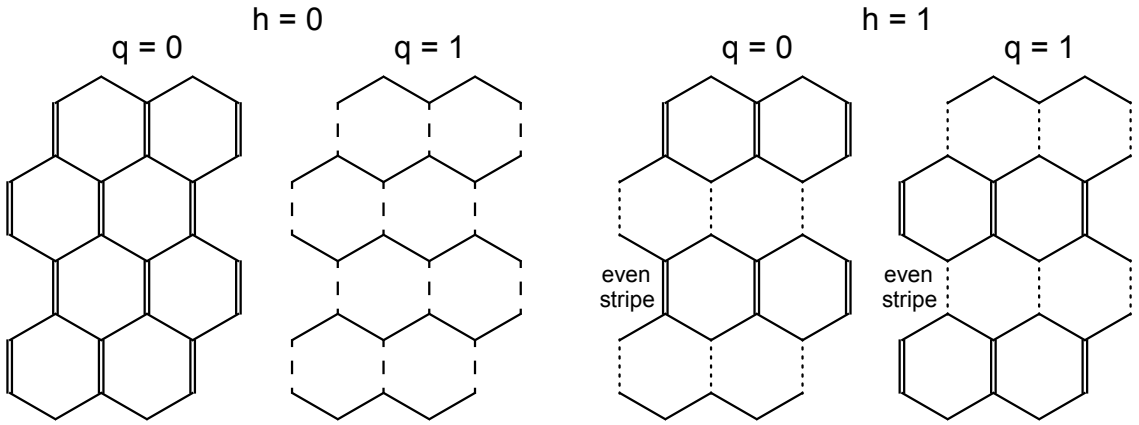

Figure 3.6: Hole hopping problems in the isolated dimer limit for different combinations of the flux quantum number $h = \{0, 1\}$ and the fermion quantum number $q = \{0, 1\}$. Each bond is labeled according to the effective hopping amplitude T along it: double solid lines indicate $T = -t$, single solid lines indicate $T = -t/2$, while dashed and dotted lines indicate $T = 0$. For dashed lines, the effective hopping amplitude vanishes only in the isolated dimer limit, while for dotted lines, it vanishes in the entire gapped phase.

fermion sectors around the hole site look the same from the point of view of the new plaquette as they did before from the point of view of the old plaquette. This implies that the hopping problem for $h = 1$ is identical to that for $h = 0$ as long as the hole hops only around the plaquettes of one particular even stripe. On the other hand, the excited plaquette can only be shifted into a neighboring odd stripe by applying the gauge transformation σ^z_l along with the transformations $c_{\tilde{z}(l)}$ and $ib^x_l b^z_l$ that switch the quantum numbers q and p. After these transformations illustrated in Fig. 3.5(b), the bond fermion and the matter fermion sectors around the hole site l look the same from the point of view of the new stripe as they did before from the point of view of the old stripe. Since the hopping is independent of p, this implies that the hopping problem for $q = 1$ around the plaquettes of odd (even) stripes is identical to that for $q = 0$ around the plaquettes of even (odd) stripes. Unlike in the case of $h = 0$, holes with different values of q do not have fundamentally different hopping problems in the case of $h = 1$: they can both hop along x and y bonds in the X direction, while hopping along z bonds in the Y direction is allowed for $q = 0$ in even stripes and for $q = 1$ in odd stripes.

3.2.4 Hopping in the gapped phase

We are now ready to discuss the hopping problem for a single isolated hole at a generic point of the gapped phase away from the isolated dimer limit ($J > 0$). From a perturbation theory in $J \ll 1$, there are possible corrections to the matrix elements in Eq. (3.14), and the importance of these corrections depends on whether the original matrix element is zero or non-zero. If there is a finite matrix element at $J = 0$, the perturbative corrections can be neglected as they only renormalize the matrix element. However, if the matrix element vanishes at $J = 0$, these corrections are extremely important as they determine the matrix element in the lowest order.

According to Eq. (3.14), the only vanishing matrix elements in the isolated dimer limit are $\tilde{T}_{h,q_1=1}$ along z bonds. Any such matrix element is zero because the matter fermion corresponding to the two sites l_1 and l_1' connected by the z bond is excited: $-ic_{l_1}c_{l_1'} = -1$. To obtain a non-zero correction for the matrix element, we must find corrections with a non-zero overlap for the ground states before and after the hopping such that $-ic_{l_1}c_{l_1'} = +1$ for both corrections. In general, these two corrections belong to two complementary sections of an open string connecting the sites l_1 and l_1'. For example, if we use the site labeling convention in Fig. 3.7 around the sites l_1 and l_1', one such pair of corrections is

$$\begin{aligned} \mathcal{F}_{q_1=1}|0\rangle &= \frac{J}{6}\left(b_5^x b_6^x c_5 c_6\right)\frac{J}{4}\left(b_3^x b_2^x c_3 c_2\right) f_1^\dagger|0\rangle, \\ \bar{\mathcal{F}}_{q_1=1}|0\rangle &= \frac{J}{6}\left(b_1^y b_2^y c_1 c_2\right)\frac{J}{4}\left(b_5^y b_4^y c_5 c_4\right) f_1^\dagger|0\rangle, \end{aligned} \tag{3.15}$$

and the resulting correction to the ground-state overlap is

$$\langle 0|\bar{\mathcal{F}}_{q_1=1}^\dagger\left(1 - ic_1c_6\right)\mathcal{F}_{q_1=1}|0\rangle = J^4 u_{1,2}u_{3,2}u_{5,4}u_{5,6}Z_P = J^4 W_P Z_P, \tag{3.16}$$

$$\begin{aligned} Z_P &= \frac{1}{576}\langle 0|f_1 c_5 c_4 c_1 c_2\left(1 - ic_1c_6\right)c_5c_6c_3c_2 f_1^\dagger|0\rangle \\ &= \frac{1}{288}\langle 0|f_1 c_5 c_4 c_1 c_2 c_5 c_6 c_3 c_2 f_1^\dagger|0\rangle = \frac{1}{288}\,. \end{aligned} \tag{3.17}$$

Note that $u_{1,6} = u_{3,4} = +1$ because $\mathcal{X}_h$ is defined in such a way that it excites only x and y bond fermions.

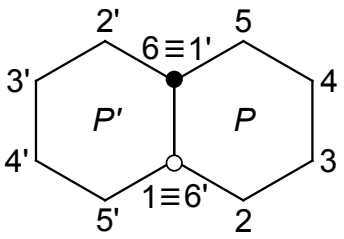

Figure 3.7: Site and plaquette labeling conventions around the sites l_1 (white dot) and l_1' (black dot) when considering the hopping along the z bond between l_1 and l_1'.

For a generic open string connecting the sites 1 and $1'$, we define a closed loop C consisting of the open string and the z bond between 1 and $1'$. Any correction to the ground-state overlap due to the open string is then proportional to $W_C Z_C$, where W_C is the corresponding loop operator eigenvalue and Z_C is an expectation value similar to that in Eq. (3.17). By means of a reflection across the middle of the z bond, we also define a dual loop C' with a loop operator eigenvalue $W_{C'}$ and a dual correction with an expectation value $Z_{C'}$. Note that the dual correction strictly corresponds to a backward hopping because the reflection exchanges the sites 1 and $1'$. On the other hand, $Z_{C'} \in \mathbb{R}$ means that there is an equivalent dual correction for the forward hopping as well. If we identify the site labels of the loop C with the dual site labels of the loop C', the explicit forms of the expectation values Z_C and $Z_{C'}$ are identical, and thus $Z_C = Z_{C'}$. Since this equality is true for all corrections, we conclude that the total corrections due to the loops C and C' have equal magnitudes, while their relative signs are determined by the loop eigenvalues $W_{C,C'}$.

This result has already strong implications for holes with a flux bound to them ($h = 1$). When the bond fermion sector is conserved by the hopping, the flux is necessarily bound to either of the plaquettes P or P'. If we then choose any two dual loops C and C' that do not enclose any other holes, one of them contains one excited plaquette and the other one contains no excited plaquettes. This implies $W_C + W_{C'} = 0$, and therefore the corrections due to all of the paired-up dual loops vanish because $(W_C + W_{C'})Z_C = 0$. The only non-zero corrections are then due to loops that are large enough such that they enclose at least one other hole with a flux

bound to it. If the smallest distance between any two holes is R, the length of such a loop is at least $2R$, and therefore the lowest-order corrections to the matrix element are $\sim J^{2R}$. Since this quantity is exponentially small in the $R \gg 1$ limit, holes with $h = 1$ can hop only along their respective stripes as long as we are in the gapped phase with $J < 1/2$.

For holes with no flux bound to them ($h = 0$), there are no excited plaquettes, and all loops have $W_C = +1$. This means that the lowest-order corrections to the ground-state overlap are due to the plaquettes P and P'. These two corrections are identical because $W_P = W_{P'} = +1$. The total expectation value Z_P is obtained by considering all possible ways of dividing the open string between the sites 1 and $1'$ into two complementary sections and all possible ways of ordering the x and y bonds within the resulting two sections. Note that the choice of the complementary sections is limited by the fact that some bonds have switched-off interactions: the bonds around the site 1 can only be used after the hopping, while the bonds around the site $1'$ can only be used before the hopping. Exploiting symmetry to reduce the number of inequivalent terms, the total expectation value becomes

$$\begin{aligned} Z_P &= \frac{2}{16}\langle 0|f_1 c_1 c_2 \hat{\epsilon}_{1,6} c_3 c_2 c_5 c_4 c_5 c_6 f_1^\dagger|0\rangle + \frac{2}{48}\langle 0|f_1 c_1 c_2 \hat{\epsilon}_{1,6} c_5 c_4 c_3 c_2 c_5 c_6 f_1^\dagger|0\rangle \\ &\quad + \frac{2}{32}\langle 0|f_1 c_1 c_2 \hat{\epsilon}_{1,6} c_3 c_2 c_5 c_6 c_5 c_4 f_1^\dagger|0\rangle + \frac{2}{64}\langle 0|f_1 c_1 c_2 \hat{\epsilon}_{1,6} c_5 c_6 c_3 c_2 c_5 c_4 f_1^\dagger|0\rangle \\ &\quad + \frac{2}{96}\langle 0|f_1 c_1 c_2 \hat{\epsilon}_{1,6} c_5 c_4 c_5 c_6 c_3 c_2 f_1^\dagger|0\rangle + \frac{2}{64}\langle 0|f_1 c_1 c_2 \hat{\epsilon}_{1,6} c_5 c_6 c_5 c_4 c_3 c_2 f_1^\dagger|0\rangle \\ &\quad + \frac{1}{16}\langle 0|f_1 c_1 c_2 c_3 c_2 \hat{\epsilon}_{1,6} c_5 c_4 c_5 c_6 f_1^\dagger|0\rangle + \frac{2}{32}\langle 0|f_1 c_1 c_2 c_3 c_2 \hat{\epsilon}_{1,6} c_5 c_6 c_5 c_4 f_1^\dagger|0\rangle \\ &\quad + \frac{1}{64}\langle 0|f_1 c_3 c_2 c_1 c_2 \hat{\epsilon}_{1,6} c_5 c_6 c_5 c_4 f_1^\dagger|0\rangle + \frac{1}{144}\langle 0|f_1 c_1 c_2 c_5 c_4 \hat{\epsilon}_{1,6} c_3 c_2 c_5 c_6 f_1^\dagger|0\rangle \\ &\quad + \frac{2}{288}\langle 0|f_1 c_1 c_2 c_5 c_4 \hat{\epsilon}_{1,6} c_5 c_6 c_3 c_2 f_1^\dagger|0\rangle + \frac{1}{576}\langle 0|f_1 c_5 c_4 c_1 c_2 \hat{\epsilon}_{1,6} c_5 c_6 c_3 c_2 f_1^\dagger|0\rangle \\ &= \frac{1}{4} + \frac{1}{12} - \frac{1}{8} - \frac{1}{16} + \frac{1}{24} - \frac{1}{16} + \frac{1}{8} - \frac{1}{8} + \frac{1}{32} + \frac{1}{72} + \frac{1}{72} + \frac{1}{288} = \frac{3}{16}, \end{aligned} \tag{3.18}$$

where $\hat{\epsilon}_{1,6} \equiv 1 - ic_1c_6 = 2$ in all the terms above. Since $W_P = W_{P'} = +1$ and $Z_P = Z_{P'} = 3/16$, the corresponding lowest-order correction to the ground-state overlap is $\langle 0|\bar{\mathcal{F}}^\dagger_{q_1=1}\hat{\epsilon}_{1,6}\mathcal{F}_{q_1=1}|0\rangle = 3J^4/8$. On the other hand, the ground-state norms

$\langle 0|\mathcal{F}_q^\dagger \mathcal{F}_q|0\rangle$ and $\langle 0|\bar{\mathcal{F}}_q^\dagger \bar{\mathcal{F}}_q|0\rangle$ are still approximately 1, and therefore the lowest-order correction to the hopping matrix element takes the form

$$\tilde{T}_{h_1=0,q_1=1} = -\frac{3}{16} J^4 t \qquad (\alpha_{l_1,l_1'} = z). \tag{3.19}$$

This result shows that holes with $h = 0$ and $q = 1$ are only confined to hop in the X direction in the limit of $J \to 0$. At a generic point of the gapped phase, holes with $h = 0$ are free to hop in both the X and the Y directions.

It is instructive to investigate the hole hopping problems across the entire gapped phase with $0 < J < 1/2$. Since the perturbation theory in $J \ll 1$ is not applicable in general, we must evaluate the hopping matrix elements in Eq. (3.12) numerically. The resulting hopping matrix elements for quantum numbers $h = 0$ and $q = \{0, 1\}$ are plotted across the gapped phase in Fig. 3.8. In the limit of $J \to 0$, when the perturbation theory is valid, the hopping matrix elements in Eqs. (3.14) and (3.19) are accurately recovered. In the opposite limit of $J \to 1/2$, when the phase transition to the gapless phase is close, the hopping matrix elements for all quantum numbers $h = \{0, 1\}$ and $q = \{0, 1\}$ become strongly dependent on the system size and exhibit a sudden drop towards zero. These results are both explained by the vanishing energy gap of the bulk fermion excitations: finite-size effects become important due to the divergent correlation length, while the hopping matrix elements vanish due to the hybridization between the hole fermions and the lowest-energy bulk fermions.

Note that the condition of slow hopping breaks down in the limit of $J \to 1/2$ as the lowest-energy bulk fermions no longer have finite excitation energies. The hopping process in this limit involves not only the respective ground states as in Sec. 3.2.1, but also the excited states in which some of the lowest-energy bulk fermions are excited. On the other hand, this means that the hopping matrix elements in Eq. (3.12) underestimate the actual hopping amplitudes, and therefore the vanishing hopping matrix elements at $J \to 1/2$ do not imply that the holes become stationary at the phase transition point.

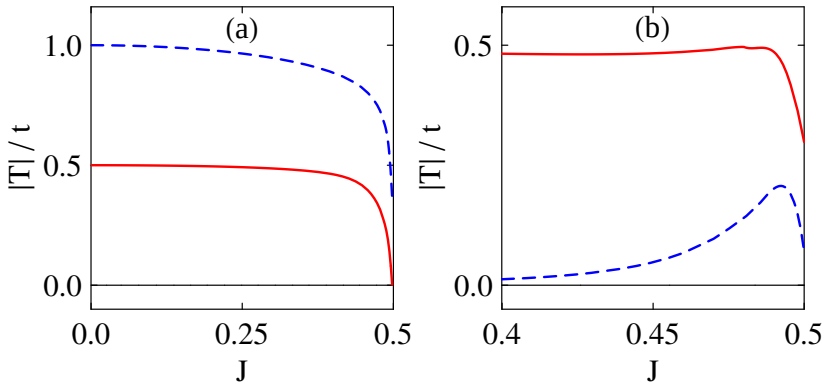

Figure 3.8: Effective hopping amplitude as a function of the x and y bond coupling strengths within the gapped phase for a hole with $h = 0$ and either $q = 0$ (a) or $q = 1$ (b) along x and y bonds (solid lines) and along z bonds (dashed lines). The lattice dimensions are $N_X = N_Y = 20$ in all cases.

3.2.5 Particle statistics

Since the quantum numbers h, q, and p are conserved by the hopping process, we can treat holes with different quantum numbers as distinct particles and determine their respective particle statistics. To this end, we consider an exchange process in which two isolated identical holes at sites 0 and ℓ are exchanged along a closed loop C that contains L sites labeled $\{1, 2, \ldots, \ell - 1, \ell, \ell + 1, \ldots, L \equiv 0\}$. If the exchange process is adiabatically slow, the final state is identical to the initial state up to a complex phase factor $\exp(i\tilde{\varphi})$. The complex phase $\tilde{\varphi}$ has two contributions: a dynamic phase from the time integral of the governing Hamiltonian that depends on the details of the exchange process, and a geometric phase θ_2 that depends only on the loop C. To determine the particle statistics, we first must obtain the phase θ_2.

The adiabatic exchange process along the loop C starts from the initial ground state $|\Omega_{h,q,p}^{\{0,\ell\}}\rangle$, ends at the exchanged ground state $|\Omega_{h,q,p}^{\{\ell,0\}}\rangle$, and happens via subsequent nearest-neighbor hopping processes through intermediate ground states $|\Omega_{h,q,p}^{\{l,l'\}}\rangle$, where $0 \leq l \leq \ell$ and $\ell \leq l' \leq L$. These hopping processes are illustrated in Fig. 3.9(a). The geometric phase θ_2 arises from the geometric connections between the intermediate ground states $|\Omega_{h,q,p}^{\{l,l'\}}\rangle$. On the other hand, it can be argued theoretically and verified numerically that these geometric connections are given by the hopping matrix

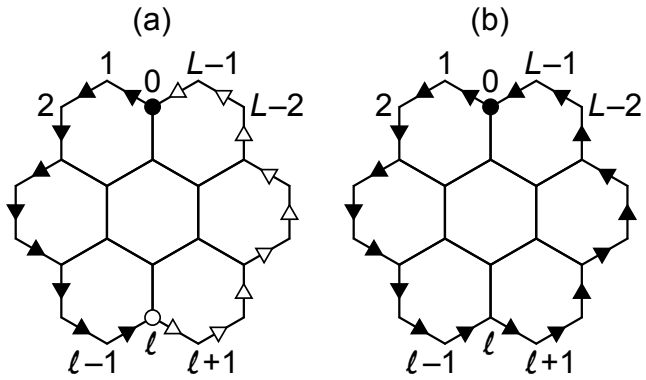

Figure 3.9: Illustrations of the two processes that are used to evaluate the statistical angle $\vartheta = \theta_2 - \theta_1$. (a) Exchange process for obtaining θ_2. Two identical holes with the given quantum numbers at sites 0 and $\ell = 9$ (black and white dots) are exchanged along a closed loop of length $L = 18$. The subsequent hopping processes for the respective holes are marked by black and white arrows. (b) Looping process for obtaining θ_1. One hole with the same quantum numbers at site 0 (black dot) is moved around the same closed loop. The subsequent hopping processes are marked by black arrows.

elements in Eq. (3.9). Since there is exactly one intermediate hopping process for each section of the loop, this suggests that the phase θ_2 is the phase of the product of all the hopping matrix elements around the loop C. In fact, we must consider two additional phase factors due to the two holes being exchanged. First, the exchanged ground state $|\Omega_{h,q,p}^{\{\ell,0\}}\rangle$ can contain a non-trivial phase factor with respect to the initial ground state $|\Omega_{h,q,p}^{\{0,\ell\}}\rangle$. Second, our hopping formalism in the hole spin picture ignores the inherent fermionic nature of the holes. Since the two hole spins are removed from both ground states $|\Omega_{h,q,p}^{\{0,\ell\}}\rangle$ and $|\Omega_{h,q,p}^{\{\ell,0\}}\rangle$ by fermionic annihilation operators, the exchange between the two holes corresponds to a non-trivial phase factor -1 in the actual hole picture. The geometric phase θ_2 thus takes the form

$$\theta_2 = \arg\left[-\langle\Omega_{h,q,p}^{\{0,\ell\}}|\Omega_{h,q,p}^{\{\ell,0\}}\rangle \prod_{l=0}^{L-1} \mathrm{T}_{l,l+1}^{(2)}\right], \tag{3.20}$$

$$\mathrm{T}_{l,l+1}^{(2)} = -\frac{t\,\langle\Omega_{h,q,p}^{\{l+1,l'\}}|\mathcal{E}_{l,l+1}|\Omega_{h,q,p}^{\{l,l'\}}\rangle}{\sqrt{\langle\Omega_{h,q,p}^{\{l+1,l'\}}|\Omega_{h,q,p}^{\{l+1,l'\}}\rangle\langle\Omega_{h,q,p}^{\{l,l'\}}|\Omega_{h,q,p}^{\{l,l'\}}\rangle}}\,. \tag{3.21}$$

Note that the matrix element $\mathrm{T}_{l,l+1}^{(2)}$ does not depend on the site l' of the other hole as the two holes are assumed to be isolated at each step of the exchange process.

The geometric phase of the exchange process can be written as a sum of two terms: $\theta_2 = \vartheta + \theta_1$. The first term ϑ is the actual statistical phase that specifies the particle statistics, while the second term θ_1 is the geometric (Berry) phase of a looping process in which a single hole at site 0 with the same quantum numbers h, q, and p is moved adiabatically slowly around the same closed loop C. Since the statistical angle is given by $\vartheta = \theta_2 - \theta_1$ in terms of the two geometric phases, we also must obtain the second phase θ_1.

The adiabatic looping process around the loop C starts from the initial ground state $|\Omega^{\{0\}}_{h,q,p}\rangle$, ends at the final ground state $|\Omega^{\{L\}}_{h,q,p}\rangle \equiv |\Omega^{\{0\}}_{h,q,p}\rangle$, and happens via subsequent nearest-neighbor hopping processes through intermediate ground states $|\Omega^{\{l\}}_{h,q,p}\rangle$, where $0 < l < L$. These hopping processes are illustrated in Fig. 3.9(b). As in the case of the exchange process, the geometric phase θ_1 of the looping process arises from the geometric connections between the intermediate ground states, and is therefore related to the product of the hopping matrix elements around the loop C. However, the two additional phase factors are absent because no holes are being exchanged. The geometric phase θ_1 thus takes the form

$$\theta_1 = \arg\left[\prod_{l=0}^{L-1} \mathrm{T}^{(1)}_{l,l+1}\right], \tag{3.22}$$

$$\mathrm{T}^{(1)}_{l,l+1} = -\frac{t\,\langle\Omega^{\{l+1\}}_{h,q,p}|\mathcal{E}_{l,l+1}|\Omega^{\{l\}}_{h,q,p}\rangle}{\sqrt{\langle\Omega^{\{l+1\}}_{h,q,p}|\Omega^{\{l+1\}}_{h,q,p}\rangle\langle\Omega^{\{l\}}_{h,q,p}|\Omega^{\{l\}}_{h,q,p}\rangle}}\,. \tag{3.23}$$

Importantly, the matrix element $\mathrm{T}^{(1)}_{l,l+1}$ is in most cases identical to the matrix element $\mathrm{T}^{(2)}_{l,l+1}$ because the presence of the other isolated hole is irrelevant. The only exception is the case of $h = 1$ and $q = 1$ when there is a string of excited bond fermions connected to the hole and the hopping is sensitive to excited bond fermions [see Eq. (3.14)]. It is then relevant for at least one section of the loop C whether the other end of the string is at the other hole moving around the same loop or at a stationary hole in the background.

We are now ready to determine the particle statistics of the various hole types. From a comparison between Eqs. (3.20) and (3.22), the statistical phase becomes

$$\vartheta = \arg\left[-\langle\Omega^{\{0,\ell\}}_{h,q,p}|\Omega^{\{\ell,0\}}_{h,q,p}\rangle \prod_{l=0}^{L-1}\left(\frac{\mathrm{T}^{(2)}_{l,l+1}}{\mathrm{T}^{(1)}_{l,l+1}}\right)\right]. \tag{3.24}$$

Furthermore, if the holes have quantum numbers other than $h = 1$ and $q = 1$, the matrix elements $\mathrm{T}^{(1)}_{l,l+1}$ and $\mathrm{T}^{(2)}_{l,l+1}$ are identical, and therefore Eq. (3.24) reduces to

$$\vartheta = \arg\left[-\langle\Omega^{\{0,\ell\}}_{h,q,p}|\Omega^{\{\ell,0\}}_{h,q,p}\rangle\right]. \tag{3.25}$$

By evaluating ϑ for all hole types, we can then directly obtain their particle statistics: $\vartheta = 0$ is indicative of bosons, while $\vartheta = \pi$ is indicative of fermions.

For holes with $h = 0$ and $q = 0$, the initial ground state $|\Omega^{\{0,\ell\}}_{0,0,p}\rangle$ and the final ground state $|\Omega^{\{\ell,0\}}_{0,0,p}\rangle$ are identical by construction. In the isolated dimer limit, the two ground states for $p = 0$ holes are $|\Omega^{\{0,\ell\}}_{0,0,0}\rangle = |\Omega^{\{\ell,0\}}_{0,0,0}\rangle = \mathcal{Q}_{\{0,\ell\}}\mathcal{P}|0\rangle$. In the general case, there are additional operators $B_p \neq 1$ and $\mathcal{F}_{0;0} \neq 1$ that set the bond fermion and the matter fermion sectors. However, these operators are the same for both ground states, and therefore the relation $|\Omega^{\{0,\ell\}}_{0,0,p}\rangle = |\Omega^{\{\ell,0\}}_{0,0,p}\rangle$ remains true. Since Eq. (3.25) then gives $\vartheta = \pi$, we conclude that holes with $h = 0$ and $q = 0$ are fermions.

For holes with $h = 0$ and $q = 1$, the initial ground state $|\Omega^{\{0,\ell\}}_{0,1,p}\rangle$ and the final ground state $|\Omega^{\{\ell,0\}}_{0,1,p}\rangle$ are only identical up to a minus sign as the two ground states have the two hole fermions at sites 0 and ℓ excited in an opposite order. In the isolated dimer limit, the two ground states for $p = 0$ holes are $|\Omega^{\{0,\ell\}}_{0,1,0}\rangle = -|\Omega^{\{\ell,0\}}_{0,1,0}\rangle = \mathcal{Q}_{\{0,\ell\}}\mathcal{P}f^{\dagger}_{\tilde{z}(0)}f^{\dagger}_{\tilde{z}(\ell)}|0\rangle$. In the general case, there are additional operators $B_p \neq 1$ and $\mathcal{F}_{1;0} \neq 1$ that set the bond fermion and the matter fermion sectors. However, these operators are the same for both ground states, and therefore the relation $|\Omega^{\{0,\ell\}}_{0,1,p}\rangle = -|\Omega^{\{\ell,0\}}_{0,1,p}\rangle$ remains true. Since Eq. (3.25) then gives $\vartheta = 0$, we conclude that holes with $h = 0$ and $q = 1$ are bosons.

It is crucial that holes with $h = 1$ can move only around the plaquettes of particular stripes: even stripes for $q = 0$ and odd stripes for $q = 1$. Furthermore, it is shown by Fig. 3.5 that $q = 0$ holes in even stripes are equivalent to $q = 1$ holes in odd

stripes. This implies that these two hole types have the same particle statistics, and therefore it is enough to consider one of them. We choose to consider holes with $h = 1$ and $q = 0$ because Eq. (3.25) is then applicable. For these holes, the only difference in the ground state with respect to holes with $h = 0$ and $q = 0$ is the presence of an additional flux-binding operator $\mathcal{X}_1 \neq 1$. However, this operator is the same for the initial and the final ground states, and therefore the two ground states are identical: $|\Omega_{1,0,p}^{\{0,\ell\}}\rangle = |\Omega_{1,0,p}^{\{\ell,0\}}\rangle$. Since Eq. (3.25) then gives $\vartheta = \pi$, we conclude that holes with $h = 1$ and $q = \{0, 1\}$ are fermions.

To supplement the above derivations, we also provide an intuitive explanation for the particle statistics found. The main principle is that the holes in the model can bind the elementary excitations of the model: fluxes and fermions. The various hole types with different quantum numbers h and q are then distinguished only by the kinds of elementary excitations that are bound to them. In particular, a hole with a non-trivial flux quantum number $h = 1$ has a bound flux, while a hole with a non-trivial fermion quantum number $q = 1$ has a bound fermion. Holes with $h = 0$ and $q = 0$ are interpreted as bare holes with no elementary excitations bound to them. Since bare holes are missing spin one-half fermions, it is natural that they are fermions themselves. Conversely, the remaining three types of holes are interpreted as composite holes made out of bare holes and elementary excitations. Due to the presence of the bound excitations, their statistics can be different from that of bare holes. For holes with $h = 0$ and $q = 1$, the binding of a fermion leads to a statistical transmutation, and therefore these holes are bosons. For holes with $h = 1$ and $q = 0$, the binding of a flux has no effect on the statistics, and therefore these holes are fermions. We might then naively expect that holes with $h = 1$ and $q = 1$ should be bosons because there is a statistical transmutation due to the binding of a fermion. However, the bound flux and the bound fermion have semionic relative statistics. Since this corresponds to an additional transmutation for the composite hole, these holes are in fact fermions. The particle statistics of the various hole types along with their interpretations in terms of the bound excitations are summarized in Table 3.4.

Hole type		Statistics	Interpretation
$h = 0$	$q = 0$	Fermion	Bare hole
	$q = 1$	Boson	Hole + fermion
$h = 1$	$q = 0$	Fermion	Hole + flux
	$q = 1$	Fermion	Hole + flux + fermion

Table 3.4: Absolute statistics of holes with flux quantum numbers $h = \{0, 1\}$ and fermion quantum numbers $q = \{0, 1\}$ from a process when two identical holes are exchanged. Interpretations are given in terms of elementary excitations bound.

It is also useful to investigate the relative statistics between the various hole types. To this end, we consider two looping processes in which a hole with quantum numbers h and q is moved around a closed loop C. In the first case, there is no hole enclosed by the loop, and Eq. (3.22) gives a geometric phase θ_1. In the second case, there is one stationary hole with quantum numbers h' and q' enclosed by the loop, and Eq. (3.22) gives a geometric phase θ_1'. The relative statistics between holes with quantum numbers h and q and holes with quantum numbers h' and q' is then specified by the relative statistical phase $\vartheta' = \theta_1' - \theta_1$. For $\vartheta' = 0$, the two hole types have trivial relative statistics, while for $\vartheta' \neq 0$, the two hole types have anyonic relative statistics. Importantly, the relative statistical phase ϑ' is symmetric in the two hole types: it does not depend on which one is kept stationary and which one is moved around the loop.

We first notice that the two looping processes giving the phases θ_1 and θ_1' are not both possible for all combinations of the quantum numbers. For mobile holes with $h = 1$, the exchange process and the looping process with no hole enclosed are barely possible, but the looping process with a stationary hole enclosed is impossible. Since these holes can move only around the plaquettes of particular stripes, there is no space for a stationary hole inside any loop they can possibly move around. This means that the mobile hole must have a trivial flux quantum number $h = 0$. On the other hand, the stationary hole can then only influence the hopping of the mobile hole if the stationary hole is connected to a string of excited bond fermions and the hopping of the mobile hole is sensitive to excited bond fermions. This corresponds to quantum numbers $h' = 1$ and $q' = \{0, 1\}$ for the stationary hole and quantum

numbers $h = 0$ and $q = 1$ for the mobile hole. In these cases, one hopping matrix element picks up a minus sign at the intersection point of the loop and the string of excited bond fermions [see Eq. (3.14)]. This implies that the relative statistical phase is $\vartheta' = \pi$, and therefore the two hole types have semionic relative statistics. In all other possible cases, the hopping of the mobile hole is not influenced by the stationary hole. This implies that the relative statistical phase is $\vartheta' = 0$, and therefore the two hole types have trivial relative statistics. The results for the relative statistics between the various hole types are summarized in Table 3.5.

Hole type		$h' = 0$		$h' = 1$	
		$q' = 0$	$q' = 1$	$q' = 0$	$q' = 1$
$h = 0$	$q = 0$	0	0	0	0
	$q = 1$	0	0	π	π
$h = 1$	$q = 0$	–	–	–	–
	$q = 1$	–	–	–	–

Table 3.5: Relative statistics between holes with quantum numbers h and q and holes with quantum numbers h' and q' from a process when the former hole type is moved around the latter hole type: $\vartheta' = 0$ indicates trivial statistics, $\vartheta' = \pi$ indicates semionic statistics, while there is no value if the process is impossible.

We can also interpret the relative statistics in terms of the elementary excitations bound to the holes. First, two bare holes or two identical elementary excitations have trivial relative statistics. Second, the relative statistics between a bare hole and an elementary excitation is trivial, while that between a flux and a fermion is semionic. As a result of these properties, the relative statistics between two identical holes and that between a bare hole and a composite hole is trivial, while that between two distinct composite holes is semionic. The entries of Table 3.5 can then be obtained, even the ones that correspond to impossible processes: the diagonal entries and the entries of the first row or the first column are $\vartheta' = 0$, while the remaining entries are $\vartheta' = \pi$. We finally remark that all of our results for the absolute and the relative particle statistics are consistent with the correspondence between the various hole types and the superselection sectors (see Table 3.3).

Chapter 4

Finite doping of the gapped phase

In this chapter, we again consider the gapped phase of the Kitaev honeycomb model, but now we aim to characterize the multi-particle ground state for a finite density of mobile holes. Given the different hole types discussed in the previous chapter, it is natural to ask which hole types appear in the multi-particle ground state and what their manifestations are in the physical properties at finite doping. Furthermore, the multi-particle ground state from our exact description can be compared with those obtained from related mean-field treatments.

The structure of this chapter is summarized as follows. In Sec. 4.1, we describe the multi-hole state representing a finite density of mobile holes, and determine the internal quantum numbers that correspond to the ground state. Depending on the model parameters, there are two complementary regimes with different hole types in the multi-hole ground state, and the different hopping dimensionalities of these hole types manifest themselves in an electrical conductivity that is either approximately isotropic or extremely anisotropic. We also discuss the effect of hole interactions on our conclusions in the two complementary regimes. In Sec. 4.2, we provide a qualitative description of the multi-hole ground state in the case when the bulk excitations are no longer negligible because the hole hopping amplitude becomes larger the bulk energy gap. In Sec. 4.3, we compare our results for the multi-hole ground state with those obtained from the most closely related mean-field treatment in Ref. [70], and discuss the main discrepancies between the two approaches.

4.1 Finite density of mobile holes

4.1.1 Non-interacting treatment

We now consider the Kitaev honeycomb model with a finite density of mobile holes. The hole density $\rho = n/2N$ gives the fraction of sites l that are hole sites $l \in \Delta$. For simplicity, we assume a small hole density $\rho \ll 1$ and neglect any hole interactions. The ground state of the model is then a multi-hole state of n non-interacting holes: depending on their particle statistics, these holes either form a Bose condensate or fill up a Fermi sea. By evaluating the multi-hole energy for all combinations of $h = \{0, 1\}$ and $q = \{0, 1\}$, we can determine the ground-state quantum numbers.

The most straightforward way to represent the multi-hole state is to use appropriate single-hole creation and annihilation operators. If the operator $a^{(\dagger)}_{h,q,p}(\mathbf{R}_l)$ annihilates (creates) a hole at site l with quantum numbers h, q, and p, the multi-hole state of n stationary holes at sites $\Delta = \{l_j\}$ with quantum numbers $\{h_j\}$, $\{q_j\}$, and $\{p_j\}$ is given by

$$|\Omega^{\Delta}_{h,q,p}\rangle = \prod_{j=1}^{n} a^{\dagger}_{h_j,q_j,p_j}(\mathbf{R}_{l_j})\,|\Omega\rangle, \tag{4.1}$$

where $|\Omega\rangle$ is the ground state of the model with no holes, and the lattice position $\mathbf{R}_l = (X_l, Y_l)$ of the site l is measured in units of the lattice constant. We now assume and later verify that holes with distinct flux quantum numbers $h = \{0, 1\}$ are not simultaneously present in this multi-hole state. Since Table 3.5 shows that no anyonic relative statistics manifests itself between holes with identical flux quantum numbers, the single-hole operators $a^{(\dagger)}_{h,q,p}(\mathbf{R}_l)$ can then be treated as standard bosonic and fermionic operators. In particular, they satisfy bosonic commutation relations in the case of $h = 0$ and $q = 1$, and fermionic anticommutation relations in all other cases, except for an overall hard-core constraint that there can be at most one hole of any type at each site. However, if the hole density ρ is sufficiently small, this hard-core constraint is practically irrelevant. We can then write an effective Hamiltonian for the model with n mobile holes in terms of the standard bosonic and fermionic operators $a^{(\dagger)}_{h,q,p}(\mathbf{R}_l)$. In the absence of hole interactions, this Hamiltonian is quadratic: it

contains an onsite potential term corresponding to the flux-binding energy discussed in Sec. 3.1.2 and several hopping terms corresponding to the hopping problems in Fig. 3.6. Taking the isolated dimer limit and keeping only the lowest-order terms in $J \ll 1$, the effective Hamiltonian takes the form

$$\begin{aligned} H_a &= \Gamma_0 - \frac{9J^8}{1024} \sum_l \sum_{q,p} \hat{n}_{1,q,p}(\mathbf{R}_l) \\ &\quad - \frac{t}{2} \sum_{l\in A} \sum_{\alpha=x,y} \sum_{h,q,p} \left[a^\dagger_{h,q,p}(\mathbf{R}_l)\, a_{h,q,p}(\mathbf{R}_{\alpha(l)}) + \text{H.c.} \right] \\ &\quad - t \sum_{l\in A} \sum_p \left[a^\dagger_{0,0,p}(\mathbf{R}_l)\, a_{0,0,p}(\mathbf{R}_{z(l)}) + \text{H.c.} \right] \\ &\quad - \frac{3J^4\, t}{16} \sum_{l\in A} \sum_p \left[a^\dagger_{0,1,p}(\mathbf{R}_l)\, a_{0,1,p}(\mathbf{R}_{z(l)}) + \text{H.c.} \right] \\ &\quad - t \sum_{l\in A'} \sum_p \left[a^\dagger_{1,0,p}(\mathbf{R}_l)\, a_{1,0,p}(\mathbf{R}_{z(l)}) + \text{H.c.} \right] \\ &\quad - t \sum_{l\in A''} \sum_p \left[a^\dagger_{1,1,p}(\mathbf{R}_l)\, a_{1,1,p}(\mathbf{R}_{z(l)}) + \text{H.c.} \right], \end{aligned} \tag{4.2}$$

where Γ_0 is the ground-state energy of the model with n stationary $h = 0$ holes, and $\hat{n}_{h,q,p}(\mathbf{R}_l) \equiv a^\dagger_{h,q,p}(\mathbf{R}_l) a_{h,q,p}(\mathbf{R}_l)$ is the number operator. The fixed total number of holes is enforced by the constraint $n = \sum_l \sum_{h,q,p} \langle \hat{n}_{h,q,p}(\mathbf{R}_l) \rangle$. Note that the coefficients of the hopping terms in Eq. (4.2) are the hopping amplitudes in Fig. 3.6: those along the bonds marked by dashed lines are given by Eq. (3.19), while those along the bonds marked by dotted lines are exactly zero. Since the hopping problems for $h = 1$ holes break the translational symmetry of the lattice, it is necessary to divide each sublattice A and B into two further sublattices: $A = A' \cup A''$ and $B = B' \cup B''$, where sites in the sublattices A' and B' are pairwise connected by z bonds within even stripes, and sites in the sublattices A'' and B'' are pairwise connected by z bonds within odd stripes.

The Hamiltonian in Eq. (4.2) is quadratic, and therefore it becomes diagonal after an appropriate transformation of the single-hole operators $a^{(\dagger)}_{h,q,p}(\mathbf{R}_l)$. Due to the translational symmetry of the hopping problems, the new single-hole operators

$\tilde{a}^{(\dagger)}_{h,q,p}(\mathbf{K},\nu)$ are labeled with the lattice momentum $\mathbf{K}=(K_X,K_Y)$ conjugate to the lattice position $\mathbf{R}=(X,Y)$. In terms of the original real-space operators, these new momentum-space operators can be written as

$$\begin{aligned}
\tilde{a}_{0,q,p}(\mathbf{K},\nu) &= \frac{1}{\sqrt{N}}\sum_{l\in A}\Big[\beta^{A}_{0,q}(\mathbf{K},\nu)\,a_{0,q,p}(\mathbf{R}_l)\,e^{-i\mathbf{K}\cdot\mathbf{R}_l} \\
&\quad + \beta^{B}_{0,q}(\mathbf{K},\nu)\,a_{0,q,p}(\mathbf{R}_{z(l)})\,e^{-i\mathbf{K}\cdot\mathbf{R}_{z(l)}}\Big], \\
\tilde{a}_{1,q,p}(\mathbf{K},\nu) &= \sqrt{\frac{2}{N}}\sum_{l\in A'}\Big[\beta^{A'}_{1,q}(\mathbf{K},\nu)\,a_{1,q,p}(\mathbf{R}_l)\,e^{-i\mathbf{K}\cdot\mathbf{R}_l} \\
&\quad + \beta^{B'}_{1,q}(\mathbf{K},\nu)\,a_{1,q,p}(\mathbf{R}_{z(l)})\,e^{-i\mathbf{K}\cdot\mathbf{R}_{z(l)}} \\
&\quad + \beta^{A''}_{1,q}(\mathbf{K},\nu)\,a_{1,q,p}(\mathbf{R}_{x(z(l))})\,e^{-i\mathbf{K}\cdot\mathbf{R}_{x(z(l))}} \\
&\quad + \beta^{B''}_{1,q}(\mathbf{K},\nu)\,a_{1,q,p}(\mathbf{R}_{y(l)})\,e^{-i\mathbf{K}\cdot\mathbf{R}_{y(l)}}\Big],
\end{aligned} \tag{4.3}$$

where the coefficients $\beta_{h,q}(\mathbf{K},\nu)\sim 1$ for the different sublattices distinguish two bands $\nu=\{1,2\}$ in the case of $h=0$ and four bands $\nu=\{1,2,3,4\}$ in the case of $h=1$. In terms of the momentum-space operators $\tilde{a}^{(\dagger)}_{h,q,p}(\mathbf{K},\nu)$, the Hamiltonian in Eq. (4.2) takes the free-particle form

$$H_a=\Gamma_0+\sum_{h,q,p}\sum_{\mathbf{K},\nu}\Lambda_{h,q}(\mathbf{K},\nu)\,\tilde{n}_{h,q,p}(\mathbf{K},\nu), \tag{4.4}$$

where $\tilde{n}_{h,q,p}(\mathbf{K},\nu)\equiv\tilde{a}^{\dagger}_{h,q,p}(\mathbf{K},\nu)\tilde{a}_{h,q,p}(\mathbf{K},\nu)$ is the number operator in momentum space. The corresponding constraint enforcing the total number of holes is then $n=\sum_{h,q,p}\sum_{\mathbf{K},\nu}\langle\tilde{n}_{h,q,p}(\mathbf{K},\nu)\rangle$.

To evaluate the multi-hole energy as the expectation value of the Hamiltonian in Eq. (4.4), we must know the energies $\Lambda_{h,q}(\mathbf{K},\nu)$ and the occupation numbers $\langle\tilde{n}_{h,q,p}(\mathbf{K},\nu)\rangle$ of the single-hole states. In the ground state of the model, holes occupy only the lowest-energy single-hole states, and it is therefore enough to determine the single-hole energy $\Lambda_{h,q}(\mathbf{K},\nu)$ around its overall minimum. On the other hand, the overall minimum of $\Lambda_{h,q}(\mathbf{K},\nu)$ in the lowest band $\nu=1$ is at zero momentum because the hopping amplitudes in Fig. 3.6 are all non-positive. Expanding $\Lambda_{h,q}(\mathbf{K},1)$ up to quadratic order in the momentum around $\mathbf{K}=\mathbf{0}$, and keeping the lowest-order terms

in $J \ll 1$, the single-hole dispersion relations for the different quantum numbers are

$$\begin{aligned}
\Lambda_{0,0}(\mathbf{K},1) &= \left[-2+\frac{3K_X^2}{8}+\frac{9K_Y^2}{16}\right]t, \\
\Lambda_{0,1}(\mathbf{K},1) &= \left[-1+\frac{3K_X^2}{8}+\frac{27J^4K_Y^2}{128}\right]t, \\
\Lambda_{1,q}(\mathbf{K},1) &= -\frac{9J^8}{1024}+\left[-\frac{1+\sqrt{5}}{2}+\frac{3K_X^2}{4\sqrt{5}}\right]t.
\end{aligned} \tag{4.5}$$

Since $h = 1$ holes are not allowed to hop at all between their stripes, their dispersion relation is independent of the component K_Y at all orders of the momentum.

When turning our attention to the corresponding occupation numbers $\langle \tilde{n}_{h,q,p}(\mathbf{K},1)\rangle$ around zero momentum, we assume that all holes in the multi-hole state have identical quantum numbers h and q. It is then crucial to notice that certain holes are bosons, while others are fermions. If the holes are bosons, they all occupy the zero-momentum state. For holes with $h = 0$ and $q = 1$, the average single-hole energy in the multi-hole state is then $\langle \Lambda_{0,1}(\mathbf{K},\nu)\rangle = -t$. If the holes are fermions, they fill up a Fermi sea around the zero-momentum state: each state inside the Fermi surface is occupied by two holes with different quantum numbers $p = \{0,1\}$, while the states outside the Fermi surface are unoccupied. For holes with $h = 0$ and $q = 0$, the equipotential curves are ellipses of similar half-axes. The Fermi sea is therefore an ellipse of half-axes $\Delta K_X \sim \Delta K_Y \sim \sqrt{\rho}$, and the average single-hole energy is $\langle \Lambda_{0,0}(\mathbf{K},\nu)\rangle = -2t + \kappa_1 t\rho$, where $\kappa_1 \sim 1$. For holes with $h = 1$ and $q = \{0,1\}$, the equipotential curves are lines parallel to the K_Y direction. The Fermi sea is therefore a strip of half-width $\Delta K_X \sim \rho$, and the average single-hole energy is $\langle \Lambda_{1,q}(\mathbf{K},\nu)\rangle = -9J^8/1024 - (1+\sqrt{5})t/2 + \kappa_2 t\rho^2$, where $\kappa_2 \sim 1$. The occupation numbers of the single-hole states for the different quantum numbers h and q are illustrated in Fig. 4.1, while the resulting average single-hole energies in the multi-hole state are summarized in Table 4.1.

We are now ready to identify the ground-state quantum numbers of the model. Since the total number of holes is fixed, the average single-hole energies $\langle \Lambda_{h,q}(\mathbf{K},\nu)\rangle$ for the different quantum numbers can be compared directly. Furthermore, the assumption of small hole density $\rho \ll 1$ means that the energies $\sim t\rho$ and $\sim t\rho^2$

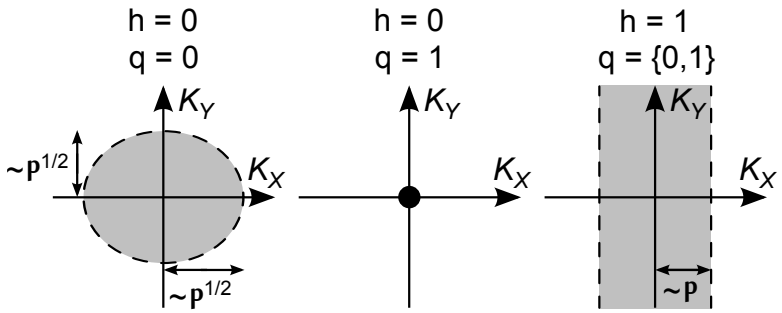

Figure 4.1: Occupations of the single-hole states for different combinations of the flux quantum number $h = \{0, 1\}$ and the fermion quantum number $q = \{0, 1\}$. In the bosonic case, the lowest-energy state of macroscopic occupation is marked by a black dot. In the fermionic cases, the Fermi sea states of constant occupation are marked by gray shading, while the Fermi surface separating occupied and unoccupied states is marked by a dashed line.

are negligible compared to the energies $\sim t$. The results in Table 4.1 then indicate two complementary regimes in the behavior of the model. In the first regime with $J^8 \ll t \ll J^4$, holes with $h = 0$ and $q = 0$ have the lowest average energy. This means that all holes in the ground state have quantum numbers $h = 0$ and $q = 0$. At each momentum $\mathbf{K}$ within the Fermi ellipse of Fig. 4.1, there are two holes with quantum numbers $p = \{0, 1\}$. In the second regime with $t \ll J^8$, holes with $h = 1$ and $q = \{0, 1\}$ have the lowest average energy. This means that all holes in the ground state have quantum numbers $h = 1$. At each momentum $\mathbf{K}$ within the Fermi strip of Fig. 4.1, there are four holes with quantum numbers $q = \{0, 1\}$ and $p = \{0, 1\}$. Note that our original assumption of no anyonic relative statistics is found to be self-consistent as all holes in the ground state are $h = 0$ holes in the first regime and $h = 1$ holes in the second regime.

Hole type		Average single-hole energy
$h = 0$	$q = 0$	$-2t + \kappa_1 t\rho$
	$q = 1$	$-t$
$h = 1$	$q = 0$	$-9J^8/1024 - (1 + \sqrt{5})t/2 + \kappa_2 t\rho^2$
	$q = 1$	

Table 4.1: Average single-hole energy $\langle \Lambda_{h,q}(\mathbf{K}, \nu) \rangle$ in the model containing a small density $\rho \ll 1$ of mobile holes with flux quantum numbers $h = \{0, 1\}$ and fermion quantum numbers $q = \{0, 1\}$.

Due to the distinct ground states, the model also has different physical properties in the two regimes. We consider the net magnetization and the electrical conductivities in the X and Y directions. The net magnetization is the sum of the local hole magnetizations $(-1)^{q+p}$ and is zero in both regimes because each hole with quantum numbers h, q, and p has a pair with quantum numbers h, q, and $1-p$. In terms of the partial densities $\rho_{h,q} = \sum_p \sum_{\mathbf{K}} \langle \tilde{n}_{h,q,p}(\mathbf{K},1)\rangle / 2N$ of the various hole types, the conductivities in the two directions are given by

$$\sigma^*_{X,Y} = e_*^2 \tau \sum_{h,q} \rho_{h,q} \left[\frac{\partial^2 \Lambda_{h,q}(\mathbf{K},1)}{\partial K^2_{X,Y}} \right]_{\mathbf{K}=\mathbf{0}}, \tag{4.6}$$

where e_* is the hole charge, and τ is the elastic scattering time. In the first regime with $J^8 \ll t \ll J^4$, the partial hole densities are $\rho_{0,0} = \rho$ and $\rho_{1,q} = \rho_{h,1} = 0$. Since the effective masses $[\partial^2 \Lambda_{0,0}(\mathbf{K},1)/\partial K^2_{X,Y}]^{-1}$ are similar in the X and Y directions, the conductivity is approximately isotropic: $\sigma^*_X \sim \sigma^*_Y \sim t\rho e_*^2 \tau$. In the second regime with $t \ll J^8$, the partial hole densities are $\rho_{1,q} = \rho/2$ and $\rho_{0,q} = 0$. Since the effective masses $[\partial^2 \Lambda_{1,q}(\mathbf{K},1)/\partial K^2_{X,Y}]^{-1}$ are finite in the X direction and infinite in the Y direction, the conductivity is extremely anisotropic: $\sigma^*_X \sim t\rho e_*^2 \tau$ and $\sigma^*_Y = 0$.

4.1.2 Mean-field treatment of interactions

We now consider hole interactions in the model with a small density $\rho \ll 1$ of mobile holes. To represent an interaction of strength $\Delta\Gamma_0$ between two holes at a relative lattice position $\mathbf{R} = \mathbf{R}_2 - \mathbf{R}_1$, we must add an appropriate quartic term to the Hamiltonian in Eq. (4.2). Considering only the Coulomb repulsion and the two attraction mechanisms discussed in Sec. 3.1.3, this quartic term takes the general form

$$\begin{aligned} \Delta H_a &= \Delta\Gamma_0 \sum_{\mathbf{R}_1} a^\dagger_{h_1,q_1',p_1}(\mathbf{R}_1)\, a^\dagger_{h_2,q_2',p_2}(\mathbf{R}_1+\mathbf{R}) \\ &\quad \times a_{h_2,q_2,p_2}(\mathbf{R}_1+\mathbf{R})\, a_{h_1,q_1,p_1}(\mathbf{R}_1). \end{aligned} \tag{4.7}$$

The flux quantum numbers $h_{1,2}$ and the plaquette quantum numbers $p_{1,2}$ are conserved by such a general hole interaction, while the fermion quantum numbers $q_{1,2} \neq q'_{1,2}$ satisfy the relation $q'_1 + q'_2 = q_1 + q_2$ modulo 2 so that the global constraint $\sum_j q_j = \text{even}$ is not violated.

Since the flux quantum numbers are conserved, the two complementary regimes found in Sec. 4.1.1 remain applicable in the presence of hole interactions: all holes in the ground state have quantum numbers $h = 0$ in the first regime with $J^8 \ll t \ll J^4$, while they all have quantum numbers $h = 1$ in the second regime with $t \ll J^8$. We can then consider the two regimes independently from each other with only $h \equiv h_{1,2} = 0$ holes in the first regime and only $h \equiv h_{1,2} = 1$ holes in the second regime. On the other hand, this means that our assumption of no anyonic relative statistics remains self-consistent in the presence of hole interactions. Expressing the real-space operators $a^{(\dagger)}_{h,q,p}(\mathbf{R}_l)$ in terms of the momentum-space operators $\tilde{a}^{(\dagger)}_{h,q,p}(\mathbf{K},\nu)$, and considering only the lowest band $\nu = 1$, the quartic term in Eq. (4.7) becomes

$$\begin{aligned}\Delta H_a &= \frac{\Delta\Gamma_0}{N}\sum_{\mathbf{K}_1,\mathbf{K}_2,\mathbf{K}'} \Upsilon_{h,\hat{q}}(\mathbf{K})\, e^{i\mathbf{K}'\cdot\mathbf{R}}\; \tilde{a}^{\dagger}_{h,q_1',p_1}(\mathbf{K}_1+\mathbf{K}') \\ &\quad\times \tilde{a}^{\dagger}_{h,q_2',p_2}(\mathbf{K}_2-\mathbf{K}')\, \tilde{a}_{h,q_2,p_2}(\mathbf{K}_2)\, \tilde{a}_{h,q_1,p_1}(\mathbf{K}_1), \end{aligned} \tag{4.8}$$

where $\tilde{a}^{(\dagger)}_{h,q,p}(\mathbf{K}) \equiv \tilde{a}^{(\dagger)}_{h,q,p}(\mathbf{K},1)$, and the quantity $\Upsilon_{h,\hat{q}}(\mathbf{K}) \sim 1$ with $\hat{q} \equiv \{q_1, q_2, q_1', q_2'\}$ depends on the coefficients $\beta_{h,q}(\mathbf{K}) \equiv \beta_{h,q}(\mathbf{K},1) \sim 1$ for the different sublattices.

The behavior of the model is influenced by hole interactions in several ways. We aim to specify the extent of applicability of the results in Sec. 4.1.1 for the ground-state quantum numbers and the corresponding physical properties. To this end, we investigate how hole interactions renormalize the average single-hole energies in Table 4.1 as a function of the partial hole densities $\rho_{h,q}$. In practice, we apply a standard mean-field decomposition to the Hamiltonian: each quartic term in Eq. (4.8) is decomposed into two constituent quadratic terms, and each quadratic term is coupled to the expectation value of the other one. The single-hole energies $\Lambda_{h,q}(\mathbf{K}) \equiv \Lambda_{h,q}(\mathbf{K},1)$ in Eq. (4.4) are then renormalized by the mean-field decomposition of any quartic term that is a product of two number operators $\tilde{n}_{h,q,p}(\mathbf{K}) \equiv \tilde{n}_{h,q,p}(\mathbf{K},1)$. In general, if we keep all such quartic terms in Eq. (4.8), and include all the equivalent quartic terms that differ only in their conserved plaquette quantum numbers $p_{1,2}$, the resulting mean-field decomposition takes the approximate form

$$\Delta\tilde{H}_a \sim \frac{\Delta\Gamma_0}{N}\sum_{\mathbf{K}_1,\mathbf{K}_2}\Big[\langle\tilde{n}_{h,q_1}(\mathbf{K}_1)\rangle\, \tilde{n}_{h,q_2}(\mathbf{K}_2) + \langle\tilde{n}_{h,q_2}(\mathbf{K}_2)\rangle\, \tilde{n}_{h,q_1}(\mathbf{K}_1)\Big], \tag{4.9}$$

where $\tilde{n}_{h,q}(\mathbf{K}) \equiv \sum_p \tilde{n}_{h,q,p}(\mathbf{K})$. Since $\rho = \sum_{h,q} \rho_{h,q}$ and $\sum_{\mathbf{K}} \langle \tilde{n}_{h,q}(\mathbf{K}) \rangle = 2N\rho_{h,q}$, the single-hole energies in Eq. (4.4) are renormalized by $\Delta\Lambda_{h,q}(\mathbf{K}) \sim \Delta\Gamma_0\, \rho$.

4.1.2.1 First regime: $J^8 \ll t \ll J^4$

In the first regime with $J^8 \ll t \ll J^4$, all holes in the ground state have flux quantum numbers $h = 0$, and therefore all quartic terms in Eq. (4.7) have $h \equiv h_{1,2} = 0$. In the region around zero momentum occupied by holes, the coefficients $\beta_{0,q}(\mathbf{K})$ for the two sublattices A and B are

$$\begin{aligned} \beta^A_{0,0}(\mathbf{K}) &= \frac{1}{\sqrt{2}}\,, \qquad & \beta^B_{0,0}(\mathbf{K}) &= \frac{1}{\sqrt{2}}\, e^{iK_Y/4}, \\ \beta^A_{0,1}(\mathbf{K}) &= \frac{1}{\sqrt{2}}\,, \qquad & \beta^B_{0,1}(\mathbf{K}) &= \frac{1}{\sqrt{2}}\, e^{-iK_Y/2}. \end{aligned} \tag{4.10}$$

Furthermore, the total hole density is $\rho = \rho_{0,0} + \rho_{0,1}$ in terms of the respective partial hole densities $\rho_{h,q}$.

It is instructive to first consider hole interactions that conserve the fermion quantum numbers $q_{1,2} = q'_{1,2}$ and are also independent of them. Hole interactions of this type include the Coulomb repulsion and the first attraction mechanism of Sec. 3.1.3. In this case, each quartic term in Eq. (4.8) with $\mathbf{K}' = \mathbf{0}$ is a product of two number operators. Keeping only the terms with $\mathbf{K}' = \mathbf{0}$, using that $\Upsilon_{0,\hat{q}}(\mathbf{K}) = 1/4$ for all such terms, and summing over the quantum numbers $q_{1,2}$ and $p_{1,2}$, the mean-field decomposition becomes

$$\Delta\tilde{H}_a = \frac{\Delta\Gamma_0}{4N} \sum_{q_1,q_2} \sum_{\mathbf{K}_1,\mathbf{K}_2} \Big[\langle \tilde{n}_{0,q_1}(\mathbf{K}_1) \rangle\, \tilde{n}_{0,q_2}(\mathbf{K}_2) + \langle \tilde{n}_{0,q_2}(\mathbf{K}_2) \rangle\, \tilde{n}_{0,q_1}(\mathbf{K}_1) \Big]. \tag{4.11}$$

Since $\sum_q \sum_{\mathbf{K}} \langle \tilde{n}_{0,q}(\mathbf{K}) \rangle = 2N\rho$ for both equivalent terms inside its square brackets, Eq. (4.11) reduces to

$$\Delta\tilde{H}_a = \Delta\Gamma_0\, \rho \sum_q \sum_{\mathbf{K}} \tilde{n}_{0,q}(\mathbf{K}). \tag{4.12}$$

From a comparison between Eqs. (4.4) and (4.12), we conclude that the single-hole energies for $h = 0$ and $q = \{0, 1\}$ are renormalized by $\Delta\Lambda_{0,q}(\mathbf{K}) = \Delta\Gamma_0\, \rho$. Since this energy depends only on the total hole density ρ, it corresponds to a constant shift

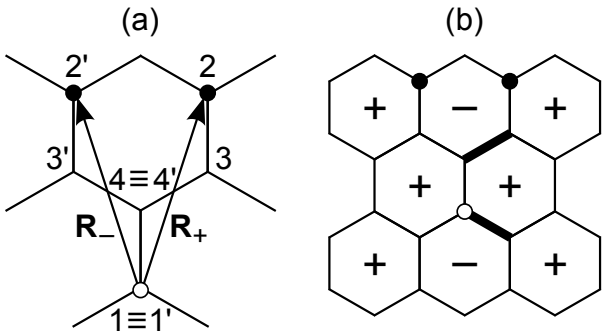

Figure 4.2: (a) Site labeling convention around two interacting holes (white and black dots) at the relative lattice positions $\mathbf{R}_\pm$. (b) Bond fermion sector around the same two holes when fluxes are bound to them: it is labeled with the excited bond fermions (thick lines) and the corresponding plaquette operator eigenvalues (± 1).

for all the single-hole energies. This means that the results for the ground state in Sec. 4.1.1 are not affected by hole interactions of this type.

Importantly, the second attraction mechanism of Sec. 3.1.3 switches the fermion quantum numbers $q_{1,2} = 1 - q'_{1,2}$. It is therefore represented by quartic terms in Eq. (4.8) where either $q_1 = q_2$ and $q'_1 = q'_2$ or $q_1 = q'_2$ and $q'_1 = q_2$. In the first case, the quartic term is never a product of two number operators, while in the second case, it is a product of two number operators when $\mathbf{K}' = \mathbf{K}_2 - \mathbf{K}_1$. According to the discussion in Sec. 3.1.3, this interaction has the largest strength $|\Delta\Gamma_0| = 1$ when the two holes are at neighboring sites connected by a z bond, or equivalently, at a relative lattice position $\mathbf{R}_z = (0, 1)$. However, the two holes in this case have a mutual hole fermion, and therefore their fermion quantum numbers become ill-defined. If we require the fermion quantum numbers to be well-defined, the interaction has the largest strength $|\Delta\Gamma_0| = J$ when the two holes are at the relative lattice positions $\mathbf{R}_\pm = (\pm\sqrt{3}/2, 5/2)$ shown in Fig. 4.2. Setting $q_1 = q'_2 = \tilde{q}$ and $q'_1 = q_2 = 1 - \tilde{q}$, keeping only the terms with $\mathbf{K}' = \mathbf{K}_2 - \mathbf{K}_1$ for both relative positions $\mathbf{R}_\pm$, and summing over $\tilde{q}$ and $p_{1,2}$, the mean-field decomposition becomes

$$\begin{aligned} \Delta\tilde{H}_a &= \frac{1}{N}\sum_{\tilde{q}}\sum_{\mathbf{K}_1,\mathbf{K}_2}\sum_{\pm}\Delta\Gamma_0(\tilde{q},\pm)\,\Upsilon_{0,\hat{q}}(\mathbf{K})\,e^{i(\mathbf{K}_2-\mathbf{K}_1)\cdot\mathbf{R}_\pm} \\ &\quad\times\Big[\langle\tilde{n}_{0,\tilde{q}}(\mathbf{K}_1)\rangle\,\tilde{n}_{0,1-\tilde{q}}(\mathbf{K}_2) + \langle\tilde{n}_{0,1-\tilde{q}}(\mathbf{K}_2)\rangle\,\tilde{n}_{0,\tilde{q}}(\mathbf{K}_1)\Big], \end{aligned} \tag{4.13}$$

$$\Upsilon_{0,\hat{q}}(\mathbf{K}) = \begin{cases} \frac{1}{4} e^{i(\mathbf{K}_1+2\mathbf{K}_2)\cdot\mathbf{R}_z/4} & (\tilde{q}=0) \\ \frac{1}{4} e^{-i(2\mathbf{K}_1+\mathbf{K}_2)\cdot\mathbf{R}_z/4} & (\tilde{q}=1). \end{cases} \tag{4.14}$$

The four interaction strengths $\Delta\Gamma_0(\tilde{q},\pm)$ can be obtained by treating the Ising couplings $-J\sigma_l^x\sigma_{x(l)}^x$ and $-J\sigma_l^y\sigma_{y(l)}^y$ as perturbations around the isolated dimer limit. Using the site labeling convention in Fig. 4.2, the interaction strength in the case of $\tilde{q}=0$ for the relative position $\mathbf{R}_+$ is

$$\begin{aligned} \Delta\Gamma_0(0,+) &= +J\langle 0|f_1(ib_3^x c_3)(ib_4^x c_4)f_3^\dagger|0\rangle \\ &= -iJ\langle 0|\hat{u}_{3,4}f_1 c_3 c_4 f_3^\dagger|0\rangle = -Ju_{3,4} = -J, \end{aligned} \tag{4.15}$$

where an additional minus sign arises because the corresponding quartic term in Eq. (4.7) does not only transfer the bound matter fermion from $\mathbf{R}_2$ to $\mathbf{R}_1$ but also exchanges the two bare holes at $\mathbf{R}_{1,2}$. Note that $u_{l,\alpha(l)} = +1$ for all bonds because no bond fermions are excited. The interaction strength in the other case $\tilde{q}=1$ is the Hermitian conjugate of Eq. (4.15), while that for the other relative position $\mathbf{R}_-$ is equivalent to it via site relabeling, and thus $\Delta\Gamma_0(\tilde{q},\pm) = -J$ in both cases and for both relative positions. On the other hand, this implies that the mean-field decomposition in Eq. (4.13) becomes

$$\begin{aligned} \Delta\tilde{H}_a &= -\frac{J}{N}\sum_{\mathbf{K}_1,\mathbf{K}_2}\cos\left[\tfrac{\sqrt{3}}{2}\tilde{K}_X\right]\cos\left[\tfrac{9}{4}K_{1,Y}-3K_{2,Y}\right] \\ &\quad\times\Big[\langle\tilde{n}_{0,0}(\mathbf{K}_1)\rangle\,\tilde{n}_{0,1}(\mathbf{K}_2)+\langle\tilde{n}_{0,1}(\mathbf{K}_2)\rangle\,\tilde{n}_{0,0}(\mathbf{K}_1)\Big], \end{aligned} \tag{4.16}$$

where $\tilde{\mathbf{K}} = (\tilde{K}_X,\tilde{K}_Y) \equiv \mathbf{K}_1-\mathbf{K}_2$ is the relative lattice momentum. Since the original single-hole energies $\Lambda_{0,q}(\mathbf{K})$ in Eq. (4.5) and their renormalizations $\Delta\Lambda_{0,q}(\mathbf{K})$ resulting from Eq. (4.16) are both minimal for $\mathbf{K}_{1,2}=\mathbf{0}$, the smallest renormalized single-hole energies $\Lambda'_{0,q}(\mathbf{K}) \equiv \Lambda_{0,q}(\mathbf{K})+\Delta\Lambda_{0,q}(\mathbf{K})$ are obtained if holes occupy the single-hole states around zero momentum. By approximating $\sum_{\mathbf{K}}\psi(\mathbf{K})\langle\tilde{n}_{0,q}(\mathbf{K})\rangle$ with $\psi(\langle\mathbf{K}\rangle)\sum_{\mathbf{K}}\langle\tilde{n}_{0,q}(\mathbf{K})\rangle$ for any function $\psi(\mathbf{K})$ in terms of the respective central momenta $\langle\mathbf{K}_{1,2}\rangle=\mathbf{0}$, and using $\sum_{\mathbf{K}}\langle\tilde{n}_{0,q}(\mathbf{K})\rangle = 2N\rho_{0,q}$, Eq. (4.16) reduces to

$$\begin{aligned} \Delta\tilde{H}_a &= -2J\rho_{0,1}\sum_{\mathbf{K}}\cos\left[\tfrac{\sqrt{3}}{2}K_X\right]\cos\left[\tfrac{9}{4}K_Y\right]\tilde{n}_{0,0}(\mathbf{K}) \\ &\quad -2J\rho_{0,0}\sum_{\mathbf{K}}\cos\left[\tfrac{\sqrt{3}}{2}K_X\right]\cos\left[3K_Y\right]\tilde{n}_{0,1}(\mathbf{K}). \end{aligned} \tag{4.17}$$

From a comparison between Eqs. (4.4) and (4.17), we conclude that the single-hole energies for $h = 0$ and $q = \{0, 1\}$ are approximately renormalized by $\Delta\Lambda_{0,q}(\mathbf{0}) = -2J\rho_{0,1-q}$ in the region around zero momentum. If we keep only the leading-order terms in $\rho \ll 1$, the average single-hole energies in Table 4.1 are then given by $\langle\Lambda'_{0,0}(\mathbf{K})\rangle = -2t - 2J\rho_{0,1}$ and $\langle\Lambda'_{0,1}(\mathbf{K})\rangle = -t - 2J\rho_{0,0}$.

Assuming that the results for the ground state in Sec. 4.1.1 remain applicable so that $\rho_{0,0} = \rho$ and $\rho_{0,1} = 0$, the two average single-hole energies $\langle\Lambda'_{0,q}(\mathbf{K})\rangle$ become equal at the critical hole density $\rho = \rho_C = t/2J$. At subcritical densities $\rho < \rho_C$, we find that $\langle\Lambda'_{0,0}(\mathbf{K})\rangle < \langle\Lambda'_{0,1}(\mathbf{K})\rangle$ for all possible values of the partial densities $\rho_{0,q}$. This means that the ground-state values are $\rho_{0,0} = \rho$ and $\rho_{0,1} = 0$, and that the results in Sec. 4.1.1 indeed remain applicable. At supercritical densities $\rho > \rho_C$, there are equilibrium values of the partial densities $\rho_{0,q}$ at which $\langle\Lambda'_{0,0}(\mathbf{K})\rangle = \langle\Lambda'_{0,1}(\mathbf{K})\rangle$. By solving $\langle\Lambda'_{0,0}(\mathbf{K})\rangle = \langle\Lambda'_{0,1}(\mathbf{K})\rangle$ and $\rho = \rho_{0,0} + \rho_{0,1}$ for the two unknowns $\rho_{0,q}$, the ground-state partial densities are

$$\rho_{0,0} = \frac{1}{2}\left(\rho + \rho_C\right), \qquad \rho_{0,1} = \frac{1}{2}\left(\rho - \rho_C\right). \tag{4.18}$$

To summarize, only holes with $h = 0$ and $q = 0$ are present in the low-density limit $\rho \to 0$, while holes with $h = 0$ and $q = 1$ appear above the critical density $\rho = \rho_C$. Note that $\rho_C = t/2J$ is small due to $t \ll J$[4].

The subcritical and the supercritical regimes are also distinct in terms of their physical properties. At subcritical densities, the physical properties of the model are as discussed in Sec. 4.1.1, except for a renormalization of the effective masses and hence the electrical conductivities. At supercritical densities, the physical properties are changed in an essential way by the presence of holes with $h = 0$ and $q = 1$. Since these holes are bosons, they all condense into the lowest-energy single-hole state at zero momentum. This condensation then leads to charged superfluid behavior in the presence of the Coulomb repulsion. Furthermore, due to the coherent condensation of both $p = 0$ and $p = 1$ holes, the model spontaneously develops a net magnetization.

4.1.2.2 Second regime: $t \ll J^8$

In the second regime with $t \ll J^8$, all holes in the ground state have flux quantum numbers $h = 1$, and therefore all quartic terms in Eq. (4.7) have $h \equiv h_{1,2} = 1$. The coefficients $\beta_{1,q}(\mathbf{K})$ for the four sublattices A', B', A'', and B'' are

$$\begin{aligned}
\beta_{1,0}^{A'}(\mathbf{K}) &= \beta_{1,1}^{A''}(\mathbf{K}) = \xi_1(K_X), \\
\beta_{1,0}^{B'}(\mathbf{K}) &= \beta_{1,1}^{B''}(\mathbf{K}) = \xi_1(K_X)\, e^{iK_Y}, \\
\beta_{1,0}^{A''}(\mathbf{K}) &= \beta_{1,1}^{A'}(\mathbf{K}) = \xi_2(K_X)\, e^{3iK_Y/2}, \\
\beta_{1,0}^{B''}(\mathbf{K}) &= \beta_{1,1}^{B'}(\mathbf{K}) = \xi_2(K_X)\, e^{-iK_Y/2},
\end{aligned} \tag{4.19}$$

where $\xi_{1,2}(K_X) \in \mathbb{R}$, and $\xi_1^2(K_X)+\xi_2^2(K_X) = 1/2$. Furthermore, the total hole density is $\rho = \rho_{1,0} + \rho_{1,1}$ in terms of the respective partial hole densities $\rho_{h,q}$.

We first notice that the mean-field decomposition of a hole interaction that is independent of the conserved fermion quantum numbers $q_{1,2}$ no longer takes the form of Eq. (4.12). Since $\Upsilon_{1,\hat{q}}(\mathbf{K})$ is not $1/4$ for all quartic terms with $\mathbf{K}' = \mathbf{0}$ in Eq. (4.8), the renormalizations $\Delta\Lambda_{1,q}(\mathbf{K})$ of the single-hole energies become dependent on the individual partial hole densities $\rho_{1,q}$. If we consider the Coulomb repulsion and the first attraction mechanism of Sec. 3.1.3 for all relative lattice positions $\mathbf{R}$, the single-hole energies in Eq. (4.4) are renormalized by $\Delta\Lambda_{1,q}(\mathbf{K}) = \Delta\Gamma_0'\,\rho_{1,q} + \Delta\Gamma_0''\,\rho_{1,1-q}$, where the exact values of $\Delta\Gamma_0'$ and $\Delta\Gamma_0''$ depend on the detailed form of the Coulomb repulsion. In the case of $\Delta\Gamma_0' > \Delta\Gamma_0''$, the partial hole densities remain $\rho_{1,0} = \rho_{1,1} = \rho/2$, while in the case of $\Delta\Gamma_0' < \Delta\Gamma_0''$, the partial hole densities become either $\rho_{1,0} = \rho$ and $\rho_{1,1} = 0$ or $\rho_{1,0} = 0$ and $\rho_{1,1} = \rho$. We assume the first case in the following so that there are equal densities of $q = 0$ and $q = 1$ holes in the ground state.

For the second attraction mechanism of Sec. 3.1.3 at the relative lattice positions $\mathbf{R}_\pm$, the mean-field decomposition takes the form of Eq. (4.13) with $\Upsilon_{1,\hat{q}}(\mathbf{K}) = \frac{1}{4}\Xi(K_X)e^{i(\mathbf{K}_2-\mathbf{K}_1)\cdot\mathbf{R}_z/2}$ and $\Xi(K_X) = 16\xi_1(K_{1,X})\xi_2(K_{1,X})\xi_1(K_{2,X})\xi_2(K_{2,X})$. Since Fig. 4.2 shows that $u_{3,4} = -1$ and $u_{3',4'} = +1$, the interaction strengths are $\Delta\Gamma_0(\tilde{q},\pm) = \pm J$.

On the other hand, this implies that mean-field decomposition becomes

$$\begin{aligned}\Delta\tilde{H}_a &= -\frac{J}{N}\sum_{\mathbf{K}_1,\mathbf{K}_2}\Xi(K_X)\,\sin\left[\tfrac{\sqrt{3}}{2}\tilde{K}_X\right]\sin\left[3\tilde{K}_Y\right] \\ &\quad\times\Big[\langle\tilde{n}_{1,0}(\mathbf{K}_1)\rangle\,\tilde{n}_{1,1}(\mathbf{K}_2)+\langle\tilde{n}_{1,1}(\mathbf{K}_2)\rangle\,\tilde{n}_{1,0}(\mathbf{K}_1)\Big].\end{aligned} \tag{4.20}$$

Unlike the original single-hole energies $\Lambda_{1,q}(\mathbf{K})$ in Eq. (4.5), their renormalizations $\Delta\Lambda_{1,q}(\mathbf{K})$ resulting from Eq. (4.20) are not minimal for $\mathbf{K}_1=\mathbf{K}_2=\mathbf{0}$. We therefore must determine the ground-state occupations of the single-hole states that correspond to the smallest renormalized single-hole energies $\Lambda'_{1,q}(\mathbf{K})\equiv\Lambda_{1,q}(\mathbf{K})+\Delta\Lambda_{1,q}(\mathbf{K})$. Exploiting the equivalence between $q=0$ holes at momenta $\mathbf{K}_1$ and $q=1$ holes at momenta $\mathbf{K}_2$, and noticing that both sine factors in Eq. (4.20) depend only on the relative momentum $\tilde{\mathbf{K}}\equiv\mathbf{K}_1-\mathbf{K}_2$, we conclude that the respective central momenta are related by $\langle\mathbf{K}\rangle=(\langle K_X\rangle,\langle K_Y\rangle)\equiv\langle\mathbf{K}_1\rangle=-\langle\mathbf{K}_2\rangle$, and minimize the single-hole energies with respect to $\langle\mathbf{K}\rangle$. Since $\Lambda_{1,q}(\mathbf{K})$ does not depend on the momentum component K_Y, the second sine factor in Eq. (4.20) can be maximized independently. In particular, its maximum $\sin[3\tilde{K}_Y]=+1$ corresponds to the ground-state value $\langle K_Y\rangle=\pi/12$. Furthermore, if we assume $\langle K_X\rangle\ll 1$, the first sine factor is approximately $\sqrt{3}\langle K_X\rangle$. Due to $\sum_{\mathbf{K}}\langle\tilde{n}_{1,q}(\mathbf{K})\rangle=2N\rho_{1,q}=N\rho$, the single-hole energies around the central momenta $\langle\mathbf{K}_{1,2}\rangle=\pm\langle\mathbf{K}\rangle$ are then renormalized by $\Delta\Lambda_{1,q}(\mathbf{K})\sim-J\rho\,\langle K_X\rangle$, and the average single-hole energies in Table 4.1 take the form

$$\langle\Lambda'_{1,q}(\mathbf{K})\rangle=C'(t,J)-\kappa_0 J\rho\,\langle K_X\rangle+\frac{3}{4\sqrt{5}}\,t\,\langle K_X\rangle^2, \tag{4.21}$$

where $C'(t,J)$ and $\kappa_0\sim 1$ are independent of $\langle K_X\rangle$. The minimum of $\langle\Lambda'_{1,q}(\mathbf{K})\rangle$ with respect to $\langle K_X\rangle$ corresponds to the ground-state value $\langle K_X\rangle\sim J\rho/t$. By approximating $\sum_{\mathbf{K}}\psi(\mathbf{K})\langle\tilde{n}_{1,q}(\mathbf{K})\rangle$ with $\psi(\langle\mathbf{K}\rangle)\sum_{\mathbf{K}}\langle\tilde{n}_{1,q}(\mathbf{K})\rangle$ for any function $\psi(\mathbf{K})$ in terms of the respective central momenta $\langle\mathbf{K}_{1,2}\rangle=\pm\langle\mathbf{K}\rangle$, and assuming $\langle K_X\rangle\sim J\rho/t\ll 1$, Eq. (4.20) reduces to

$$\Delta\tilde{H}_a=-\frac{J^2\rho^2}{t}\sum_q\sum_{\mathbf{K}}\tilde{\Xi}[K_X-(-1)^q\langle K_X\rangle]\cos\left\{3[K_Y-(-1)^q\langle K_Y\rangle]\right\}\tilde{n}_{1,q}(\mathbf{K}), \tag{4.22}$$

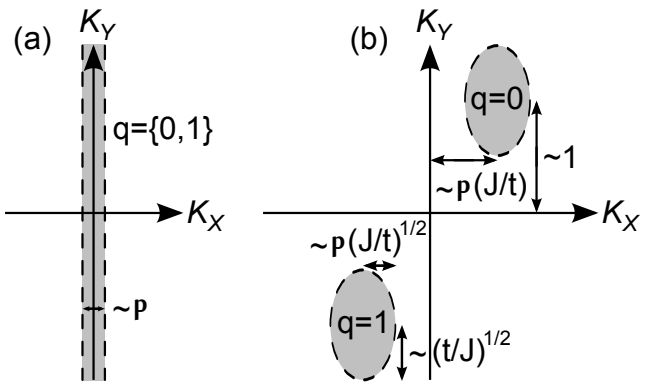

Figure 4.3: Single-hole states occupied by holes with quantum numbers $h = 1$ and $q = \{0, 1\}$ in the non-interacting treatment (a) and in the interacting treatment (b). Fermi sea states of constant occupation are marked by gray shading, while the Fermi surface separating occupied and unoccupied states is marked by a dashed line.

where $\tilde{\Xi}[K_X - (-1)^q \langle K_X \rangle] \sim 1$ contains all dependence on the momentum component K_X. Importantly, the renormalized single-hole energies $\Lambda'_{1,q}(\mathbf{K})$ resulting from Eq. (4.22) depend on the momentum component K_Y as well. In fact, the single-hole dispersion relations for $q = \{0, 1\}$ holes around their respective central momenta $\pm\langle \mathbf{K} \rangle$ are quadratic in both the K_X and the K_Y directions: the leading-order terms are $\sim t(K_X \mp \langle K_X \rangle)^2$ and $\sim J^2\rho^2(K_Y \mp \langle K_Y \rangle)^2/t$. This implies that the Fermi seas for the two hole types are ellipses of half-axes $\Delta K_X \sim \rho\sqrt{J/t}$ and $\Delta K_Y \sim \sqrt{t/J}$ centered at $\pm\langle \mathbf{K} \rangle$. Note that $\Delta K_Y \ll 1$ due to $t \ll J$[8] and that $\Delta K_X \sim \langle K_X \rangle \, \Delta K_Y \ll 1$ due to $\langle K_X \rangle \ll 1$ and $\Delta K_Y \ll 1$. Since our calculation is valid for any hole density $\rho > 0$, the Fermi strip described in Sec. 4.1.1 is unstable against an arbitrarily small hole interaction. The Fermi ellipses of the interacting treatment and the Fermi strip of the non-interacting treatment are contrasted in Fig. 4.3.

In terms of physical properties, the main difference with respect to the results in Sec. 4.1.1 is a finite electrical conductivity in the Y direction. The conductivities in the X and Y directions are still calculated by Eq. (4.6), except that we use the renormalized single-hole energies $\Lambda'_{1,q}(\mathbf{K})$ and take their second derivatives at the central momenta $\pm\langle \mathbf{K} \rangle$. Since the partial hole densities are $\rho_{1,q} = \rho/2$, and the second derivatives are $\partial^2\Lambda'_{1,q}(\mathbf{K})/\partial K_X^2 \sim t$ and $\partial^2\Lambda'_{1,q}(\mathbf{K})/\partial K_Y^2 \sim J^2\rho^2/t$, the conductivities

in the two directions take the respective forms

$$\sigma_X^* \sim t\rho e_*^2 \tau, \qquad \sigma_Y^* \sim \frac{J^2 \rho^3 e_*^2 \tau}{t}\,. \tag{4.23}$$

Note in particular that $\sigma_X^* \propto \rho$ and $\sigma_Y^* \propto \rho^3$. Since the ratio of the two conductivities is $\sigma_Y^*/\sigma_X^* \sim (J\rho/t)^2 \ll 1$, the model has a strong conductivity anisotropy that becomes weaker as we increase the hole density ρ.

4.2 Mobile holes beyond slow hopping

By relaxing the condition of slow hopping, we qualitatively describe the Kitaev honeycomb model with mobile holes in the regimes of intermediate hopping ($J^4 \ll t \ll 1$) and fast hopping ($t \gg 1$). We first consider a single isolated hole and investigate the applicability of the internal quantum numbers h, q, and p. Since the original definitions of these quantum numbers in Sec. 3.1.2 are in terms of the internal modes only, they are not applicable beyond the limit of slow hopping when the excitations in the bulk modes can no longer be neglected. In the regime of intermediate hopping when $t \gg E_P \sim J^4$, the bulk flux excitations are no longer negligible, and the hole is surrounded by a cloud of fluctuating fluxes. In the regime of fast hopping when $t \gg E_f \sim 1$, the bulk fermion excitations are no longer negligible, and the hole is also surrounded by a cloud of fluctuating fermions. On the other hand, the hole combined with these excitation clouds has a well-defined superselection sector that is conserved by the hopping process due to the locality of the exchange operator $\mathcal{E}_{l,l'}$. This means that the definitions of the quantum numbers h and q can be generalized in terms of their correspondence to these conserved superselection sectors. Furthermore, the only non-trivial terms in the exchange operator $\mathcal{E}_{l,l'}$ are the Heisenberg terms in Eq. (3.5) that conserve the product of dimer operators $\lambda_l = \sigma_l^z \sigma_{z(l)}^z$ and the products of plaquette operators W_P both in even stripes and in odd stripes (see Sec. 3.1.4). This means that the definitions of all quantum numbers h, q, and p can be generalized in terms of these products such that they are conserved by the hopping process: $(-1)^{q+p} = \prod_{l\in A} \lambda_l$, $(-1)^{h+p} = \prod_{P\in\eta} W_P$, and $(-1)^p = \prod_{P\in\mu} W_P$,

where each product is taken over a sufficiently large region that contains the clouds of fluctuating fluxes and fermions. The quantum numbers h, q, and p are then valid if the distances between holes exceed the radii of these excitation clouds.

To provide an upper bound on the radius of each excitation cloud, we notice that the fluctuating fluxes and fermions increase the potential energy and decrease the kinetic energy of the hole. This means that the two radii are determined by a balance between the potential and the kinetic energies. Since the excitation energy of a bulk flux is $E_P \sim J^4$ and that of a bulk fermion is $E_f \sim 1$, the increase in the potential energy is on the order of $R_P^2 E_P \sim R_P^2 J^4$ for a flux cloud of radius R_P and on the order of $R_f^2 E_f \sim R_f^2$ for a fermion cloud of radius R_f. On the other hand, since the decrease in the kinetic energy due to both excitation clouds is at most $\sim t$, the increase in the potential energy due to either excitation cloud must be bounded by $\lesssim t$. We therefore conclude that the upper bound on the flux cloud radius is $R_P \lesssim \sqrt{t/J^4}$ and that on the fermion cloud radius is $R_f \lesssim \sqrt{t}$.

We are now ready to investigate the ground-state quantum numbers h and q for a finite density of mobile holes. For simplicity, we consider the case of $J^4 \ll t \ll 1$ when only the plauqettes are fluctuating around the holes. To ensure that the quantum numbers h and q are valid, we assume a small hole density $\rho \ll R_P^{-2}$ and neglect any hole interactions. Since the hopping matrix elements are independent of the quantum numbers p, we also set $p = q$ for each hole without loss of generality. Due to the lack of broken dimers in the isolated dimer limit, the plaquette sector is then conserved by all hopping processes along z bonds. Since the hopping processes along x and y bonds either flip no plaquettes or two plaquettes in each of two neighboring stripes (see Fig. 3.4), this implies that the number of excited plaquettes has a conserved parity in each stripe. If there are an odd number of excited plaquettes in any stripe around any hole, the given hole can hop in the Y direction only if it leaves behind an excited plaquette in the given stripe. Since the kinetic energy decreases by $\sim t$ for each hole that can hop in the Y direction, this process happens spontaneously for $t \gg J^4$, and there remain an even number of excited plaquettes in each stripe around

each hole. Due to the relations $\prod_{P\in\eta} W_P = (-1)^{h+q}$ and $\prod_{P\in\mu} W_P = (-1)^q$, this means that any hole with quantum numbers other than $h = 0$ and $q = 0$ is unstable against a spontaneous decay into a hole with quantum numbers $h = 0$ and $q = 0$. Note that this result remains valid away from the isolated dimer limit and in the case of $t \gg 1$ when the fermions are also fluctuating. Holes with quantum numbers $h = 0$ and $q = 0$ are then energetically favorable because their hopping is the least constrained in the Y direction.

In conclusion, the quantum numbers h, q, and p generalize beyond the regime of slow hopping, but they are valid only for smaller hole densities due to the clouds of fluctuating excitations around holes. Furthermore, any hole with quantum numbers other than $h = 0$ and $q = 0$ is unstable against a spontaneous decay into a hole with quantum numbers $h = 0$ and $q = 0$. This means that all holes in the ground state have quantum numbers $h = 0$ and $q = 0$, and that the ground state is identical to that in the case of $J^8 \ll t \ll J^4$. The only difference is that there are clouds of fluctuating excitations around each hole. Importantly, when the hole density becomes $\rho \gtrsim R_{P,f}^{-2}$, the clouds of fluctuating fluxes (fermions) around different holes merge, and the holes hop in an entire lattice of fluctuating fluxes (fermions).

4.3 Comparison with mean-field results

4.3.1 Holes in the parton description

We now discuss the relation between our exact results for the Kitaev honeycomb model with mobile holes and the corresponding mean-field results in Ref. [70]. In their description, the physical operators $\mathbf{c}_{l,\uparrow}^{(\dagger)}$ and $\mathbf{c}_{l,\downarrow}^{(\dagger)}$ that annihilate (create) a spin-up and a spin-down particle at site l, respectively, are expressed in terms of the fermionic spinon operators $\mathbf{f}_{l,\uparrow}^{(\dagger)}$ and $\mathbf{f}_{l,\downarrow}^{(\dagger)}$ and the bosonic holon operators $\mathbf{b}_{l,1}^{(\dagger)}$ and $\mathbf{b}_{l,2}^{(\dagger)}$. The resulting relations between the physical operators and the parton (spinon and holon) operators can be summarized in the matrix form $\mathbf{C}_l = \mathbf{F}_l \cdot \mathbf{B}_l/\sqrt{2}$, where the

physical-operator matrix takes the form

$$\mathbf{C}_l = \begin{pmatrix} \mathbf{c}_{l,\uparrow} & -\mathbf{c}^\dagger_{l,\downarrow} \\ \mathbf{c}_{l,\downarrow} & \mathbf{c}^\dagger_{l,\uparrow} \end{pmatrix}, \tag{4.24}$$

while the spinon-operator and the holon-operator matrices are given by

$$\mathbf{F}_l = \begin{pmatrix} \mathbf{f}_{l,\uparrow} & -\mathbf{f}^\dagger_{l,\downarrow} \\ \mathbf{f}_{l,\downarrow} & \mathbf{f}^\dagger_{l,\uparrow} \end{pmatrix}, \qquad \mathbf{B}_l = \begin{pmatrix} \mathbf{b}^\dagger_{l,1} & -\mathbf{b}_{l,2} \\ \mathbf{b}^\dagger_{l,2} & \mathbf{b}_{l,1} \end{pmatrix}. \tag{4.25}$$

Importantly, the physical-operator matrix $\mathbf{C}_l$ is invariant under the combined gauge transformation $\mathbf{F}_l \to \mathbf{F}_l \cdot \mathbf{G}_l$ and $\mathbf{B}_l \to \mathbf{G}_l \cdot \mathbf{B}_l$ for any $\mathbf{G}_l \in \mathrm{SU}(2)$. Since a physical state $|\Phi\rangle$ should also be invariant under such an SU(2) gauge transformation at any site l, it must satisfy $\mathcal{K}^\alpha_l|\Phi\rangle = 0$ for all corresponding SU(2) generators $\mathcal{K}^\alpha_l$ with $\alpha = \{x, y, z\}$. If the spinon operators are related to the Majorana fermions introduced in Sec. 2.1.3 by $\mathbf{f}_{l,\uparrow} = (c_l + ib^z_l)/2$ and $\mathbf{f}_{l,\downarrow} = (ib^x_l - b^y_l)/2$, these SU(2) generators take the form [see Eq. (20) in Ref. [70]]

$$\mathcal{K}^\alpha_l = \frac{i}{4} b^\alpha_l c_l - \frac{i}{8} \sum_{\alpha_1,\alpha_2} \tilde{\epsilon}_{\alpha\alpha_1\alpha_2} b^{\alpha_1}_l b^{\alpha_2}_l - \frac{1}{2} \sum_{\zeta_1,\zeta_2} \mathbf{b}_{l,\zeta_1} \tilde{\sigma}^\alpha_{\zeta_1\zeta_2} \mathbf{b}^\dagger_{l,\zeta_2}, \tag{4.26}$$

where $\tilde{\sigma}^\alpha$ are the Pauli matrices, $\tilde{\epsilon}$ is the completely antisymmetric tensor, and the summations are over $\alpha_{1,2} = \{x, y, z\}$ and $\zeta_{1,2} = \{1, 2\}$. For a single site l, there are only three physical states: the empty hole state $|\times_l\rangle$, the spin-up particle state $|\uparrow_l\rangle$, and the spin-down particle state $|\downarrow_l\rangle$. The projection of any state in the parton description onto the physical subspace with $\mathcal{K}^\alpha_l = 0$ is then a superposition of $|\times_l\rangle$, $|\uparrow_l\rangle$, and $|\downarrow_l\rangle$. In terms of the parton operators, these three physical states are given by [see Eq. (18) in Ref. [70]]

$$\begin{aligned} |\times_l\rangle &= \frac{1}{\sqrt{2}} \left(\mathbf{b}^\dagger_{l,1} + \mathbf{b}^\dagger_{l,2} \mathbf{f}^\dagger_{l,\uparrow} \mathbf{f}^\dagger_{l,\downarrow} \right) |\mathbf{0}_l\rangle, \\ |\uparrow_l\rangle &= \mathbf{c}^\dagger_{l,\uparrow} |\times_l\rangle = \mathbf{f}^\dagger_{l,\uparrow} |\mathbf{0}_l\rangle, \\ |\downarrow_l\rangle &= \mathbf{c}^\dagger_{l,\downarrow} |\times_l\rangle = \mathbf{f}^\dagger_{l,\downarrow} |\mathbf{0}_l\rangle, \end{aligned} \tag{4.27}$$

where $|\mathbf{0}_l\rangle$ is the vacuum of the parton operators that is defined by $\mathbf{f}_{l,\uparrow}|\mathbf{0}_l\rangle = \mathbf{f}_{l,\downarrow}|\mathbf{0}_l\rangle = 0$ and $\mathbf{b}_{l,1}|\mathbf{0}_l\rangle = \mathbf{b}_{l,2}|\mathbf{0}_l\rangle = 0$. Note that these three states are indeed physical because they satisfy $\mathcal{K}^\alpha_l|\times_l\rangle = \mathcal{K}^\alpha_l|\uparrow_l\rangle = \mathcal{K}^\alpha_l|\downarrow_l\rangle = 0$ for all $\alpha = \{x, y, z\}$.

Before investigating the mean-field treatment, we consider a single stationary hole and aim to make a connection between its parton description and its internal quantum numbers h, q, and p. In the isolated dimer limit, there is an effective two-site system around the hole consisting of the hole site l and the neighboring site $l' = z(l)$. We assume $l \in A$ without loss of generality. Since there is a hole at site l and there is no hole at site l', one holon is excited at site l and no holon is excited at site l'. Due to the four spinons at sites l and l' that are either excited or not and the two holons at site l from which exactly one is excited, the Hilbert space of the two-site system in the parton description is then 32 dimensional. However, the physical Hilbert space of the two-site system is only 2 dimensional because it is spanned by the two physical states $|\times_l\rangle \otimes |\uparrow_{l'}\rangle$ and $|\times_l\rangle \otimes |\downarrow_{l'}\rangle$. This means that the projection of any state in the parton description onto the subspace with $\mathcal{K}_l^\alpha = \mathcal{K}_{l'}^\alpha = 0$ is a superposition of these two physical states. Since the effective Hamiltonian of the two-site system is $H = -b_l^z b_{l'}^z c_l c_{l'}$, its ground state has expectation values $\langle i b_l^z b_{l'}^z \rangle = \langle -i c_l c_{l'} \rangle = \pm 1$. In fact, there are 16 such ground states in the parton description that take the form

$$\begin{aligned} |\Psi_{\zeta,\pm}^{r_1,r_2}\rangle &= \left(1 \mp i \mathbf{f}_{l,\uparrow}^\dagger \mathbf{f}_{l',\uparrow}^\dagger\right) (\mathbf{f}_{l,\downarrow}^\dagger)^{r_1} (\mathbf{f}_{l',\downarrow}^\dagger)^{r_2} \mathbf{b}_{l,\zeta}^\dagger (|\mathbf{0}_l\rangle \otimes |\mathbf{0}_{l'}\rangle) \\ &= \left[(\mathbf{f}_{l,\downarrow}^\dagger)^{r_1} \mathbf{b}_{l,\zeta}^\dagger |\mathbf{0}_l\rangle\right] \otimes \left[(\mathbf{f}_{l',\downarrow}^\dagger)^{r_2} |\mathbf{0}_{l'}\rangle\right] \\ &\quad \mp i \left[\mathbf{f}_{l,\uparrow}^\dagger (-\mathbf{f}_{l,\downarrow}^\dagger)^{r_1} \mathbf{b}_{l,\zeta}^\dagger |\mathbf{0}_l\rangle\right] \otimes \left[\mathbf{f}_{l',\uparrow}^\dagger (\mathbf{f}_{l',\downarrow}^\dagger)^{r_2} |\mathbf{0}_{l'}\rangle\right], \end{aligned} \tag{4.28}$$

where $\zeta = \{1, 2\}$ and $r_{1,2} = \{0, 1\}$. On the other hand, the projection of the ground state $|\Psi_{\zeta,\pm}^{r_1,r_2}\rangle$ onto the subspace with $\mathcal{K}_l^\alpha = \mathcal{K}_{l'}^\alpha = 0$ is non-zero only if the overlap of $|\Psi_{\zeta,\pm}^{r_1,r_2}\rangle$ is non-zero with either of the two physical states $|\times_l\rangle \otimes |\uparrow_{l'}\rangle$ or $|\times_l\rangle \otimes |\downarrow_{l'}\rangle$. For $\zeta = 1$, we must choose $r_1 = 0$ and $r_2 = 1$, in which case the first term in Eq. (4.28) has a non-zero overlap with $|\times_l\rangle \otimes |\downarrow_{l'}\rangle$. For $\zeta = 2$, we must choose $r_1 = 1$ and $r_2 = 0$, in which case the second term in Eq. (4.28) has a non-zero overlap with $|\times_l\rangle \otimes |\uparrow_{l'}\rangle$. This means that the choice of exciting either $\mathbf{b}_{l,1}^\dagger$ or $\mathbf{b}_{l,2}^\dagger$ at the hole site l before the projection determines the local magnetization at the neighboring site $l' = z(l)$ after the projection. We therefore conclude that these two different choices correspond to different plaquette quantum numbers $p = \{0, 1\}$.

Since the two-site system around the hole has only two physical states that are distinguished by the plaquette quantum number p, the remaining quantum numbers h and q are necessarily determined by the spinons around the hole site. In the regime of slow hopping, the definitions of these quantum numbers in Sec. 3.1.2 are straightforward to express in terms of the Majorana fermions b_l^α and c_l, or equivalently, in terms of the spinon operators $\mathbf{f}_{l,\uparrow}^{(\dagger)}$ and $\mathbf{f}_{l,\downarrow}^{(\dagger)}$. Beyond the regime of slow hopping, the exact expressions become more complicated, but the general principle remains the same. For our purposes, it is enough to establish an intuitive picture from the general principle by using the interpretation in which the various hole types with different quantum numbers h and q have different kinds of elementary excitations bound to them. This interpretation has a simple translation in the parton description: some of the spinons around the hole site are bound to the holon at the hole site, and the quantum numbers h and q are determined by the structure of these bound spinons.

4.3.2 Mean-field treatment of the model

In the mean-field treatment of Ref. [70], the Hamiltonian of the model is first expressed in terms of the parton operators and then subjected to an appropriate mean-field decomposition. The resulting mean-field Hamiltonian of the model with a small density $\rho \ll 1$ of mobile holes takes the form [see Eqs. (24) and (25) in Ref. [70]]

$$\begin{aligned}
\tilde{H} \;=\; & \sum_{l\in A}\sum_{\alpha=x,y,z}\Bigg\{\Big[J_\alpha u_\alpha^\alpha - \frac{t}{4}\sum_{\zeta=1}^{2}\big(w_\alpha^\zeta + \text{c.c.}\big)\Big]\, ic_l c_{\alpha(l)} \\
& - \sum_{\alpha'=x,y,z}\Big[J_\alpha\delta_{\alpha,\alpha'}v_\alpha + \frac{t}{4}\sum_{\zeta=1}^{2}\big(w_\alpha^\zeta + \text{c.c.}\big)\Big]\, ib_l^{\alpha'}b_{\alpha(l)}^{\alpha'} \\
& + \frac{t}{4}\Big[v_\alpha - \sum_{\alpha'=x,y,z}u_\alpha^{\alpha'}\Big]\sum_{\zeta=1}^{2}\Big[i\mathbf{b}_{l,\zeta}^\dagger\mathbf{b}_{\alpha(l),\zeta} + \text{H.c.}\Big]\Bigg\} \\
& + \sum_l\sum_{\alpha=x,y,z}\tilde{\beta}_l^\alpha\mathcal{K}_l^\alpha - \tilde{\mu}\sum_l\sum_{\zeta=1}^{2}\mathbf{b}_{l,\zeta}^\dagger\mathbf{b}_{l,\zeta},
\end{aligned} \tag{4.29}$$

where $u_\alpha^{\alpha'}$, v_α, and w_α^ζ are the respective expectation values of the generalized bond fermion operators $\hat{u}_\alpha^{\alpha'} \equiv i b_l^{\alpha'} b_{\alpha(l)}^{\alpha'}$, the generalized matter fermion operators $\hat{v}_\alpha \equiv -i c_l c_{\alpha(l)}$, and the holon coherence operators $\hat{w}_\alpha^\zeta \equiv i \mathbf{b}_{l,\zeta}^\dagger \mathbf{b}_{\alpha(l),\zeta}$. The number constraint $\sum_l \sum_\zeta \langle \mathbf{b}_{l,\zeta}^\dagger \mathbf{b}_{l,\zeta} \rangle = 2N\rho$ is enforced by the chemical potential $\tilde{\mu}$, while the softened gauge constraint $\langle \mathcal{K}_l^\alpha \rangle = 0$ is enforced by the Lagrange multiplier $\tilde{\beta}_l^\alpha$ for all l and α. Importantly, the mean-field Hamiltonian in Eq. (4.29) is an extension of that in Ref. [70]. It is applicable to the gapped phase of the model, where the coupling strengths J_α are different: $J_z = 1$ and $J \equiv J_x = J_y \ll 1$.

The mean-field Hamiltonian in Eq. (4.29) can be solved by a self-consistent procedure in terms of the expectation values $u_\alpha^{\alpha'}$, v_α, and w_α^ζ. In the absence of holes ($\rho = 0$), there is a coupling of strength J_α between the bond fermion expectation value u_α^α and the matter fermion expectation value v_α along each bond of α type. Keeping only the lowest-order terms in $J \ll 1$, the self-consistent solutions for these expectation values are $u_\alpha^\alpha = v_z = 1$ and $v_x = v_y = J/2$. Note that the same expectation values are obtained from the exact solution of the model in Sec. 2.1. In the presence of holes ($\rho > 0$), the holons all condense into their lowest-energy state at zero momentum, and hence the holon coherence expectation values are $w_\alpha^\zeta \sim \rho$. This means that the original terms $J_\alpha u_\alpha^\alpha$ and $J_\alpha \delta_{\alpha,\alpha'} v_\alpha$ in the first two square brackets of Eq. (4.29) are in competition with new terms on the order of $t\rho$. The expectation values u_α^α and v_α for $\rho > 0$ are then close to those for $\rho = 0$ as long as these new terms are negligible with respect to the original terms. In particular, the bond fermion expectation values u_x^x and u_y^y remain close to 1 as long as $t\rho \ll J_{x,y} v_{x,y} \sim J^2$, while the bond fermion expectation value u_z^z and the matter fermion expectation value v_z remain close to 1 as long as $t\rho \ll J_z v_z, J_z u_z^z \sim 1$.

4.3.3 Discussion of ground-state properties

We are now ready to make a comparison between the mean-field ground state obtained from Eq. (4.29) and the exact ground state discussed in Secs. 4.1.1 and 4.2. Although there are general trends in the phase diagram of the model that are common to

both approaches, this comparison reveals several interesting discrepancies between the exact description and the mean-field treatment. In particular, there are two significant discrepancies concerning the internal degrees of freedom and the particle statistics of mobile holes.

The most important result of our exact study is that each hole has three internal degrees of freedom and that it can be characterized by three corresponding quantum numbers h, q, and p. The quantum number p describes a local magnetization around the hole, while the quantum numbers h and q capture the possibility of an elementary excitation (flux or fermion) being bound to it. The parton description in Ref. [70] incorporates the quantum number p via the introduction of two distinct holon species (see Sec. 4.3.1). However, the mean-field treatment is unable to represent the quantum numbers h and q: it ignores the possibility of bound states between holes and elementary excitations as it inherently neglects any correlations between these independent degrees of freedom.

In the regime of slow hopping, it is straightforward to verify explicitly that all holes in the mean-field ground state have quantum numbers $h = 0$ and $q = 0$ as they have no elementary excitations bound to them. Since $t \ll J^4$ and $\rho \ll 1$ in this regime, the conditions $t\rho \ll J^2$ and $t\rho \ll 1$ are both satisfied, and hence the mean-field expectation values u_α^α and v_α for $\rho > 0$ are close to those at $\rho = 0$. On the other hand, these expectation values are the same as those obtained from the exact solution of the undoped model. Since the exact ground state of the undoped model is free of elementary excitations by definition, the mean-field ground state of the doped model has no elementary excitations either. Note that the quantum numbers of the mean-field ground state are then consistent with those of the exact ground state in the case of $J^8 \ll t \ll J^4$ but not in the case of $t \ll J^8$ (see Sec. 4.1.1).

The particle statistics of the various hole types are further important results of our exact study. Unsurprisingly, the particle statistics depends on the quantum numbers h and q as the binding of an elementary excitation can lead to a statistical transmutation. Since only bare holes with $h = 0$ and $q = 0$ are captured by the mean-field

treatment, the relevant comparison is between the bare holes of the exact description and the holons of the mean-field treatment. We find a remarkable discrepancy in this respect: the bare holes of our exact study are fermions, while the holons of the parton description in Ref. [70] are bosons. It would then be interesting to resolve this discrepancy by considering a fermionic analogue of the mean-field treatment in Ref. [70]. For example, an appropriate transformation between spinful bosons and spinful fermions [79] could be used to relate the two species of bosonic holons and the fermionic bare holes with $p = \{0, 1\}$. Alternatively, an analysis going beyond the mean-field saddle point could provide the correct statistics.

Beyond the regime of slow hopping, we can compare the evolution of the mean-field ground state as a function of t, J, and ρ with our picture of the exact ground state where holes are surrounded by clouds of fluctuating excitations. In the mean-field treatment, there are two important characteristic scales of $t\rho$. First, the bond fermion expectation values u_x^x, u_y^y, and u_z^z are all close to 1 only for $t\rho \ll J^2$, and flux excitations then start appearing at $(t\rho)_P \sim J^2$. Second, the matter fermion expectation values v_z are close to 1 only for $t\rho \ll 1$, and fermion excitations then start appearing at $(t\rho)_f \sim 1$. In the language of the exact description in Sec. 4.2, the critical value $(t\rho)_{P,f}$ corresponds to the critical density at which the fluctuating fluxes (fermions) around different holes merge. If we assume that our upper bounds on the excitation cloud radii are good estimates so that $R_P \sim \sqrt{t/J^4}$ and $R_f \sim \sqrt{t}$, the corresponding critical values from Sec. 4.2 are $(t\rho)_P \sim J^4$ and $(t\rho)_f \sim 1$. These results have a simple interpretation: each kind of excitation starts appearing when the kinetic energy density $t\rho$ reaches its excitation energy. However, by using this interpretation, we obtain inconsistent values for the flux excitation energy as it is $E_P \sim J^4$ in the exact description and $E_P \sim J^2$ in the mean-field treatment. The reason for this inconsistency is that flux excitations do not appear explicitly in the mean-field treatment but instead are decoupled as independent bond fermion excitations.

Chapter 5

Single isolated hole in the gapless phase

In this chapter, we consider the gapless phase of the Kitaev honeycomb model, and aim to discuss the propagation of a single isolated hole. Unlike in the gapped phase, it is far from obvious whether the hole can be described by a coherent quasiparticle because there is a strong hybridization between the hole and the gapless excitations of the spin liquid. In fact, this kind of question is surprisingly delicate [80]: after the discovery of high-temperature superconductors and their relation to doped Mott insulators, it took more than a decade to establish that a single mobile hole in a two-dimensional antiferromagnet has a coherent quasiparticle description [17, 81, 82, 83, 84, 85, 86]. The analogous problem for a mobile hole in a gapless spin liquid has been recently studied by Trousselet *et al.* using exact diagonalization [87]. Within the limits of their calculation, they find that a fast hole with hopping amplitude $t \gg J_{x,y,z}$ is completely incoherent in the gapless phase of the Kitaev honeycomb model. Our study is complementary to theirs in two ways because we consider a slow hole with hopping amplitude $t \ll J_{x,y,z}$ and employ the exact solution of the model to obtain analytic results that are directly applicable in the thermodynamic limit.

To address the possibility of a coherent quasiparticle description, we must consider the single-hole spectral function $\mathcal{A}(\varepsilon, \mathbf{K})$, which is the imaginary part of the single-hole Green's function $\mathcal{G}(\varepsilon, \mathbf{K})$. Depending on the behavior of this quantity, there are two fundamentally distinct scenarios [17, 80, 86]. If the spectral function has a

delta-function peak at some hole energy ε, we can identify this peak as a signature of a coherent quasiparticle. In this scenario, the main quantity of interest is the spectral weight $\mathcal{Z} > 0$ of the quasiparticle peak, which typically appears at the lower edge of the spectrum. Furthermore, the quasiparticle energy ε as a function of the hole momentum $\mathbf{K}$ corresponds to a quasiparticle dispersion relation with an effective mass at the bottom of the resulting quasiparticle band [17]. If the spectral function has no such delta-function peak, the hole is completely incoherent with a vanishing quasiparticle weight $\mathcal{Z} = 0$, and therefore a coherent quasiparticle description is impossible. Nevertheless, the behavior of the spectral function is interesting at the lower edge of the spectrum as it often exhibits a power-law singularity with a non-trivial exponent that is indicative of spin-charge separation [86]. For example, this scenario is found in the case of the one-dimensional Hubbard model [6]. Importantly, the spectral function is also relevant from an experimental point of view as it can be measured directly by angle-resolved photoemission spectroscopy [88].

Since the Kitaev honeycomb model is not exactly solvable in the presence of a mobile hole, it is extremely hard to evaluate the single-hole spectral function $\mathcal{A}(\varepsilon, \mathbf{K})$ in general. To obtain a problem that is analytically tractable, we initially introduce two important simplifications. First, we restrict our attention to a special point in the gapless phase characterized by Ising coupling strengths $J_x = J_y = J_0$ and $J_z = 0$. At this point, the two-dimensional (2D) spin-liquid ground state of the undoped model breaks down into a set of one-dimensional (1D) gapless spin liquids. Second, instead of considering the actual ground state of the doped model containing a mobile hole ($t > 0$), we employ a variational approach using a single-parameter trial state that interpolates smoothly between the ground state of the doped model containing a stationary hole ($t \to 0$) and the ground state of the undoped model. The two limiting ground states are available via the exact solution of the model, and the best variational state in between is determined by a competition between the potential energy $E_J \propto J_0$ and the kinetic energy $E_t \propto t$. Discussing our results, we finally argue that they remain valid beyond the two simplifying assumptions.

The structure of this chapter is summarized as follows. In Sec. 5.1, we introduce the problem by defining the main quantities of interest, including the spectral function and the expectation values of the potential and the kinetic energies, and by explaining the main approximations used, including the simplified limit of the 1D spin liquids. In Sec. 5.2, we solve the problem exactly in the case of a stationary hole ($t \to 0$). The methods described and the results obtained in this section serve as useful starting points towards the more involved considerations in the remaining sections. In Sec. 5.3, we carry out the variational approach in the case of a slow hole ($t \ll J_0$) and obtain the best possible trial state that optimizes both potential and kinetic energies. Our main result is that the hole has a finite quasiparticle weight $\mathcal{Z} > 0$ for any finite hopping amplitude $t > 0$ but a vanishing quasiparticle weight $\mathcal{Z} \to 0$ for a vanishing hopping amplitude $t \to 0$. In Sec. 5.4, we discuss the results obtained in the previous sections, and argue that they are applicable even beyond our approximations.

5.1 General formulation

5.1.1 Eigenstates and spectral function

The main aim of this chapter is to determine whether a coherent quasiparticle description is possible for an isolated mobile hole in the gapless phase of the Kitaev honeycomb model. To this end, we consider the single-hole spectral function, which is defined in terms of the ground state $|\Omega\rangle$ of the undoped model containing no holes and the eigenstates $|\Phi_{h,q,p}(\mathbf{K})\rangle$ of the doped model containing a single mobile hole with momentum $\mathbf{K}$ and quantum numbers h, q, and p. Due to translational and sublattice symmetries, the eigenstates of the doped model take the general form

$$|\Phi_{h,q,p}(\mathbf{K})\rangle = \frac{1}{\sqrt{2N}} \sum_{l \in A} e^{i\mathbf{K}\cdot\mathbf{R}_l} \, |\Phi^{\{l\}}_{h,q,p}(\mathbf{K})\rangle + \frac{1}{\sqrt{2N}} \sum_{l \in B} e^{i\mathbf{K}\cdot\mathbf{R}_l + i\varpi^{\Phi}_{h,q}(\mathbf{K})} \, |\Phi^{\{l\}}_{h,q,p}(\mathbf{K})\rangle, \tag{5.1}$$

where $\varpi^{\Phi}_{h,q}(\mathbf{K})$ is a phase difference between the two sublattices, and $|\Phi^{\{l\}}_{h,q,p}(\mathbf{K})\rangle$ is a single-hole state corresponding to a definite hole site l. Importantly, two such states with different hole sites l and l' are related by a translation when l and l' are in the

same sublattice and by a spatial inversion when l and l' are in opposite sublattices. In terms of the eigenstates $|\Phi_{h,q,p}(\mathbf{K})\rangle$ and the their energies $E^{\Phi}_{h,q}(\mathbf{K})$, the spectral function of a single hole has the Lehmann representation

$$\begin{aligned}\mathcal{A}(\varepsilon,\mathbf{K}) &= \frac{1}{2N}\sum_{h,q,p}\sum_{\Phi}\sum_{l,l'}\sum_{\sigma=\uparrow,\downarrow}\langle\Omega|\mathbf{c}^{\dagger}_{l',\sigma}|\Phi_{h,q,p}(\mathbf{K})\rangle\,\langle\Phi_{h,q,p}(\mathbf{K})|\mathbf{c}_{l,\sigma}|\Omega\rangle \\ &\quad\times\delta\left[\varepsilon-E^{\Phi}_{h,q}(\mathbf{K})\right]\,e^{i\mathbf{K}\cdot(\mathbf{R}_{l}-\mathbf{R}_{l'})}. \qquad (5.2)\end{aligned}$$

Even for the smallest hopping amplitudes $t\to 0$ and the smallest hole energies $\varepsilon\to 0$, the states $|\Phi^{\{l\}}_{h,q,p}(\mathbf{K})\rangle$ have large numbers of bulk fermion excitations because the bulk fermions have vanishing excitation energies $E_f\to 0$ in the gapless phase. However, the bulk fluxes have finite excitation energies $E_P\sim J_{x,y,z}$, and therefore the states $|\Phi^{\{l\}}_{h,q,p}(\mathbf{K})\rangle$ have no bulk flux excitations, at least for sufficiently small hopping amplitudes $t\ll E_P$ and sufficiently small hole energies $\varepsilon\ll E_P$. Furthermore, since the hole is created by a local operator $\mathbf{c}_{l,\sigma}$, the resulting single-hole states $\mathbf{c}_{l,\sigma}|\Omega\rangle$ in Eq. (5.2) have zero overlaps with $|\Phi^{\{l\}}_{h,q,p}(\mathbf{K})\rangle$ unless $h=0$ and $q=0$. Using the hole spin picture, the states $|\Phi^{\{l\}}_{h,q,p}(\mathbf{K})\rangle$ with $h=0$ and $q=0$ can then be written as

$$|\Phi^{\{l\}}_{0,0,p}(\mathbf{K})\rangle=\mathcal{P}\,\frac{1+ib^{z}_{l}c_{l}}{2}\,(ib^{x}_{l}b^{z}_{l})^{p}\,|\phi^{\{l\}}(\mathbf{K})\rangle, \qquad (5.3)$$

where $|\phi^{\{l\}}(\mathbf{K})\rangle$ is a generic state in the matter-fermion space $\{\phi_k\}$ spanned by the free matter fermions ϕ_k of the undoped model. Note that the lack of flux excitations translates into a lack of bond fermion excitations and therefore $\chi^{\alpha}_{l'}|\phi^{\{l\}}(\mathbf{K})\rangle=0$ for all l' and α. Since $|\Omega\rangle=\mathcal{P}|\omega\rangle$ in terms of the matter-fermion vacuum state $|\omega\rangle\in\{\phi_k\}$ satisfying $\phi_k|\omega\rangle=0$ for all k, the single-hole states $\mathbf{c}_{l,\sigma}|\Omega\rangle$ in the hole spin picture are given by

$$\mathbf{c}_{l,\uparrow}|\Omega\rangle=\mathcal{P}\,\frac{1+ib^{z}_{l}c_{l}}{2}\,|\omega\rangle,\qquad \mathbf{c}_{l,\downarrow}|\Omega\rangle=\mathcal{P}\,(ib^{x}_{l}b^{z}_{l})\,\frac{1-ib^{z}_{l}c_{l}}{2}\,|\omega\rangle. \qquad (5.4)$$

After projecting onto the subspaces with $\sigma^{z}_{l}=\pm 1$ in the two cases, respectively, the operator $ib^{x}_{l}b^{z}_{l}$ in the second case applies a spin rotation $\sigma^{x,z}_{l}\to-\sigma^{x,z}_{l}$ so that the hole spin ends up in the $\sigma^{z}_{l}=+1$ state. The matrix elements in Eq. (5.2) then become

$$\langle\Phi_{h,q,0}(\mathbf{K})|\mathbf{c}_{l,\downarrow}|\Omega\rangle = \langle\Phi_{h,q,1}(\mathbf{K})|\mathbf{c}_{l,\uparrow}|\Omega\rangle=0,$$

$$
\begin{aligned}
\langle \Phi_{h,q,0}(\mathbf{K})|\mathbf{c}_{l\in A,\uparrow}|\Omega\rangle &= \langle \Phi_{h,q,1}(\mathbf{K})|\mathbf{c}_{l\in A,\downarrow}|\Omega\rangle \\
&= \frac{1}{2\sqrt{N}}\,\delta_{h,0}\,\delta_{q,0}\,\langle \phi^{\{l\}}(\mathbf{K})|\omega\rangle\, e^{-i\mathbf{K}\cdot\mathbf{R}_l}, \qquad (5.5)\\
\langle \Phi_{h,q,0}(\mathbf{K})|\mathbf{c}_{l\in B,\uparrow}|\Omega\rangle &= \langle \Phi_{h,q,1}(\mathbf{K})|\mathbf{c}_{l\in B,\downarrow}|\Omega\rangle \\
&= \frac{1}{2\sqrt{N}}\,\delta_{h,0}\,\delta_{q,0}\,\langle \phi^{\{l\}}(\mathbf{K})|\omega\rangle\, e^{-i\mathbf{K}\cdot\mathbf{R}_l - i\varpi^{\Phi}_{h,q}(\mathbf{K})},
\end{aligned}
$$

and the spectral function can be expressed in terms of the matter fermions ϕ_k as

$$
\mathcal{A}(\varepsilon,\mathbf{K}) = \frac{1}{2}\sum_{\Phi}\left\{1+\cos\left[\varpi_{\Phi}(\mathbf{K})\right]\right\}|\langle\phi^{\{0\}}(\mathbf{K})|\omega\rangle|^2\,\delta\left[\varepsilon - E_{\Phi}(\mathbf{K})\right]. \qquad (5.6)
$$

Note that $E_{\Phi}(\mathbf{K}) \equiv E^{\Phi}_{0,0}(\mathbf{K})$ and $\varpi_{\Phi}(\mathbf{K}) \equiv \varpi^{\Phi}_{0,0}(\mathbf{K})$ are independent of p and that $\langle\phi^{\{l\}}(\mathbf{K})|\omega\rangle$ is independent of l due to the symmetries of the model. We can therefore restrict our attention to a special site $l=0$ in the sublattice B.

5.1.2 Potential and kinetic energies

The energy $E_{\Phi}(\mathbf{K})$ of the doped-model eigenstate $|\Phi_{0,0,p}(\mathbf{K})\rangle$ is a sum of two contributions: a potential energy due to the matter fermions excited in each single-hole state $|\Phi^{\{l\}}_{0,0,p}(\mathbf{K})\rangle$ and a kinetic energy due to the hole hopping between the states $|\Phi^{\{l\}}_{0,0,p}(\mathbf{K})\rangle$ that correspond to neighboring hole sites. Since the states $|\Phi^{\{l\}}_{0,0,p}(\mathbf{K})\rangle$ with different hole sites l are related by symmetry, the potential energy is determined entirely by the state $|\Phi^{\{0\}}_{0,0,p}(\mathbf{K})\rangle$ corresponding to the special site $l=0$. Using the hole spin picture and the matter-fermion state $|\phi^{\{0\}}(\mathbf{K})\rangle$, the expectation value of the potential energy is

$$
E_J(\mathbf{K}) = \langle\Phi^{\{0\}}_{0,0,p}(\mathbf{K})|\tilde{H}_{\sigma}|\Phi^{\{0\}}_{0,0,p}(\mathbf{K})\rangle = \langle\phi^{\{0\}}(\mathbf{K})|\tilde{H}_{\phi}|\phi^{\{0\}}(\mathbf{K})\rangle, \qquad (5.7)
$$

where $\tilde{H}_{\sigma}$ is the Hamiltonian of the undoped model with switched-off Ising couplings around the hole site $l=0$, and $\tilde{H}_{\phi}$ is the exclusively matter-fermion form of the same Hamiltonian that takes the form

$$
\tilde{H}_{\phi} = \sum_{l\in A}\sum_{\alpha=x,y,z} iJ_{\alpha}c_l c_{\alpha(l)} - \sum_{\alpha=x,y,z} iJ_{\alpha}c_{\alpha(0)}c_0. \qquad (5.8)
$$

As in the gapped phase, we find that the potential energy is independent of p. To determine the kinetic energy, we must consider the states $|\Phi^{\{0\}}_{0,0,p}(\mathbf{K})\rangle$ and $|\Phi^{\{\alpha(0)\}}_{0,0,p}(\mathbf{K})\rangle$

that correspond to neighboring hole sites 0 and $\alpha(0)$ with $\alpha = \{x, y, z\}$. If we set $\mathbf{R}_0 \equiv 0$ without loss of generality, the expectation value of the kinetic energy is

$$E_t(\mathbf{K}) = \sum_{\alpha=x,y,z} T^{\alpha}(\mathbf{K}) \cos\left[\mathbf{K} \cdot \mathbf{R}_{\alpha(0)} - \varpi_{\Phi}(\mathbf{K})\right], \tag{5.9}$$

where the effective hopping amplitudes $T^{\alpha}(\mathbf{K})$ in the hole spin picture are given by

$$\begin{aligned} T^{\alpha}(\mathbf{K}) &= -t \, \langle \Phi^{\{0\}}_{0,0,p}(\mathbf{K}) | \mathcal{E}_{0,\alpha(0)} | \Phi^{\{\alpha(0)\}}_{0,0,p}(\mathbf{K}) \rangle \\ &= -\frac{t}{2} \, \langle \phi^{\{0\}}(\mathbf{K}) | (1 - i c_{\alpha(0)} c_0) | \phi^{\{\alpha(0)\}}(\mathbf{K}) \rangle. \end{aligned} \tag{5.10}$$

As in the gapped phase, we find that the kinetic energy is independent of p because the hopping process conserves this quantum number and the effective hopping amplitudes are independent of it. Note that these conclusions are also in accordance with $E_{\Phi}(\mathbf{K})$ and $\varpi_{\Phi}(\mathbf{K})$ being independent of p. Furthermore, there are two possible values of $\varpi_{\Phi}(\mathbf{K})$ for each $|\phi^{\{0\}}(\mathbf{K})\rangle$ that are determined by $T^{\alpha}(\mathbf{K})$ in such a way that they minimize and maximize the kinetic energy, respectively.

5.1.3 Effective hopping amplitudes

The effective hopping amplitudes $T^{\alpha}(\mathbf{K})$ are important due to their role in determining the kinetic energy $E_t(\mathbf{K})$. Although Eq. (5.10) gives $T^{\alpha}(\mathbf{K})$ exclusively in terms of the free matter fermions ϕ_k of the undoped model, it contains a matrix element between two different matter-fermion states $|\phi^{\{0\}}(\mathbf{K})\rangle$ and $|\phi^{\{\alpha(0)\}}(\mathbf{K})\rangle$. Since these two matter-fermion states are related by a spatial inversion $\mathcal{R}^{\alpha}_{\pi}$ around the middle of the α bond connecting sites 0 and $\alpha(0)$ [see Fig. 5.1], the matrix element can be turned into an expectation value by expressing the two matter-fermion states in terms of each other as $|\phi^{\{\alpha(0)\}}(\mathbf{K})\rangle = \hat{\mathcal{R}}^{\alpha}_{\pi} |\phi^{\{0\}}(\mathbf{K})\rangle$, where $\hat{\mathcal{R}}^{\alpha}_{\pi}$ is an operator representation of $\mathcal{R}^{\alpha}_{\pi}$ acting in the matter-fermion space $\{\phi_k\}$.

To determine the operator $\hat{\mathcal{R}}^{\alpha}_{\pi}$, we first notice that the matter-fermion vacuum state must be invariant under any spatial inversion and therefore $\hat{\mathcal{R}}^{\alpha}_{\pi} |\omega\rangle = |\omega\rangle$. It is also known that the original Majorana fermions c_l transform as $\hat{\mathcal{R}}^{\alpha}_{\pi}(c_{l \in A}) = c_{\mathcal{R}^{\alpha}_{\pi}(l)}$ and $\hat{\mathcal{R}}^{\alpha}_{\pi}(c_{l \in B}) = -c_{\mathcal{R}^{\alpha}_{\pi}(l)}$, where the minus sign is necessary in the second case because

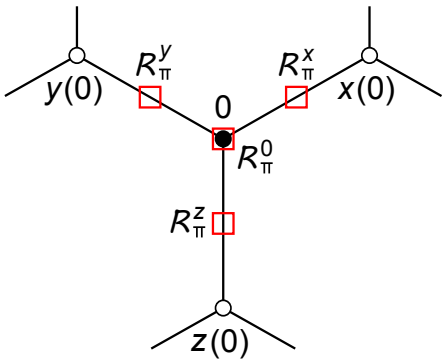

Figure 5.1: Illustration of the special site $l = 0$ and its neighborhood: the special site 0 is marked by a black dot, the neighboring sites $\alpha(0)$ are marked by white dots, while the centers of the spatial inversions $\mathcal{R}^0_\pi$ and $\mathcal{R}^\alpha_\pi$ are marked by red rectangles.

$\mathcal{R}^\alpha_\pi$ exchanges the two sublattices. We must then determine how the free matter fermions ϕ_k transform under $\hat{\mathcal{R}}^\alpha_\pi$. Importantly, due to the translational symmetry of the undoped model, the fermions ϕ_k are labeled by their momenta k, and due to the inversion symmetry $\mathcal{R}^\alpha_\pi$, they always come in degenerate pairs of momenta $\pm k$ such that $E_{+k} = E_{-k}$. It is then possible to consider standing-wave representations instead of traveling-wave representations, and we introduce two different kinds of standing-wave representations with their nodal structures centered at different points [see Fig. 5.1]. First, we define the set of unshifted fermions in such a way that their Majorana fermion components have either even (η) or odd (μ) envelope functions under a spatial inversion $\mathcal{R}^0_\pi$ around the special site $l = 0$. Note that this spatial inversion is not a symmetry of the model but even (odd) fermions can still be defined in such a way that they have antinodes (nodes) at its center. Mathematically, these even and odd unshifted fermions are given by

$$\phi_{k,\eta} = \frac{1}{2}[\gamma_{k,\eta,A} + i\gamma_{k,\eta,B}], \qquad \phi_{k,\mu} = \frac{1}{2}[\gamma_{k,\mu,A} + i\gamma_{k,\mu,B}], \tag{5.11}$$

and their respective Majorana fermion components take the forms

$$\gamma_{k,\eta,\upsilon} = \sqrt{\frac{2}{N}} \sum_{l\in\upsilon} \cos\left[\mathbf{k}\cdot\mathbf{R}_l\right] c_l, \qquad \gamma_{k,\mu,\upsilon} = \sqrt{\frac{2}{N}} \sum_{l\in\upsilon} \sin\left[\mathbf{k}\cdot\mathbf{R}_l\right] c_l, \tag{5.12}$$

where we recall $\mathbf{R}_0 \equiv \mathbf{0}$ and use the notation $\upsilon = \{A, B\}$. The unshifted fermions become useful when we break translational symmetry by introducing a hole at the special site $l = 0$. In the resulting doped model, the odd fermions remain completely decoupled, while the even fermions are coupled only among themselves. Second, we also define three sets of shifted fermions in such a way that their Majorana fermion components have either even (η) or odd (μ) envelope functions under the spatial inversions $\mathcal{R}_\pi^{x,y,z}$ defined above, respectively. Mathematically, these even and odd shifted fermions are given by

$$\begin{aligned} \hat{\phi}_{k,\eta}(\alpha) &= \frac{1}{2}[\hat{\gamma}_{k,\eta,A}(\alpha) + i\hat{\gamma}_{k,\eta,B}(\alpha)], \\ \hat{\phi}_{k,\mu}(\alpha) &= \frac{1}{2}[\hat{\gamma}_{k,\mu,A}(\alpha) + i\hat{\gamma}_{k,\mu,B}(\alpha)], \end{aligned} \tag{5.13}$$

and their respective Majorana fermion components take the forms

$$\begin{aligned} \hat{\gamma}_{k,\eta,\upsilon}(\alpha) &= \sqrt{\frac{2}{N}} \sum_{l\in\upsilon} \cos\left[\mathbf{k}\cdot(\mathbf{R}_l - \mathbf{R}_{\alpha(0)}/2)\right] c_l, \\ \hat{\gamma}_{k,\mu,\upsilon}(\alpha) &= \sqrt{\frac{2}{N}} \sum_{l\in\upsilon} \sin\left[\mathbf{k}\cdot(\mathbf{R}_l - \mathbf{R}_{\alpha(0)}/2)\right] c_l. \end{aligned} \tag{5.14}$$

The shifted fermions are useful because they transform in a straightforward way under the spatial inversion $\mathcal{R}_\pi^\alpha$. In particular, the Majorana fermion components transform as $\hat{\mathcal{R}}_\pi^\alpha[\hat{\gamma}_{k,\eta,A}(\alpha)] = \hat{\gamma}_{k,\eta,B}(\alpha)$, $\hat{\mathcal{R}}_\pi^\alpha[\hat{\gamma}_{k,\eta,B}(\alpha)] = -\hat{\gamma}_{k,\eta,A}(\alpha)$, $\hat{\mathcal{R}}_\pi^\alpha[\hat{\gamma}_{k,\mu,A}(\alpha)] = -\hat{\gamma}_{k,\mu,B}(\alpha)$, and $\hat{\mathcal{R}}_\pi^\alpha[\hat{\gamma}_{k,\mu,B}(\alpha)] = \hat{\gamma}_{k,\mu,A}(\alpha)$, which implies that the shifted fermions themselves transform as $\hat{\mathcal{R}}_\pi^\alpha[\hat{\phi}_{k,\eta}(\alpha)] = -i\hat{\phi}_{k,\eta}(\alpha)$ and $\hat{\mathcal{R}}_\pi^\alpha[\hat{\phi}_{k,\mu}(\alpha)] = i\hat{\phi}_{k,\mu}(\alpha)$. Furthermore, the shifted fermions are related to the unshifted fermions by

$$\begin{aligned} \hat{\phi}_{k,\eta}(\alpha) &= \cos(\mathbf{k}\cdot\mathbf{R}_{\alpha(0)}/2)\,\phi_{k,\eta} + \sin(\mathbf{k}\cdot\mathbf{R}_{\alpha(0)}/2)\,\phi_{k,\mu}, \\ \hat{\phi}_{k,\mu}(\alpha) &= -\sin(\mathbf{k}\cdot\mathbf{R}_{\alpha(0)}/2)\,\phi_{k,\eta} + \cos(\mathbf{k}\cdot\mathbf{R}_{\alpha(0)}/2)\,\phi_{k,\mu}. \end{aligned} \tag{5.15}$$

Importantly, all sets of fermions have the same vacuum state $|\omega\rangle$, and the different fermions $\phi_{k,\eta}$, $\phi_{k,\mu}$, $\hat{\phi}_{k,\eta}(\alpha)$, and $\hat{\phi}_{k,\mu}(\alpha)$ corresponding to the same momentum pair $\pm k$ all have identical excitation energies $E_k \equiv E_{\pm k}$.

We are now ready to obtain the operator $\hat{\mathcal{R}}_\pi^\alpha$ by noticing that it leaves the vacuum state $|\omega\rangle$ invariant while it multiplies the creation operators $\hat{\phi}_{k,\eta}^\dagger(\alpha)$ and $\hat{\phi}_{k,\mu}^\dagger(\alpha)$ by

factors of $+i$ and $-i$, respectively. Its general form then becomes

$$\begin{aligned}\hat{\mathcal{R}}_{\pi}^{\alpha} &= \exp\left\{\frac{i\pi}{2}\sum_{\pm k}\left[\hat{\phi}_{k,\eta}^{\dagger}(\alpha)\,\hat{\phi}_{k,\eta}(\alpha)-\hat{\phi}_{k,\mu}^{\dagger}(\alpha)\,\hat{\phi}_{k,\mu}(\alpha)\right]\right\} \\ &= \prod_{\pm k}\left\{\left[1-(1-i)\,\hat{\phi}_{k,\eta}^{\dagger}(\alpha)\,\hat{\phi}_{k,\eta}(\alpha)\right]\left[1-(1+i)\,\hat{\phi}_{k,\mu}^{\dagger}(\alpha)\,\hat{\phi}_{k,\mu}(\alpha)\right]\right\},\end{aligned} \tag{5.16}$$

where the notation $\pm k$ indicates that the sum (product) is over pairs of momenta. Finally, using $|\phi^{\{\alpha(0)\}}(\mathbf{K})\rangle = \hat{\mathcal{R}}_{\pi}^{\alpha}|\phi^{\{0\}}(\mathbf{K})\rangle$ and $\hat{\mathcal{R}}_{\pi}^{\alpha}c_0 = -c_{\alpha(0)}\hat{\mathcal{R}}_{\pi}^{\alpha}$, the effective hopping amplitude in Eq. (5.10) takes the expectation-value form

$$T^{\alpha}(\mathbf{K}) = -\frac{t}{2}\,\langle\phi^{\{0\}}(\mathbf{K})|\hat{\mathcal{T}}^{\alpha}|\phi^{\{0\}}(\mathbf{K})\rangle, \qquad \hat{\mathcal{T}}^{\alpha} = \hat{\mathcal{R}}_{\pi}^{\alpha} - ic_0\hat{\mathcal{R}}_{\pi}^{\alpha}c_0. \tag{5.17}$$

This final result for $T^{\alpha}(\mathbf{K})$ has a straightforward interpretation: instead of looking at the hopping process from a passive point of view in which the hole jumps to a neighboring site and the fermions are unchanged, we look at it from an active point of view in which the hole stays at the same site (due to a relabeling of sites) and the fermions are shifted accordingly. The main advantage of this point of view is that we can evaluate the effective hopping amplitude by considering only one matter-fermion state $|\phi^{\{0\}}(\mathbf{K})\rangle$ which corresponds to the hole being at the special site $l = 0$.

5.1.4 Simplified one-dimensional problem

In the rest of this chapter, we consider a spatially anisotropic special point in the gapless phase, at which the Kitaev honeycomb model breaks down into non-interacting 1D chains along the x and y bonds. This special point is characterized by Ising coupling strengths $J_x = J_y = J_0$ and $J_z = 0$ and belongs to the boundary of the gapless phase. Although the hole can hop between neighboring chains as we take the bare hopping amplitude t to be the same for all bond types $\alpha = \{x, y, z\}$, the spectral function and the effective hopping amplitudes can be calculated by restricting our attention to a single chain.

Indeed, the spectral function in Eq. (5.6) is to be evaluated in terms of the single-chain states $|\omega\rangle$ and $|\phi^{\{0\}}(\mathbf{K})\rangle$ because only one chain is affected by the introduction of a single hole. For hopping along x and y bonds, the hopping process occurs within a

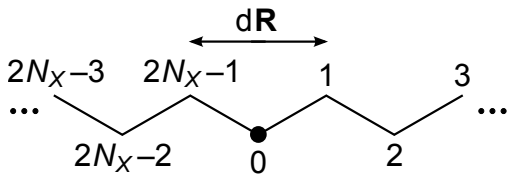

Figure 5.2: Site labeling convention for the one-dimensional (1D) chain of lattice constant $\delta\mathbf{R}$ around the special site $l = 0$ (black dot).

single chain, and therefore Eq. (5.17) gives the effective hopping amplitude in terms of the single-chain state $|\phi^{\{0\}}(\mathbf{K})\rangle$ and the corresponding single-chain fermions ϕ_k. For hopping along z bonds, the hopping process occurs between two neighboring chains. In this case, we consider two chains and use Eq. (5.10) to evaluate the effective hopping amplitude as

$$\begin{aligned} T^z(\mathbf{K}) &= -\frac{t}{2}\left[\langle\omega| \otimes \langle\phi^{\{0\}}(\mathbf{K})|\right]\left(1 - ic_{z(0)}c_0\right)\left[|\phi^{\{z(0)\}}(\mathbf{K})\rangle \otimes |\omega\rangle\right] \\ &= -\frac{t}{2}\left|\langle\phi^{\{0\}}(\mathbf{K})|\omega\rangle\right|^2. \end{aligned} \tag{5.18}$$

Similarly to the spectral function in Eq. (5.6), the effective hopping amplitude in Eq. (5.18) is a function of the single-chain states $|\omega\rangle$ and $|\phi^{\{0\}}(\mathbf{K})\rangle$, which are in turn expressed in terms of the single-chain fermions ϕ_k.

For a single chain of length $2N_X$, the sites labeled $\{1, 2, \ldots, 2N_X \equiv 0\}$ are illustrated in Fig. 5.2, and the fermion momenta are written as $k = \mathbf{k} \cdot \delta\mathbf{R}$, where $\delta\mathbf{R} \equiv \mathbf{R}_{y(x(0))}$ is the lattice constant. However, since the fermions $\phi_{k,\eta}$ and $\phi_{k,\mu}$ are defined for pairs of momenta $\pm k$, we consider non-negative momenta only, and deduce that its possible values are $k = \{0, \delta k, 2\delta k, \ldots, \pi\}$, where $\delta k = 2\pi/N_X$ is the momentum spacing. Note that the total number of fermions is N_X as expected because there are two fermions $\phi_{k,\eta}$ and $\phi_{k,\mu}$ for each $0 < k < \pi$ while there is one fermion $\phi_{k,\eta}$ for each of $k = 0$ and $k = \pi$.

5.2 Exact treatment of a stationary hole

When hopping is switched off and the hole becomes stationary ($t \to 0$), the lack of kinetic energy means that the total energy is identical to the potential energy. The

energy eigenvalues $E_\Phi \equiv E_\Phi(\mathbf{K}) = E_J(\mathbf{K})$ of the doped model and the corresponding matter-fermion states $|\phi^{\{0\}}\rangle \equiv |\phi^{\{0\}}(\mathbf{K})\rangle$ are then independent of the hole momentum $\mathbf{K}$. Furthermore, the eigenstates come in degenerate pairs with identical matter-fermion configurations $|\phi^{\{0\}}\rangle$ and opposite sublattice phase differences $\varpi_\Phi(\mathbf{K}) = 0$ and $\varpi_\Phi(\mathbf{K}) = \pi$. From Eq. (5.6), the momentum-independent spectral function $\mathcal{A}(\varepsilon) \equiv \mathcal{A}(\varepsilon, \mathbf{K})$ is then given by

$$\mathcal{A}(\varepsilon) = \sum_\Phi |\langle \phi^{\{0\}} | \omega \rangle|^2 \, \delta \left[\varepsilon - E_\Phi \right], \tag{5.19}$$

where the sum is over the different matter-fermion configurations $|\phi^{\{0\}}\rangle$. In fact, these configurations $|\phi^{\{0\}}\rangle$ are the eigenstates of the stationary doped model that contains a single stationary hole at the special site $l = 0$. Since this model is exactly solvable, we can obtain exact analytic expressions for the spectral function and the effective hopping amplitudes.

5.2.1 Free matter fermions

In the hole spin picture, the undoped model and the stationary doped model are each described by a quadratic matter-fermion Hamiltonian. For the undoped model, this quadratic Hamiltonian reads

$$H_\phi = i J_0 \sum_{l \in A} \left[c_l c_{x(l)} + c_l c_{y(l)} \right]. \tag{5.20}$$

Since translational symmetry is intact, the resulting free matter fermions are the (even and odd) unshifted fermions $\phi_{k,\eta}$ and $\phi_{k,\mu}$ in Eq. (5.11). Their degenerate excitation energies are given by $E_{k,\eta} = E_{k,\mu} = 4J_0 \cos(k/2)$. Using the notation of the 1D chain, the corresponding Majorana fermion components in Eq. (5.12) become

$$\begin{aligned}
\gamma_{k=0,\eta,A} &= \frac{1}{\sqrt{N_X}} \sum_{l \in A} c_l, & \gamma_{k=0,\eta,B} &= \frac{1}{\sqrt{N_X}} \sum_{l \in B} c_l, \\
\gamma_{k=\pi,\eta,A} &= \frac{1}{\sqrt{N_X}} \sum_{l \in A} (-1)^{(l-1)/2} \, c_l, & \gamma_{k=\pi,\eta,B} &= \frac{1}{\sqrt{N_X}} \sum_{l \in B} (-1)^{l/2} \, c_l, \\
\gamma_{0<k<\pi,\eta,v} &= \sqrt{\frac{2}{N_X}} \sum_{l \in v} \cos\left[\frac{kl}{2}\right] c_l, & \gamma_{0<k<\pi,\mu,v} &= \sqrt{\frac{2}{N_X}} \sum_{l \in v} \sin\left[\frac{kl}{2}\right] c_l.
\end{aligned} \tag{5.21}$$

For the stationary doped model, the quadratic Hamiltonian takes the form

$$\tilde{H}_\phi = iJ_0 \sum_{l\in A} \left[c_l c_{x(l)} + c_l c_{y(l)}\right] - iJ_0 \left[c_{x(0)} c_0 + c_{y(0)} c_0\right], \tag{5.22}$$

where the additional terms with respect to Eq. (5.20) correspond to the two bonds with switched-off Ising couplings around the hole site $l = 0$. Importantly, the odd unshifted fermions $\phi_{k,\mu}$ of the undoped model are completely unaffected by these additional terms because their Majorana fermion components $\gamma_{k,\mu,B}$ have vanishing coefficients at the hole site. The free matter fermions of the doped model are therefore either even ($\tilde{\phi}_{k,\eta}$) or odd ($\tilde{\phi}_{k,\mu}$), and the odd fermions are identical to their counterparts in the undoped model: $\tilde{\phi}_{k,\mu} = \phi_{k,\mu}$ and $\tilde{E}_{k,\mu} = E_{k,\mu} = 4J_0 \cos(k/2)$. Furthermore, due to the simplicity of the 1D chain, the even fermions $\tilde{\phi}_{k,\eta}$ are also straightforward to express. In particular, their Majorana fermion components read

$$\begin{aligned} \tilde{\gamma}_{k=\pi,\eta,A} = \gamma_{k=\pi,\eta,A} = \frac{1}{\sqrt{N_X}} \sum_{l\in A} (-1)^{(l-1)/2}\, c_l, \qquad \tilde{\gamma}_{k=\pi,\eta,B} = c_0, \\ \tilde{\gamma}_{k<\pi,\eta,\upsilon} = \sqrt{\frac{2}{N_X}} \sum_{l\in \upsilon} \sin\left[\left(k + \frac{\delta k}{2}\right)\frac{l}{2}\right] c_l, \end{aligned} \tag{5.23}$$

and their excitation energies are $\tilde{E}_{k=\pi,\eta} = 0$ and $\tilde{E}_{k<\pi,\eta} = 4J_0 \cos[(k + \delta k/2)/2]$. The zero-energy fermion $\tilde{\phi}_{k=\pi,\eta}$ corresponds to the localized hole fermion discussed in relation to the gapped phase. However, in the gapless phase, only one of its Majorana fermion components is localized around the hole site.

It is important to emphasize that the undoped Hamiltonian H_ϕ and the stationary doped Hamiltonian $\tilde{H}_\phi$ have different ground states $|\omega\rangle$ and $|\tilde{\omega}\rangle$. To establish a relation between these two fermion-vacuum states, we first express the corresponding fermions in terms of one another. Since the odd fermions $\tilde{\phi}_{k,\mu} = \phi_{k,\mu}$ are identical in the two models, it is enough to concentrate on the even fermions $\phi_k \equiv \phi_{k,\eta}$ and $\tilde{\phi}_k \equiv \tilde{\phi}_{k,\eta}$. If we write the respective Majorana fermion components as $\gamma_{k,A} = \sum_{l\in A} U_{l,k} c_l$, $\gamma_{k,B} = \sum_{l\in A} V_{l,k} c_{x(l)}$, $\tilde{\gamma}_{k,A} = \sum_{l\in A} \tilde{U}_{l,k} c_l$, and $\tilde{\gamma}_{k,B} = \sum_{l\in A} \tilde{V}_{l,k} c_{x(l)}$ in terms of the original Majorana fermions, they are related to each other by $\tilde{\gamma}_{k,A} = \sum_{k'} \hat{U}_{k,k'} \gamma_{k',A}$ and $\tilde{\gamma}_{k,B} = \sum_{k'} \hat{V}_{k,k'} \gamma_{k',B}$, where $\hat{U} = \tilde{U}^T \cdot U$ and $\hat{V} = \tilde{V}^T \cdot V$ are real orthogonal

matrices. From Eqs. (5.21) and (5.23), the corresponding matrix elements are

$$\begin{aligned}
\hat{U}_{k<\pi,\,0<k'<\pi} &= \frac{2}{N_X}\sum_{l\in A}\sin\left[\left(k+\frac{\delta k}{2}\right)\frac{l}{2}\right]\cos\left[\frac{k'l}{2}\right] \\
&= \frac{1}{N_X}\left\{\csc\left[\frac{k+k'}{2}+\frac{\delta k}{4}\right]+\csc\left[\frac{k-k'}{2}+\frac{\delta k}{4}\right]\right\}, \\
\hat{U}_{k<\pi,\,k'=0} &= \frac{\sqrt{2}}{N_X}\,\csc\left[\frac{k}{2}+\frac{\delta k}{4}\right], \qquad \hat{U}_{k<\pi,\,k'=\pi} = 0, \\
\hat{U}_{k=\pi,\,k'<\pi} &= 0, \qquad \hat{U}_{k=\pi,\,k'=\pi} = 1, \\
\hat{V}_{k<\pi,\,0<k'<\pi} &= \frac{2}{N_X}\sum_{l\in B}\sin\left[\left(k+\frac{\delta k}{2}\right)\frac{l}{2}\right]\cos\left[\frac{k'l}{2}\right] \\
&= \frac{1}{N_X}\left\{\cot\left[\frac{k+k'}{2}+\frac{\delta k}{4}\right]+\cot\left[\frac{k-k'}{2}+\frac{\delta k}{4}\right]\right\}, \\
\hat{V}_{k<\pi,\,k'=0} &= \frac{\sqrt{2}}{N_X}\,\cot\left[\frac{k}{2}+\frac{\delta k}{4}\right], \qquad \hat{V}_{k<\pi,\,k'=\pi} = -\frac{\sqrt{2}}{N_X}\,\tan\left[\frac{k}{2}+\frac{\delta k}{4}\right], \\
\hat{V}_{k=\pi,\,0<k'<\pi} &= \sqrt{\frac{2}{N_X}}, \qquad \hat{V}_{k=\pi,\,k'=0} = \frac{1}{\sqrt{N_X}}, \qquad \hat{V}_{k=\pi,\,k'=\pi} = \frac{1}{\sqrt{N_X}}.
\end{aligned} \tag{5.24}$$

Note that the matrices $\hat{U}$ and $\hat{V}$ are not identical. The two Majorana fermion components transform differently between the two models, and therefore the transformations between the fermions ϕ_k and $\tilde{\phi}_k$ are anomalous in the sense that they mix the creation and the annihilation operators. This fact is in accordance with the corresponding vacuum states $|\omega\rangle$ and $|\tilde{\omega}\rangle$ being different.

5.2.2 Spectral function at low energies

We are now ready to consider the spectral function $\mathcal{A}(\varepsilon)$ in Eq. (5.19), and to determine whether a single hole has a coherent quasiparticle description in the stationary limit. Since we are interested in the behavior of the spectral function $\mathcal{A}(\varepsilon)$ at small energies $\varepsilon \to 0$, we investigate its Laplace transform $\mathcal{A}'(s)$ at large arguments $s \to \infty$. This Laplace transform is given by

$$\begin{aligned}
\mathcal{A}'(s) &\equiv \int_0^\infty \mathcal{A}(\varepsilon)e^{-s\varepsilon}d\varepsilon = \sum_\Phi |\langle\phi^{\{0\}}|\omega\rangle|^2\, e^{-sE_\Phi} \\
&= \langle\omega|\Big[\sum_\Phi |\phi^{\{0\}}\rangle\langle\phi^{\{0\}}|e^{-sE_\Phi}\Big]|\omega\rangle.
\end{aligned} \tag{5.25}$$

Since the matter-fermion eigenstates are $|\phi^{\{0\}}\rangle = \tilde{\phi}^\dagger_{k_1}\tilde{\phi}^\dagger_{k_2}\ldots\tilde{\phi}^\dagger_{k_j}|\tilde{\omega}\rangle$ with respective energies $E_\Phi = \tilde{E}_{k_1} + \tilde{E}_{k_2} + \ldots + \tilde{E}_{k_j}$, the term in the square brackets factorizes, and the Laplace transform of the spectral function takes the simplified form

$$\begin{aligned}\mathcal{A}'(s) &= \langle\omega|\exp\Big[-s\sum_k \tilde{E}_k\tilde{\phi}^\dagger_k\tilde{\phi}_k\Big]|\omega\rangle \\ &= \langle\omega|\prod_k\Big[1-\Big(1-e^{-s\tilde{E}_k}\Big)\tilde{\phi}^\dagger_k\tilde{\phi}_k\Big]|\omega\rangle. \end{aligned} \tag{5.26}$$

If we express the fermions $\tilde{\phi}_k$ in terms of the fermions ϕ_k corresponding to the vacuum state $|\omega\rangle$, this expectation value can be calculated using Wick's theorem. However, we can simplify this calculation considerably by defining a set of intermediate fermions ϕ'_k with Majorana fermion components $\gamma'_{k,A} = \sum_{k'}\hat{U}_{k,k'}\gamma_{k',A} = \tilde{\gamma}_{k,A}$ and $\gamma'_{k,B} = \sum_{k'}\hat{U}_{k,k'}\gamma_{k',B}$. These intermediate fermions are useful for two reasons. On one hand, the transformations between $\tilde{\phi}_k$ and ϕ'_k are non-trivial in only one Majorana fermion component. On the other hand, the transformations between ϕ_k and ϕ'_k are identical in the two Majorana fermion components, and therefore the corresponding vacuum states $|\omega\rangle$ and $|\omega'\rangle$ are identical. Substituting $|\omega\rangle$ with $|\omega'\rangle$ in Eq. (5.26), and using $\tilde{\gamma}_{k,B} = \sum_{k'}\hat{W}_{k,k'}\gamma'_{k',B}$, the Laplace transform then becomes

$$\begin{aligned}\mathcal{A}'(s) &= \langle\omega'|\prod_k\left[\frac{1}{2}\left(1+e^{-s\tilde{E}_k}\right)-\frac{i}{2}\left(1-e^{-s\tilde{E}_k}\right)\gamma'_{k,A}\sum_{k'}\hat{W}_{k,k'}\,\gamma'_{k',B}\right]|\omega'\rangle \\ &= \det\left[\frac{1}{2}\left(1+e^{-s\tilde{E}_k}\right)\delta_{k,k'}+\frac{1}{2}\left(1-e^{-s\tilde{E}_k}\right)\hat{W}_{k,k'}\right] \\ &\equiv \det\Big[\bar{W}_{k,k'}(s)\Big], \end{aligned} \tag{5.27}$$

where $\hat{W} = \hat{V}\cdot\hat{U}^T$ is a real orthogonal matrix. To obtain the final determinant form, we must appreciate that Majorana fermions anticommute and that the expectation value vanishes unless each $\gamma'_{k,A}$ has a pair $\gamma'_{k,B}$.

Since there is a zero-energy fermion $\tilde{\phi}_{k=\pi}$ with excitation energy $\tilde{E}_{k=\pi} = 0$, the corresponding elements of the matrix $\bar{W}(s)$ are given by $\bar{W}_{k=\pi,\,k'}(s) = \delta_{k,k'}$. Note that this result applies to any finite s and also to the limit of $s\to\infty$. The Laplace transform in Eq. (5.27) is then reduced to $\mathcal{A}'(s) = \det[\bar{W}_{k<\pi,\,k'<\pi}(s)]$ and becomes a function of the corresponding matrix elements $\hat{W}_{k<\pi,\,k'<\pi}$ only. Using Eq. (5.24),

these matrix elements take the exact form

$$\begin{aligned}\hat{W}_{k<\pi,\,k'<\pi} &= \sum_{k''} \hat{V}_{k<\pi,\,k''}\,\hat{U}_{k'<\pi,\,k''} = \frac{2}{N_X^2}\,\cot\left[\frac{k}{2}+\frac{\delta k}{4}\right]\csc\left[\frac{k'}{2}+\frac{\delta k}{4}\right] \\ &+ \frac{1}{N_X^2}\sum_{0<k''<\pi}\left\{\cot\left[\frac{k+k''}{2}+\frac{\delta k}{4}\right]+\cot\left[\frac{k-k''}{2}+\frac{\delta k}{4}\right]\right\} \\ &\times\left\{\csc\left[\frac{k'+k''}{2}+\frac{\delta k}{4}\right]+\csc\left[\frac{k'-k''}{2}+\frac{\delta k}{4}\right]\right\}. \end{aligned} \tag{5.28}$$

In the thermodynamic limit, the sum in k'' can be turned into an integral, but care must be taken as the integrand diverges at $k''=k$ and $k''=k'$. Furthermore, there are two distinct cases to consider. For the diagonal matrix elements with $k=k'$, there are two divergent terms $(k''-k)^{-1}$ and $(k''-k)^{-2}$ at a single divergent point $k''=k$. Since the possible arguments of the cot and the csc functions are symmetric around $k''=k$ due to the shift $\delta k/2$ with respect to $k''-k$, the integral of the divergent term $(k''-k)^{-1}$ can be substituted with its principal value. However, for the integral of the divergent term $(k''-k)^{-2}$, the infinite contribution picked up at $k''=k$ must be substituted with a corresponding sum given by

$$\frac{1}{N_X^2}\left(\frac{4}{\delta k}\right)^2\sum_{r=-\infty}^{+\infty}\frac{1}{(1+2r)^2}=1. \tag{5.29}$$

Neglecting any contributions $\mathcal{O}(N_X^{-2})$, recognizing that the indefinite integral is

$$\begin{aligned}&\int\left\{\cot\left[\frac{k+k''}{2}\right]+\cot\left[\frac{k-k''}{2}\right]\right\}\left\{\csc\left[\frac{k+k''}{2}\right]+\csc\left[\frac{k-k''}{2}\right]\right\}dk'' \\ &\quad= -2\csc\left[\frac{k+k''}{2}\right]+2\csc\left[\frac{k-k''}{2}\right] \\ &\qquad+4\cot\left(\frac{k}{2}\right)\operatorname{arctanh}\left[\frac{\sin(k''/2)}{\sin(k/2)}\right],\end{aligned} \tag{5.30}$$

and taking care of the divergent terms, the diagonal matrix elements take the form

$$\begin{aligned}\hat{W}_{k<\pi,\,k<\pi} &= 1-\frac{2G_{k,k}}{N_X}+\mathcal{O}(N_X^{-2}), \\ G_{k,k} &= \frac{1}{\pi}\left\{\csc\left[\frac{\pi-k}{2}\right]-\tan\left[\frac{\pi-k}{2}\right]\ln\cot\left[\frac{\pi-k}{4}\right]\right\}.\end{aligned} \tag{5.31}$$

For the off-diagonal matrix elements with $k\neq k'$, there are two divergent terms $(k''-k)^{-1}$ and $(k''-k')^{-1}$ at two separate divergent points $k''=k$ and $k''=k'$.

Since the possible arguments of the cot and the csc functions are symmetric around $k'' = k$ and $k'' = k'$, respectively, the integrals of the divergent terms can both be substituted with their principal values. Once again, neglecting any contributions $\mathcal{O}(N_X^{-2})$, recognizing that the indefinite integral is

$$\begin{aligned}\int \left\{\cot\left[\frac{k+k''}{2}\right] + \cot\left[\frac{k-k''}{2}\right]\right\}\left\{\csc\left[\frac{k'+k''}{2}\right] + \csc\left[\frac{k'-k''}{2}\right]\right\} dk'' \\ = 8\cos\left(\frac{k}{2}\right)\csc\left[\frac{k+k'}{2}\right]\csc\left[\frac{k-k'}{2}\right] \\ \times\left\{\sin\left(\frac{k}{2}\right)\operatorname{arctanh}\left[\frac{\sin(k''/2)}{\sin(k'/2)}\right] - \sin\left(\frac{k'}{2}\right)\operatorname{arctanh}\left[\frac{\sin(k''/2)}{\sin(k/2)}\right]\right\},\end{aligned} \tag{5.32}$$

and taking care of the divergent terms, the diagonal and the off-diagonal matrix elements take the unified form

$$\begin{aligned}\hat{W}_{k<\pi,\,k'<\pi} &= \delta_{k,k'} - \frac{2G_{k,k'}}{N_X} + \mathcal{O}(N_X^{-2}), \\ G_{k,k'} &= \frac{2}{\pi}\cos\left(\frac{k}{2}\right)\csc\left[\frac{k+k'}{2}\right]\csc\left[\frac{k-k'}{2}\right] \\ &\quad\times\left\{\sin\left(\frac{k'}{2}\right)\ln\cot\left[\frac{\pi-k}{4}\right] - \sin\left(\frac{k}{2}\right)\ln\cot\left[\frac{\pi-k'}{4}\right]\right\}.\end{aligned} \tag{5.33}$$

Note that $G_{k,k'} \geq 0$ for all $0 \leq k \neq k' < \pi$ and that $G_{k,k} \geq 0$ in Eq. (5.31) is recovered for $k' \to k$. Furthermore, the above steps can be repeated to verify that $\sum_{k''}\hat{U}_{k,k''}\hat{U}_{k',k''} = \sum_{k''}\hat{V}_{k,k''}\hat{V}_{k',k''} = \delta_{k,k'} + \mathcal{O}(N_X^{-2})$.

For simplicity, we first consider the Laplace transform $\mathcal{A}'(s)$ in the limit of $s \to \infty$. Exploiting the relation between the trace and the determinant of a matrix, and using $\bar{W}_{k<\pi,\,k'<\pi}(s\to\infty) = \delta_{k,k'} - N_X^{-1}G_{k,k'}$, this quantity can be expanded as

$$\begin{aligned}\mathcal{A}'(s\to\infty) &= \det\left[\bar{W}_{k<\pi,\,k'<\pi}(s\to\infty)\right] \\ &= \exp\left[\operatorname{tr}\left\{\ln\left[\delta_{k,k'} - N_X^{-1}G_{k,k'}\right]\right\}\right] = \exp\left[-\sum_{r=1}^{\infty}\mathcal{S}_r\right], \\ \mathcal{S}_1 &= N_X^{-1}\sum_k G_{k,k}, \quad \mathcal{S}_2 = \frac{N_X^{-2}}{2}\sum_{k_1,k_2} G_{k_1,k_2}G_{k_2,k_1}, \\ \mathcal{S}_3 &= \frac{N_X^{-3}}{3}\sum_{k_1,k_2,k_3} G_{k_1,k_2}G_{k_2,k_3}G_{k_3,k_1}, \quad \ldots,\end{aligned} \tag{5.34}$$

where the first expansion term $\mathcal{S}_1$ approximates the determinant as the product of the diagonal matrix elements, and the remaining expansion terms $\mathcal{S}_r$ refine this approximation by taking r-cycles of off-diagonal matrix elements into account. We evaluate the first two expansion terms analytically by turning the sums into integrals. For the first expansion term, this procedure gives

$$\begin{aligned} \mathcal{S}_1 &= \frac{1}{2\pi}\int_0^\pi G_{k,k}\,dk \\ &= \frac{1}{2\pi^2}\int_0^\pi \left\{\csc\left[\frac{\pi-k}{2}\right] - \tan\left[\frac{\pi-k}{2}\right]\ln\cot\left[\frac{\pi-k}{4}\right]\right\} dk. \end{aligned} \tag{5.35}$$

Importantly, the first term of the integrand diverges at $k \to \pi$, and the expansion term $\mathcal{S}_1$ is dominated by this divergence in the thermodynamic limit. Substituting $G_{k,k}$ with its divergent part $G_{k,k} \sim (2/\pi)[\pi - k]^{-1}$, and noticing that there is a cut-off at $\hat{k} \equiv \pi - k \to 0$ given by the momentum spacing $\delta k = 2\pi/N_X$, the first expansion term takes the approximate form

$$\mathcal{S}_1 \sim \frac{1}{2\pi}\int_{\delta k}^{\pi} \frac{2}{\pi\hat{k}}\,d\hat{k} \sim \frac{1}{\pi^2}\,\ln N_X. \tag{5.36}$$

For the second expansion term $\mathcal{S}_2$, we immediately substitute $G_{k_1,k_2}G_{k_2,k_1}$ with its divergent part at $k_{1,2} \to \pi$. Introducing radial and angular parameters as $\hat{k}_1 \equiv \pi - k_1 = \hat{k}\cos\hat{\vartheta}_k$ and $\hat{k}_2 \equiv \pi - k_2 = \hat{k}\sin\hat{\vartheta}_k$, this divergent part is given by

$$G_{k_1,k_2}G_{k_2,k_1} \sim \frac{8}{\pi^2\hat{k}^2}\,\tan(2\hat{\vartheta}_k)\sec(2\hat{\vartheta}_k)\ln^2[\tan\hat{\vartheta}_k], \tag{5.37}$$

and the second expansion term takes the approximate form

$$\begin{aligned} \mathcal{S}_2 &\sim \frac{1}{8\pi^2}\int_{\delta k}^{\pi}\frac{8}{\pi^2\hat{k}^2}\,\hat{k}\,d\hat{k}\int_0^{\pi/2}\tan(2\hat{\vartheta}_k)\sec(2\hat{\vartheta}_k)\ln^2[\tan\hat{\vartheta}_k]\,d\hat{\vartheta}_k \\ &\sim \frac{1}{6\pi^2}\,\ln N_X. \end{aligned} \tag{5.38}$$

The dominant contribution to the r-th expansion term is given by a similar expression: it has the same logarithmic divergence in the radial integral with a different coefficient that is determined by the $r-1$ angular integrals. Instead of evaluating the remaining coefficients analytically, we determine numerically that the third and the fourth expansion terms are $\mathcal{S}_3 \sim (2/45\pi^2)\ln N_X$ and $\mathcal{S}_4 \sim (1/70\pi^2)\ln N_X$, within

a relative accuracy of 10^{-3}, and deduce from the observed pattern that the r-th expansion term is given by

$$\mathcal{S}_r \sim \frac{2^r (r!)^2}{\pi^2 r^2 (2r)!} \ln N_X. \tag{5.39}$$

Substituting Eq. (5.39) into Eq. (5.34), the final form of the Laplace transform is

$$\begin{aligned} \mathcal{A}'(s \to \infty) &\sim \exp\left[-\sum_{r=1}^{\infty} \frac{2^r (r!)^2}{\pi^2 r^2 (2r)!} \ln N_X \right] \\ &= \exp\left[-\frac{1}{8} \ln N_X \right] \sim N_X^{-1/8} \to 0. \end{aligned} \tag{5.40}$$

Importantly, the final exponent $-1/8$ is also verified numerically within a relative accuracy of 10^{-5}. Although this exponent indicates a slow decay as a function of the chain dimension N_X, the Laplace transform $\mathcal{A}'(s \to \infty)$ nevertheless vanishes in the thermodynamic limit [89]. This result implies that the spectral function $\mathcal{A}(\varepsilon)$ has no delta-function peak at $\varepsilon = 0$ and that the hole is completely incoherent.

When the Laplace transform $\mathcal{A}'(s)$ has a finite (but large) argument s, the above calculation can be repeated using the substitution $G_{k,k'} \to G_{k,k'}(1 - e^{-s\tilde{E}_k})$. In particular, the analog of the first expansion term in Eq. (5.35) becomes

$$\mathcal{S}_1 = \frac{1}{2\pi^2} \int_0^{\pi} \left\{ \csc\left[\frac{\pi - k}{2}\right] - \tan\left[\frac{\pi - k}{2}\right] \ln\cot\left[\frac{\pi - k}{4}\right] \right\} \left(1 - e^{-2s\tilde{E}_k}\right) dk, \tag{5.41}$$

where $\tilde{E}_k \approx E_k = 4J_0 \cos(k/2)$. Since the function $1 - e^{-2s\tilde{E}_k}$ is approximately 1 in the case of $\hat{k} \gg 1/sJ_0$ and approximately $2s\tilde{E}_k \approx 4sJ_0\hat{k}$ in the case of $\hat{k} \ll 1/sJ_0$, its main effect is to cancel the $1/\hat{k}$ divergence at $\hat{k} \to 0$ and to provide a cut-off at $\hat{k} \sim \hat{k}_0 \sim 1/sJ_0$ that is independent of the chain dimension N_X. The approximate form is therefore given by

$$\mathcal{S}_1 \sim \frac{1}{2\pi} \int_{\hat{k}_0}^{\pi} \frac{2}{\pi\hat{k}}\, d\hat{k} \sim \frac{1}{\pi^2} \ln(sJ_0). \tag{5.42}$$

Anticipating the same cut-off to appear in all expansion terms $\mathcal{S}_r$, the analog of the Laplace transform in Eq. (5.40) becomes

$$\mathcal{A}'(s) \sim \exp\left[-\frac{1}{8} \ln(sJ_0) \right] \sim (sJ_0)^{-1/8}, \tag{5.43}$$

and the spectral function takes the functional form $\mathcal{A}(\varepsilon) \propto \varepsilon^{-7/8}$ for small energies $\varepsilon \ll J_0$. Note that $\mathcal{A}(\varepsilon)$ diverges at $\varepsilon \to 0$ but its integral remains finite due to the exponent of ε being larger than -1. The fact that the exponent $-7/8$ is close to -1 is consistent with the slow decay of $\mathcal{A}'(s \to \infty)$ as a function of the chain dimension N_X. If the exponent was -1, the power law would turn into a delta-function peak at $\varepsilon = 0$, and it would indicate the presence of a coherent quasiparticle [86].

5.2.3 Effective hopping amplitudes

We now investigate the effective hopping amplitudes $T^\alpha \equiv T^\alpha(\mathbf{K})$ between the ground states of the stationary doped model that correspond to neighboring hole sites 0 and $\alpha(0)$ with $\alpha = \{x, y, z\}$. These effective hopping amplitudes are completely analogous to the ones obtained in the gapped phase, and they reveal whether a perturbative treatment of the kinetic energy is possible for a finite bare hopping amplitude $t > 0$. As indicated by Eqs. (5.17) and (5.18), the effective hopping amplitudes can be calculated from a single ground state that corresponds to the hole being at the special site $l = 0$. For the hopping amplitude along z bonds, substituting $|\phi^{\{0\}}(\mathbf{K})\rangle = |\tilde{\omega}\rangle$ into Eq. (5.18) readily gives $T^z = -|\langle\tilde{\omega}|\omega\rangle|^2\, t/2$. We then notice that this result is related to the Laplace transform of the spectral function defined in Eq. (5.25). In particular, the presence of the zero-energy fermion $\tilde{\phi}_{k=\pi}$ implies that $\mathcal{A}'(s \to \infty) = |\langle\tilde{\omega}|\omega\rangle|^2 + |\langle\tilde{\omega}|\tilde{\phi}_{k=\pi}|\omega\rangle|^2$. However, since the fermions $\tilde{\phi}_k$ can only be excited pairwise in the vacuum state $|\omega\rangle$, the second term vanishes, and the relation $\mathcal{A}'(s \to \infty) = |\langle\tilde{\omega}|\omega\rangle|^2$ implies

$$T^z = -\frac{t}{2}\,\mathcal{A}'(s \to \infty) \sim -t\, N_X^{-1/8} \to 0. \tag{5.44}$$

For the hopping amplitudes along x and y bonds, substituting $|\phi^{\{0\}}(\mathbf{K})\rangle = |\tilde{\omega}\rangle$ into Eq. (5.17) readily gives

$$T^{x,y} = -\frac{t}{2}\left[\langle\tilde{\omega}|\hat{\mathcal{R}}_\pi^{x,y}|\tilde{\omega}\rangle - i\langle\tilde{\omega}|c_0\hat{\mathcal{R}}_\pi^{x,y}c_0|\tilde{\omega}\rangle\right]. \tag{5.45}$$

Initially, we restrict our attention to the first expectation value in the square brackets. Since the odd fermions $\tilde{\phi}_{k,\mu} = \phi_{k,\mu}$ are identical in the doped and the undoped models,

we express the expectation value $\langle\tilde{\omega}|\hat{\mathcal{R}}_{\pi}^{x,y}|\tilde{\omega}\rangle$ exclusively in terms of the even fermions $\phi_k \equiv \phi_{k,\eta}$. Recalling that $\mathbf{k}\cdot\mathbf{R}_{x(0)} = k/2$ and $\mathbf{k}\cdot\mathbf{R}_{y(0)} = -k/2$ for the 1D chain, we first use Eq. (5.15) to obtain the relations between the shifted and the unshifted fermions. For fermion momenta $0 < k < \pi$, these relations are

$$\begin{aligned}
\hat{\phi}_{k,\eta}(x) &= \cos(k/4)\,\phi_{k,\eta} + \sin(k/4)\,\phi_{k,\mu}, \\
\hat{\phi}_{k,\mu}(x) &= -\sin(k/4)\,\phi_{k,\eta} + \cos(k/4)\,\phi_{k,\mu}, \\
\hat{\phi}_{k,\eta}(y) &= \cos(k/4)\,\phi_{k,\eta} - \sin(k/4)\,\phi_{k,\mu}, \\
\hat{\phi}_{k,\mu}(y) &= \sin(k/4)\,\phi_{k,\eta} + \cos(k/4)\,\phi_{k,\mu},
\end{aligned} \tag{5.46}$$

while for $k = 0$ and $k = \pi$, these relations are trivial as there is only one (even) fermion for each momentum. Using the general form of $\hat{\mathcal{R}}_{\pi}^{x,y}$ in Eq. (5.16) and exploiting the fact that $\phi_{k,\mu}|\tilde{\omega}\rangle = 0$ for all k, the first expectation value in Eq. (5.45) becomes

$$\langle\tilde{\omega}|\hat{\mathcal{R}}_{\pi}^{x,y}|\tilde{\omega}\rangle = \langle\tilde{\omega}|\left[1-(1-i)\,\phi_{k=\pi}^{\dagger}\phi_{k=\pi}\right]\prod_{k<\pi}\left\{1-[1-i\cos(k/2)]\phi_k^{\dagger}\phi_k\right\}|\tilde{\omega}\rangle. \tag{5.47}$$

Turning our attention to the second expectation value $\langle\tilde{\omega}|c_0\hat{\mathcal{R}}_{\pi}^{x,y}c_0|\tilde{\omega}\rangle$, we first recall from Eq. (5.23) that $c_0 = \tilde{\gamma}_{k=\pi,B}$ and that $\tilde{\gamma}_{k=\pi,A} = \gamma_{k=\pi,A}$. If we then insert $\gamma_{k=\pi,A}^2 = 1$ twice, the second expectation value becomes

$$\begin{aligned}
\langle\tilde{\omega}|c_0\hat{\mathcal{R}}_{\pi}^{x,y}c_0|\tilde{\omega}\rangle &= \langle\tilde{\omega}|(ic_0\tilde{\gamma}_{k=\pi,A})\,\gamma_{k=\pi,A}\,\hat{\mathcal{R}}_{\pi}^{x,y}\,\gamma_{k=\pi,A}\,(ic_0\tilde{\gamma}_{k=\pi,A})|\tilde{\omega}\rangle \\
&= \langle\tilde{\omega}|\gamma_{k=\pi,A}\left[1-(1-i)\,\phi_{k=\pi}^{\dagger}\phi_{k=\pi}\right]\gamma_{k=\pi,A} \\
&\quad\times\prod_{k<\pi}\left\{1-[1-i\cos(k/2)]\phi_k^{\dagger}\phi_k\right\}|\tilde{\omega}\rangle \\
&= i\,\langle\tilde{\omega}|\left[1-(1+i)\,\phi_{k=\pi}^{\dagger}\phi_{k=\pi}\right]\prod_{k<\pi}\left\{1-[1-i\cos(k/2)]\phi_k^{\dagger}\phi_k\right\}|\tilde{\omega}\rangle,
\end{aligned} \tag{5.48}$$

and the hopping amplitude in Eq. (5.45) takes the simplified form

$$T^{x,y} = -t\,\langle\tilde{\omega}|\prod_{k}\left\{1-[1-i\cos(k/2)]\phi_k^{\dagger}\phi_k\right\}|\tilde{\omega}\rangle, \tag{5.49}$$

which is exactly the same for the x and the y bonds. Furthermore, note that the hopping amplitude is always real because the fermions ϕ_k can only be excited pairwise in the vacuum state $|\tilde{\omega}\rangle$. Since the result in Eq. (5.49) for $T^{x,y}$ is analogous to the

one in Eq. (5.26) for $\mathcal{A}'(s)$, the hopping amplitude can also be converted into a determinant form given by

$$T^{x,y} = -t \, \det \left\{ \frac{1}{2} \left[1 + i \cos(k/2) \right] \delta_{k,k'} + \frac{1}{2} \left[1 - i \cos(k/2) \right] \hat{Z}_{k,k'} \right\}, \tag{5.50}$$

where $\hat{Z} = \hat{V}^T \cdot \hat{U}$ is a real orthogonal matrix. Note that the matrices $\hat{W}$ and $\hat{Z}$ appearing in Eqs. (5.27) and (5.50) are not identical because the doped and the undoped models have exchanged roles in Eqs. (5.26) and (5.49).

The hopping amplitude $T^{x,y}$ in Eq. (5.50) can be evaluated in the same way as the Laplace transform $\mathcal{A}'(s)$. However, instead of calculating it explicitly, we use the intuition that the behavior of the model is dominated by the lowest-energy fermions at momenta $k \to \pi$. Since $\cos(k/2) \to 0$ for these fermions, the hopping amplitude in Eq. (5.49) can then be approximated as

$$T^{x,y} \sim -t \, \langle \tilde{\omega} | \prod_k \left[1 - \phi_k^\dagger \phi_k \right] | \tilde{\omega} \rangle = -t \, |\langle \omega | \tilde{\omega} \rangle|^2. \tag{5.51}$$

This approximate result has a straightforward interpretation. The ground-state overlap $|\langle \omega | \tilde{\omega} \rangle|$ differs from 1 because the matrices $\hat{U}$ and $\hat{V}$ corresponding to the two sublattices are not identical: the introduction of the hole breaks sublattice symmetry and skews the fermions towards one of the sublattices. If we introduce the hole to a neighboring site instead, it skews the fermions towards the other sublattice, and the overlap between the two ground states with the fermions skewed in opposite directions is then approximately $|\langle \omega | \tilde{\omega} \rangle|^2$. Finally, due to the relation $\mathcal{A}'(s \to \infty) = |\langle \omega | \tilde{\omega} \rangle|^2$, the hopping amplitude becomes

$$T^{x,y} \sim -t \, \mathcal{A}'(s \to \infty) \sim -t \, N_X^{-1/8} \to 0. \tag{5.52}$$

From Eqs. (5.44) and (5.52), we conclude that the effective hopping amplitudes T^α all vanish in the thermodynamic limit. Unlike in the gapped phase, the kinetic energy is therefore inherently non-perturbative in the bare hopping amplitude $t > 0$, and we must develop a more delicate approach to address the problem of a mobile hole.

5.3 Variational approach for a mobile hole

When hopping is restored and the hole becomes mobile ($t > 0$), the resulting doped model is no longer exactly solvable, and the exact ground state is not available in general. To obtain a reasonable approximation for the ground state, we use a variational approach in terms of a single-parameter trial state that interpolates smoothly between the known ground states of the stationary doped model and the undoped model. The ground state $|\phi^{\{0\}}(\mathbf{K})\rangle = |\tilde{\omega}\rangle$ of the stationary doped Hamiltonian $\tilde{H}_\phi$ provides a perfect optimization of the potential energy, and therefore it corresponds to the exact ground state in the limit of a stationary hole ($t \to 0$). The ground state $|\phi^{\{0\}}(\mathbf{K})\rangle = |\omega\rangle$ of the undoped Hamiltonian H_ϕ provides a reasonable optimization of both the potential and the kinetic energies, and therefore it might correspond to a good approximation of the ground state in the case of a moderately fast hole ($t \sim J_0$). Note that the ground state in the limit of an infinitely fast hole ($t \to \infty$) is a ferromagnetic state that provides a perfect optimization of the kinetic energy [90]. For the trial state, it is natural to choose the ground state $|\tilde{\omega}'\rangle$ of the Hamiltonian $\tilde{H}'_\phi = (1-\varrho)\tilde{H}_\phi + \varrho H_\phi$, which interpolates smoothly between $\tilde{H}_\phi$ and H_ϕ as a function of the variational parameter $0 \leq \varrho \leq 1$. Using this trial state, we obtain analytic expressions for the spectral function and the effective hopping amplitudes, and find the best variational parameter ϱ for each value of the bare hopping amplitude $t \ll J_0$.

5.3.1 Free matter fermions

In the framework of our variational approach, the undoped model and the doped model are once again described by quadratic matter-fermion Hamiltonians in the hole spin picture. The Hamiltonian and the free matter fermions of the undoped model are given by Eqs. (5.20) and (5.21), while the Hamiltonian of the doped model takes the form

$$\tilde{H}'_\phi = iJ_0 \sum_{l \in A} \left[c_l c_{x(l)} + c_l c_{y(l)} \right] - i(1-\varrho) J_0 \left[c_{x(0)} c_0 + c_{y(0)} c_0 \right], \tag{5.53}$$

where $0 \leq \varrho \leq 1$ is the variational parameter. Note that we recover the stationary doped Hamiltonian $\tilde{H}_\phi$ for $\varrho = 0$ and the undoped Hamiltonian H_ϕ for $\varrho = 1$. Since the odd unshifted fermions $\phi_{k,\mu}$ of the undoped model are unaffected by the additional terms in Eq. (5.53) with respect to Eq. (5.20), the free matter fermions of the doped model are either even ($\tilde{\phi}'_{k,\eta}$) or odd ($\tilde{\phi}'_{k,\mu}$), and the odd fermions are identical to their counterparts in the undoped model: $\tilde{\phi}'_{k,\mu} = \phi_{k,\mu}$ and $\tilde{E}'_{k,\mu} = E_{k,\mu} = 4J_0 \cos(k/2)$. The Majorana fermion components of the even fermions $\tilde{\phi}'_k \equiv \tilde{\phi}'_{k,\eta}$ read

$$
\begin{aligned}
\tilde{\gamma}'_{k=\pi,A} &= \gamma_{k=\pi,A} = \frac{\mathcal{N}_{k=\pi,A}}{\sqrt{N_X}} \sum_{l\in A} (-1)^{(l-1)/2}\, c_l, \qquad \mathcal{N}_{k=\pi,A} = 1, \\
\tilde{\gamma}'_{k=\pi,B} &= \frac{\mathcal{N}_{k=\pi,B}}{\sqrt{N_X}} \left\{ \frac{1}{\varrho}\, c_0 + \sum_{l\in B}^{l\neq 0} (-1)^{l/2}\, c_l \right\}, \\
\mathcal{N}_{k=\pi,B} &= 1 - \frac{1}{2N_X}\left(\frac{1}{\varrho^2} - 1\right) + \mathcal{O}(N_X^{-2}), \\
\tilde{\gamma}'_{k<\pi,A} &= \mathcal{N}_{k<\pi,A} \sqrt{\frac{2}{N_X}} \sum_{l\in A} \cos\left[\varphi_k - \left(k + \frac{\varphi_k \delta k}{\pi}\right)\frac{l}{2}\right] c_l, \\
\mathcal{N}_{k<\pi,A} &= 1 - \frac{\sin(2\varphi_k)}{2N_X \sin k} + \mathcal{O}(N_X^{-2}), \\
\tilde{\gamma}'_{k<\pi,B} &= \mathcal{N}_{k<\pi,B} \sqrt{\frac{2}{N_X}} \left\{ \frac{\cos\varphi_k}{\varrho}\, c_0 + \sum_{l\in B}^{l\neq 0} \cos\left[\varphi_k - \left(k + \frac{\varphi_k \delta k}{\pi}\right)\frac{l}{2}\right] c_l \right\}, \\
\mathcal{N}_{k<\pi,B} &= 1 - \frac{\sin(2\varphi_k)}{2N_X \tan k} - \frac{\cos^2\varphi_k}{N_X}\left(\frac{1}{\varrho^2} - 1\right) + \mathcal{O}(N_X^{-2}),
\end{aligned}
\tag{5.54}
$$

and their excitation energies are $\tilde{E}'_k \equiv \tilde{E}'_{k,\eta} = 4J_0 \cos[(k + \varphi_k \delta k/\pi)/2]$. Importantly, the actual momentum of each even fermion is shifted by $\varphi_k \delta k/\pi$ with respect to its nominal momentum k, where the shift angle φ_k satisfies

$$
\tan\varphi_k = \frac{1-\varrho^2}{\varrho^2}\, \cot\left[\frac{1}{2}\left(k + \frac{\varphi_k \delta k}{\pi}\right)\right]. \tag{5.55}
$$

In the limit of $\varrho \to 1$, the shift angle becomes $\varphi_k = 0$ for all k, and therefore Eq. (5.21) is recovered. In the opposite limit of $\varrho \to 0$, the shift angle becomes $\varphi_k = \pi/2$ for $k < \pi$ and $\varphi_k = 0$ for $k = \pi$, and therefore Eq. (5.23) is recovered. In between the two limits, the shift angle φ_k is a smooth function of the momentum k that satisfies $\varphi_{k=0} = \pi/2$ and $\varphi_{k=\pi} = 0$. This function is illustrated in Fig. 5.3 for three different values of the variational parameter ϱ. Since the shift angle $\varphi_{k=\pi} = 0$ implies

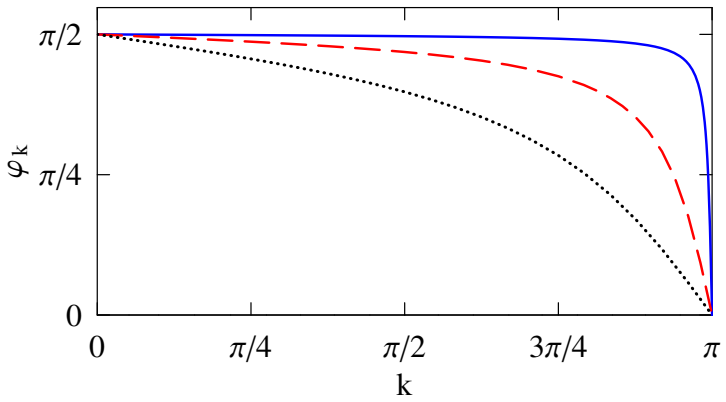

Figure 5.3: Shift angle φ_k as a function of the fermion momentum k for variational parameters $\varrho = 0.1$ (solid line), $\varrho = 0.3$ (dashed line), and $\varrho = 0.5$ (dotted line). The extremal values $\varphi_{k=0} = \pi/2$ and $\varphi_{k=\pi} = 0$ are recovered in all three cases.

a vanishing excitation energy $\tilde{E}'_{k=\pi} = 0$, we find that $\tilde{\phi}'_{k=\pi}$ is a zero-energy fermion for all $0 \leq \varrho \leq 1$. However, this zero-energy fermion behaves differently for $\varrho = 0$ and for $\varrho > 0$: in the former case, one Majorana fermion component is localized at the hole site, while in the latter case, both Majorana fermion components are delocalized across the entire chain.

To establish a relation between the respective ground states $|\omega\rangle$ and $|\tilde{\omega}'\rangle$, we must express the fermions of the undoped and the doped models in terms of each other. Restricting our attention to momenta $0 < k < \pi$, the analog of Eq. (5.24) becomes

$$\begin{aligned}
\hat{U}'_{k<\pi,\,0<k'<\pi} &= \frac{2\mathcal{N}_{k,A}}{N_X} \sum_{l\in A} \cos\left[\varphi_k - \left(k + \frac{\varphi_k \delta k}{\pi}\right)\frac{l}{2}\right] \cos\left[\frac{k'l}{2}\right] \\
&= \frac{\mathcal{N}_{k,A}}{N_X} \sin\varphi_k \left\{ \csc\left[\frac{k+k'}{2} + \frac{\varphi_k \delta k}{2\pi}\right] + \csc\left[\frac{k-k'}{2} + \frac{\varphi_k \delta k}{2\pi}\right]\right\}, \\
\hat{V}'_{k<\pi,\,0<k'<\pi} &= \frac{2\mathcal{N}_{k,B}}{N_X} \left\{ \frac{\cos\varphi_k}{\varrho} + \sum_{l\in B}^{l\neq 0} \cos\left[\varphi_k - \left(k + \frac{\varphi_k \delta k}{\pi}\right)\frac{l}{2}\right] \cos\left[\frac{k'l}{2}\right]\right\} \\
&= \frac{\mathcal{N}_{k,B}}{N_X} \left[2\cos\varphi_k \left(\frac{1}{\varrho} - 1\right) + \sin\varphi_k \left\{ \cot\left[\frac{k+k'}{2} + \frac{\varphi_k \delta k}{2\pi}\right] \right.\right. \\
&\quad \left.\left. + \cot\left[\frac{k-k'}{2} + \frac{\varphi_k \delta k}{2\pi}\right]\right\}\right].
\end{aligned} \tag{5.56}$$

Note that the shift angle φ_k has a crucial role in the matrix elements $\hat{U}'_{k,k'}$ and $\hat{V}'_{k,k'}$ and that the results in Eq. (5.24) are recovered in the limit of $\varrho \to 0$ when $\varphi_k = \pi/2$ and hence $\mathcal{N}_{k,A} = \mathcal{N}_{k,B} = 1$ for all $k < \pi$.

5.3.2 Spectral function and quasiparticle weight

We now investigate the spectral function $\mathcal{A}(\varepsilon, \mathbf{K})$ and determine whether a single mobile hole has a finite quasiparticle weight $\mathcal{Z} > 0$. For simplicity, we first consider the spectral function in the limit of zero hole momentum $\mathbf{K} \to \mathbf{0}$, and then argue that our results remain valid for small hole momenta $|\mathbf{K}||\delta\mathbf{R}| \ll 1$. Since the zero-momentum eigenstates of the doped model come in pairs with identical matter-fermion configurations $|\phi^{\{0\}}\rangle \equiv |\phi^{\{0\}}(\mathbf{0})\rangle$ and opposite sublattice phase differences $\varpi_\Phi(\mathbf{0}) = 0$ and $\varpi_\Phi(\mathbf{0}) = \pi$, the zero-momentum spectral function $\mathcal{A}(\varepsilon) \equiv \mathcal{A}(\varepsilon, \mathbf{0})$ can be evaluated using Eq. (5.19). Recalling the presence of the zero-energy fermion $\tilde{\phi}'_{k=\pi}$, the Laplace transform of the spectral function then becomes

$$\mathcal{A}'(s) = \det\left[\frac{1}{2}\left(1 + e^{-s\tilde{E}'_k}\right)\delta_{k<\pi,\,k'<\pi} + \frac{1}{2}\left(1 - e^{-s\tilde{E}'_k}\right)\hat{W}'_{k<\pi,\,k'<\pi}\right], \tag{5.57}$$

where the appropriate elements of the matrix $\hat{W}' \equiv \hat{V}' \cdot (\hat{U}')^T$ can be calculated from Eq. (5.56) by turning the sum in the dummy variable k'' into an integral [see Eq. (5.28)]. However, in this case, the arguments of the cot and the csc functions are not symmetric around the divergent points $k'' - k$ and $k'' - k'$, and there are additional corrections to the principal values of the integrals due to the divergent terms $(k'' - k)^{-1}$ and $(k'' - k')^{-1}$. The matrix elements then take the form

$$\begin{aligned}
\hat{W}'_{k<\pi,\,k'<\pi} \;=\; & \mathcal{N}_{k,B}\,\mathcal{N}_{k',A}\Bigg\{\delta_{k,k'} + \frac{1}{N_X}\cos\varphi_k \sin\varphi_{k'}\Bigg\{\csc\left[\frac{k'+k}{2}\right] \\
& + (1-\delta_{k,k'})\csc\left[\frac{k'-k}{2}\right]\Bigg\} + \frac{1}{N_X}\cos\varphi_{k'}\Bigg[2\cos\varphi_k\left(\frac{1}{\varrho} - 1\right) \\
& + \sin\varphi_k\left\{\cot\left[\frac{k+k'}{2}\right] + (1-\delta_{k,k'})\cot\left[\frac{k-k'}{2}\right]\right\}\Bigg] \\
& + \frac{4}{\pi N_X}\cos\varphi_k\sin\varphi_{k'}\left(\frac{1}{\varrho} - 1\right)\ln\cot\left[\frac{\pi-k'}{4}\right] \\
& - \frac{4}{\pi N_X}\sin\varphi_k\sin\varphi_{k'}\cos\left(\frac{k}{2}\right)\csc\left[\frac{k+k'}{2}\right]\csc\left[\frac{k-k'}{2}\right] \\
& \times\left\{\sin\left(\frac{k'}{2}\right)\ln\cot\left[\frac{\pi-k}{4}\right] - \sin\left(\frac{k}{2}\right)\ln\cot\left[\frac{\pi-k'}{4}\right]\right\} + \mathcal{O}(N_X^{-2})\Bigg\},
\end{aligned} \tag{5.58}$$

where the first term in the large curly brackets is due to the divergent term $(k''-k)^{-2}$ [see Eq. (5.29)], the second and third terms are due to the divergent terms $(k''-k)^{-1}$ and $(k''-k')^{-1}$, respectively, and the remaining terms are from the principal values of the integrals. For the off-diagonal matrix elements with $k \neq k'$, the leading term is $\mathcal{O}(N_X^{-1})$, and therefore the result follows directly from Eq. (5.58) using $\delta_{k,k'} = 0$ and $\mathcal{N}_{k',A} = \mathcal{N}_{k,B} = 1$. For the diagonal matrix elements with $k = k'$, the leading term is $\mathcal{O}(1)$. Taking proper care of $\mathcal{N}_{k',A}$ and $\mathcal{N}_{k,B}$, these matrix elements take the form

$$\begin{aligned}\hat{W}'_{k<\pi,\,k<\pi} &= 1 - \frac{1}{N_X}\Bigg[\cos^2\varphi_k \left(\frac{1}{\varrho}-1\right)^2 \\ &\quad - \frac{4}{\pi}\sin\varphi_k\cos\varphi_k\left(\frac{1}{\varrho}-1\right)\ln\cot\left[\frac{\pi-k}{4}\right] \\ &\quad + \frac{2}{\pi}\sin^2\varphi_k\left\{\csc\left[\frac{\pi-k}{2}\right] - \tan\left[\frac{\pi-k}{2}\right]\ln\cot\left[\frac{\pi-k}{4}\right]\right\}\Bigg] + \mathcal{O}(N_X^{-2}).\end{aligned} \tag{5.59}$$

Importantly, the analogous results in Eqs. (5.31) and (5.33) are recovered when $\varrho \to 0$ and hence $\varphi_k = \varphi_{k'} = \pi/2$. Furthermore, in the case of $\varrho \ll 1$, the function $\sin\varphi_k$ is approximately 1 for $\hat{k} \gg \varrho^2$ and approximately $\hat{k}/\varrho^2$ for $\hat{k} \ll \varrho^2$. Since the terms proportional to $\cos\varphi_k$ or $\cos\varphi_{k'}$ are all bounded by $\sim 1/\varrho^2$ and differ from zero in a range $\sim \varrho^2$, the Laplace transform $\mathcal{A}'(s\to\infty)$ is dominated by the divergent terms that are present in the case of $\varrho = 0$ as well. However, in the case of $\varrho > 0$, there is an additional cut-off at $\hat{k} \sim \varrho^2$, and therefore the approximate form of the Laplace transform becomes

$$\mathcal{A}'(s\to\infty) \sim \exp\left[\frac{1}{8}\ln\left(\varrho^2\right)\right] \sim \varrho^{1/4}. \tag{5.60}$$

Since the Laplace transform $\mathcal{A}'(s\to\infty)$ is finite, the spectral function $\mathcal{A}(\varepsilon)$ has a delta-function peak at $\varepsilon = 0$. In the framework of our variational approach, the hole is then a coherent quasiparticle with finite spectral weight $\mathcal{Z} = \mathcal{A}'(s\to\infty) \sim \varrho^{1/4}$.

5.3.3 Potential and kinetic energies

We are now ready to calculate the variational expectation values of the potential and the kinetic energies. Since we anticipate that the limit of $t \ll J_0$ corresponds to that of $\varrho \ll 1$, we assume throughout the calculation that the variational parameter ϱ is

small. From Eq. (5.7), the potential energy of the trial state $|\tilde{\omega}'\rangle$ with respect to the stationary ground state $|\tilde{\omega}\rangle$ is given by

$$\begin{aligned} E_J &= \langle\tilde{\omega}'|\tilde{H}_\phi|\tilde{\omega}'\rangle - \langle\tilde{\omega}|\tilde{H}_\phi|\tilde{\omega}\rangle \\ &= \left(\langle\tilde{\omega}'|\tilde{H}'_\phi|\tilde{\omega}'\rangle - \langle\tilde{\omega}|\tilde{H}_\phi|\tilde{\omega}\rangle\right) + \langle\tilde{\omega}'|\left[\tilde{H}_\phi - \tilde{H}'_\phi\right]|\tilde{\omega}'\rangle \qquad (5.61) \\ &= -\frac{1}{2}\sum_k \left(\tilde{E}'_k - \tilde{E}_k\right) + \varrho J_0 \langle\tilde{\omega}'|\left[-ic_{x(0)}c_0 - ic_{y(0)}c_0\right]|\tilde{\omega}'\rangle \equiv E_J^{(1)} + E_J^{(2)}, \end{aligned}$$

where the first term $E_J^{(1)}$ is the difference in the ground-state energies of the Hamiltonians $\tilde{H}_\phi$ and $\tilde{H}'_\phi$, while the second term $E_J^{(2)}$ is a local expectation value of the trial state $|\tilde{\omega}'\rangle$. Turning the sum in k into an integral, the first term becomes

$$\begin{aligned} E_J^{(1)} &= -\frac{N_X}{4\pi}\int_0^\pi 4J_0 \sin\left(\frac{k}{2}\right)\frac{\delta k}{2\pi}\left[\frac{\pi}{2} - \varphi_k\right]dk \\ &= -\frac{J_0}{\pi}\int_0^\pi \sin\left(\frac{k}{2}\right)\left[\frac{\pi}{2} - \varphi_k\right]dk. \qquad (5.62) \end{aligned}$$

Since Eq. (5.55) indicates that the function $\pi/2 - \varphi_k$ in the limit of $\varrho \ll 1$ is approximately 1 for $\hat{k} \ll \varrho^2$ and approximately $2\varrho^2/\hat{k}$ for $\hat{k} \gg \varrho^2$, the integral in Eq. (5.62) takes the approximate form

$$E_J^{(1)} \sim -\frac{J_0}{\pi}\int_{\varrho^2}^\pi \frac{2\varrho^2}{\hat{k}}\,d\hat{k} \sim -\frac{4J_0\varrho^2}{\pi}\,\ln(1/\varrho), \qquad (5.63)$$

where the remaining range between 0 and ϱ^2 gives a subdominant correction $\sim J_0\varrho^2$. Using Eq. (5.54) to express $-ic_{\alpha(0)}c_0$ in terms of $-i\tilde{\gamma}'_{k,A}\tilde{\gamma}'_{k,B}$, and turning the sum in k into an integral, the second term in Eq. (5.61) becomes

$$\begin{aligned} E_J^{(2)} &= \frac{4\varrho J_0}{N_X}\sum_{k<\pi}\cos\left[\varphi_k - \frac{k}{2}\right]\frac{\cos\varphi_k}{\varrho} \\ &= \frac{2J_0}{\pi}\int_0^\pi \left[\cos^2\varphi_k\,\cos\left(\frac{k}{2}\right) + \sin\varphi_k\cos\varphi_k\,\sin\left(\frac{k}{2}\right)\right]dk. \qquad (5.64) \end{aligned}$$

Substituting $\tan\varphi_k$ from Eq. (5.55), and taking the limit of $\varrho \ll 1$, this integral then takes the approximate form

$$\begin{aligned} E_J^{(2)} &= \frac{2J_0}{\pi}\int_0^\pi \frac{\varrho^2\cos(k/2)}{\varrho^4 + (1-\varrho^2)^2\cot^2(k/2)}\,dk \\ &\sim \frac{2J_0\varrho^2}{\pi}\int_0^\pi \frac{\hat{k}/2}{\varrho^4 + (\hat{k}/2)^2}\,d\hat{k} \sim \frac{8J_0\varrho^2}{\pi}\,\ln(1/\varrho). \qquad (5.65) \end{aligned}$$

Noticing that $E_J^{(2)} = -2E_J^{(1)}$ and that $E_J^{(1)} + E_J^{(2)} = -E_J^{(1)} > 0$, we obtain that the potential energy is approximately $E_J \sim J_0 \varrho^2 \ln(1/\varrho)$ in the limit of $\varrho \ll 1$.

To determine the kinetic energy in Eq. (5.9), we must consider the effective hopping amplitudes $T^\alpha \equiv T^\alpha(\mathbf{0})$. From Eq. (5.18), the hopping amplitude T^z along z bonds is directly related to $\mathcal{A}'(s \to \infty)$, and it is therefore given by $T^z \sim -t\varrho^{1/4}$. From Eq. (5.17), the hopping amplitudes $T^{x,y}$ along x and y bonds are given by

$$T^{x,y} = -\frac{t}{2}\left[\langle\tilde{\omega}'|\hat{\mathcal{R}}_\pi^{x,y}|\tilde{\omega}'\rangle - i\langle\tilde{\omega}'|c_0\hat{\mathcal{R}}_\pi^{x,y}c_0|\tilde{\omega}'\rangle\right]. \tag{5.66}$$

In the following, we consider the two terms in Eq. (5.66) separately. Recalling that $\cos(k/2) \to 0$ for the lowest-energy fermions at momenta $k \to \pi$, the approximate form of the first term becomes

$$\begin{aligned}
\langle\tilde{\omega}'|\hat{\mathcal{R}}_\pi^{x,y}|\tilde{\omega}'\rangle &= \langle\tilde{\omega}'|\left[1-(1-i)\,\phi_{k=\pi}^\dagger\phi_{k=\pi}\right]\prod_{k<\pi}\left\{1-[1-i\cos(k/2)]\phi_k^\dagger\phi_k\right\}|\tilde{\omega}'\rangle \\
&\sim \langle\tilde{\omega}'|\left[1-(1-i)\,\phi_{k=\pi}^\dagger\phi_{k=\pi}\right]\prod_{k<\pi}\left[1-\phi_k^\dagger\phi_k\right]|\tilde{\omega}'\rangle \\
&= |\langle\omega|\tilde{\omega}'\rangle|^2 + i|\langle\omega|\phi_{k=\pi}|\tilde{\omega}'\rangle|^2.
\end{aligned} \tag{5.67}$$

However, since the fermions ϕ_k can only be excited pairwise in the vacuum state $|\tilde{\omega}'\rangle$, the second term $i|\langle\omega|\phi_{k=\pi}|\tilde{\omega}'\rangle|^2$ vanishes, and we obtain $\langle\tilde{\omega}'|\hat{\mathcal{R}}_\pi^{x,y}|\tilde{\omega}'\rangle = |\langle\omega|\tilde{\omega}'\rangle|^2 \sim \mathcal{A}'(s \to \infty) \sim \varrho^{1/4}$. Furthermore, it is possible to rewrite the second term in Eq. (5.66) as $-i\langle\tilde{\omega}'|c_0\hat{\mathcal{R}}_\pi^{x,y}c_0|\tilde{\omega}'\rangle = -i\langle\tilde{\omega}''|\hat{\mathcal{R}}_\pi^{x,y}|\tilde{\omega}''\rangle$, where the vacuum state $|\tilde{\omega}''\rangle = c_0|\tilde{\omega}'\rangle$ corresponds to the fermions $\tilde{\phi}_k''$ with Majorana fermion components that are obtained from Eq. (5.54) via the substitution $c_0 \to -c_0$, or equivalently, via the substitution $\varrho \to -\varrho$. Since the vacuum states $|\omega\rangle$ and $|\tilde{\omega}''\rangle$ differ in an odd number of excited fermions, the first term vanishes in the analog of Eq. (5.67), and we obtain $-i\langle\tilde{\omega}''|\hat{\mathcal{R}}_\pi^{x,y}|\tilde{\omega}''\rangle = |\langle\omega|\phi_{k=\pi}|\tilde{\omega}''\rangle|^2 \sim \mathcal{A}'(s \to \infty)$. Importantly, the substitution $\varrho \to -\varrho$ does not affect the dominant terms proportional to $\sin\varphi_k$ and $\sin\varphi_{k'}$ in Eqs. (5.58) and (5.59), and therefore $\mathcal{A}'(s \to \infty) \sim \varrho^{1/4}$ is readily recovered. Noticing that the effective hopping amplitudes all take the approximate form $T^\alpha \sim -t\varrho^{1/4}$, we obtain that the kinetic energy is approximately $E_t \sim -t\varrho^{1/4}$ in the limit of $\varrho \ll 1$.

5.3.4 Variational optimization

For each value of the bare hopping amplitude $t \ll J_0$, the best possible variational state $|\tilde{\omega}'\rangle$ is found by minimizing the total energy E_Φ with respect to the variational parameter ϱ. The approximate form of the total energy reads

$$E_\Phi = E_J + E_t \sim J_0 \varrho^2 \ln(1/\varrho) - t\varrho^{1/4}, \tag{5.68}$$

and a differentiation in ϱ gives an implicit equation $t/J_0 \sim \varrho^{7/4} \ln(1/\varrho)$ for the optimal variational parameter ϱ. We can solve this equation approximately by means of an iterative procedure. In the first iteration step, we neglect the logarithm to obtain $\varrho \sim [t/J_0]^{4/7}$. In the second iteration step, we use this result inside the logarithm to obtain $\varrho \sim [(t/J_0)/\ln(J_0/t)]^{4/7}$. Further iteration steps could then provide sublogarithmic corrections, but the result obtained from the second iteration step is sufficient for our purposes. Note that $\varrho \to 0$ is recovered for $t \to 0$ and that the limit of $\varrho \ll 1$ corresponds to that of $t \ll J_0$.

Using the relationship between the optimal variational parameter ϱ and the bare hopping amplitude t, we are now ready to express our main quantities of interest in terms of t only. In particular, the quasiparticle weight $\mathcal{Z}$ becomes

$$\mathcal{Z} \sim \varrho^{1/4} \sim \frac{(t/J_0)^{1/7}}{\ln^{1/7}(J_0/t)}\,, \tag{5.69}$$

while the effective hopping amplitudes T^α and the kinetic energy E_t take the form

$$E_t \sim T^\alpha \sim -t\varrho^{1/4} \sim -J_0 \frac{(t/J_0)^{8/7}}{\ln^{1/7}(J_0/t)}\,, \tag{5.70}$$

and the potential energy E_J takes an identical form with an overall positive sign. Note that the corresponding results in Sec. 5.2 are recovered as these quantities all vanish in the limit of $t \to 0$.

We finally consider the effect of a finite (but small) hole momentum $\mathbf{K} \neq \mathbf{0}$. In the limit of $|\mathbf{K}||\delta\mathbf{R}| \ll 1$, the finite momentum enters the problem only via the factors $\cos[\mathbf{K} \cdot \mathbf{R}_{\alpha(0)}] \approx 1 - [\mathbf{K} \cdot \mathbf{R}_{\alpha(0)}]^2/2$ in Eq. (5.9). Since the matter-fermion configuration $|\phi^{\{0\}}(\mathbf{K})\rangle$ at finite momentum is then close to the matter-fermion configuration

$|\phi^{\{0\}}(\mathbf{0})\rangle$ at zero momentum, the quasiparticle weight in Eq. (5.69) and the effective hopping amplitudes in Eq. (5.70) are renormalized by small perturbative corrections only. The spectral function has an overall shift in the hole energy ε because the kinetic energy is increased by $\Delta E_t \sim T^\alpha |\mathbf{K}|^2 |\delta\mathbf{R}|^2$ due to the $\cos[\mathbf{K}\cdot\mathbf{R}_{\alpha(0)}]$ factors in Eq. (5.9). This momentum-dependent shift translates into a quasiparticle dispersion relation and gives an effective mass proportional to $1/T^\alpha$ at the bottom of the resulting quasiparticle band. In comparison with the gapped phase, we find that the effective mass is increased by a factor $t/T^\alpha \sim \varrho^{-1/4} \sim \mathcal{Z}^{-1}$ [17].

5.4 Discussion and outlook

The main result of this chapter is that an isolated slow hole ($t \ll J_0$) in the gapless phase of the Kitaev honeycomb model is a coherent quasiparticle with finite spectral weight $\mathcal{Z} > 0$. It is important to emphasize that the coherence of the hole is related to its mobility because the quasiparticle weight $\mathcal{Z}$ vanishes in the stationary limit $t \to 0$. Although our results are obtained by an approximate variational approach at a special point in the gapless phase, we argue on physical grounds that they are also valid for the exact ground state at a generic point of the gapless phase.

We first consider the variational trial state $|\tilde{\omega}'\rangle$ for a generic variational parameter $0 \leq \varrho \leq 1$, and notice that it has fundamentally distinct properties in the cases of $\varrho = 0$ and $\varrho > 0$. In particular, the ground-state overlap $|\langle\omega|\tilde{\omega}'\rangle|$ is finite for $\varrho > 0$ and zero for $\varrho = 0$. To explain these results, we recall that the ground-state overlap $|\langle\omega|\tilde{\omega}'\rangle|$ differs from 1 because the two Majorana fermion components $\gamma_{k,A}$ and $\gamma_{k,B}$ have different transformation matrices $\hat{U}$ and $\hat{V}$ between the corresponding sets of free matter fermions ϕ_k and $\tilde{\phi}'_k$. However, this asymmetry is only quantitative for $\varrho > 0$ when all fermions remain delocalized, while it is qualitative for $\varrho = 0$ when one Majorana fermion component of the zero-energy fermion $\tilde{\phi}'_{k=\pi}$ becomes localized at the hole site and the other one remains delocalized. Note that the finite ground-state overlap in the gapped phase is in accordance with these results as the zero-energy fermion is then localized in both of its Majorana fermion components.

In light of this distinction between the cases of zero and finite ground-state overlaps, we are now in a position to argue that the essential physics is captured by our variational approach. In the stationary limit $t \to 0$, the exact solution of the model corresponds to the $\varrho = 0$ Hamiltonian $\tilde{H}_\phi$, and the zero-energy fermion is localized at the hole site $l = 0$ in one of its Majorana fermion components. In the mobile limit $t > 0$, this Majorana fermion c_0 is coupled to the neighboring Majorana fermions $c_{\alpha(0)}$ by the operator $\hat{\mathcal{T}}^\alpha$ in Eq. (5.17). Although these couplings are extremely involved and not even quadratic, they are expected to delocalize the zero-energy fermion in both of its Majorana fermion components, and their essence is therefore captured by the additional terms in the $\varrho > 0$ Hamiltonian $\tilde{H}'_\phi$. We anticipate that this delocalization of the zero-energy fermion gives a finite quasiparticle weight $\mathcal{Z} = |\langle\omega|\tilde{\omega}'\rangle|^2 > 0$ for the exact $t > 0$ ground state as well.

The most important difference between a generic point of the gapless phase and the special point considered in this chapter is the dimensionality of the problem: the ground state of the undoped model is a 2D spin liquid in the first case, while it is a set of non-interacting 1D spin liquids in the second case. Since the gapless excitations of the spin liquid have Dirac point nodes in both cases, their density of states at the smallest energies $\varepsilon \to 0$ is constant in the 1D case and $\propto \varepsilon$ in the 2D case. Recalling that the potential incoherence of a mobile hole is caused by the strong hybridization between the hole and the gapless excitations, we expect that the hole must be more coherent in the 2D case than in the 1D case because the gapless excitations have a vanishing density of states instead of a constant density of states. Since we find that a mobile hole is already coherent at the special point (1D case), we anticipate that it remains coherent at a generic point (2D case).

Chapter 6

Summary and outlook

In this thesis, we presented a controlled microscopic study of mobile holes in both the (Abelian) gapped and the gapless phases of the Kitaev honeycomb model. In the gapped phase, we found that the mobile holes in the doped model have internal degrees of freedom as they can bind the fractional excitations of the undoped model and that the resulting hole types with different fractional excitations bound to them are fundamentally different in terms of their single-particle properties and their experimental signatures in the multi-particle ground state. In the gapless phase, we argued by means of a variational approach that a single mobile hole has a finite quasiparticle weight for any finite hopping amplitude but a vanishing quasiparticle weight for a vanishing hopping amplitude. We now conclude the thesis with three suggestions for the future direction of this research.

The interest in quantum spin liquids is in part due to their identification as parent states of high-temperature superconductors [20]. Indeed, if Cooper pairs are formed by extra electrons or missing electrons (holes) in a doped quantum spin liquid, the condensation of these Cooper pairs can lead to superconducting behavior. As discussed briefly in Sec. 3.1.3, the holes in the gapped phase of the model form bound pairs if the Coulomb repulsion is strong enough to counteract phase separation but not strong enough to counteract pair formation. It is then natural to ask what kind of internal degrees of freedom these hole pairs possess and what their manifestations are in the superconducting behavior of hole pairs. Importantly, since the question of superconductivity is also of central importance in the complementary mean-field

works [70], an exact study of hole pairs could further clarify the relation between the exact description and the mean-field treatments.

The binding of fractional excitations by mobile holes is interesting in part because it provides a controlled way of introducing fractional particles into the Abelian gapped phase of the model and manipulating the resulting quantum state by exploiting the anyonic statistics of these fractional particles [76]. Importantly, the model has even more exotic fractional excitations in its non-Abelian gapped phase. Since we believe that our results obtained for the Abelian gapped phase are applicable for gapped spin liquids in general, we expect that the fractional excitations can also be bound to mobile holes in the non-Abelian gapped phase. Nevertheless, it would be interesting to explore the resulting fractional particles, especially the manifestations of their non-Abelian anyonic statistics, in more detail.

We argued in Sec. 5.4 that our approximate variational results at the special point of the gapless phase (1D case) are in fact applicable for the exact ground state at a generic point of the gapless phase (2D case). However, these arguments could be substantiated by further research. In particular, we anticipate that the essence of our calculation in the 1D case can be repeated in the 2D case by concentrating on the most relevant features and neglecting any unnecessary details. Such an investigation could verify our expectations that the hole is more coherent in the 2D case than in the 1D case. Furthermore, alternative approaches complementing our variational treatment could also be employed. In the 1D case, the linear dispersion of the gapless fermions naturally lends itself to a bosonization approach, while in general, a continuum approximation could translate our discrete hopping problem into that of an appropriately perturbed Dirac equation.

Bibliography

[1] N. F. Mott, Rev. Mod. Phys. **40**, 677 (1968).

[2] M. Imada, A. Fujimori, and Y. Tokura, Rev. Mod. Phys. **70**, 1039 (1998).

[3] P. A. Lee, N. Nagaosa, and X.-G. Wen, Rev. Mod. Phys. **78**, 17 (2006).

[4] J. Hubbard, Proc. R. Soc. Lond. A **276**, 238 (1963).

[5] E. H. Lieb and F. Y. Wu, Phys. Rev. Lett. **20**, 1445 (1968).

[6] F. H. L. Essler, H. Frahm, F. Göhmann, A. Klümper, and V. E. Korepin, *The One-Dimensional Hubbard Model* (Cambridge University Press, Cambridge, 2010).

[7] F. C. Zhang and T. M. Rice, Phys. Rev. B **37**, 3759(R) (1988).

[8] J. E. Hirsch, Phys. Rev. Lett. **54**, 1317 (1985).

[9] M. Ogata and H. Fukuyama, Rep. Prog. Phys. **71**, 036501 (2008).

[10] J. G. Bednorz and K. A. Müller, Z. Phys. B: Condens. Matter **64**, 189 (1986).

[11] P. W. Anderson, *The Theory of Superconductivity in the High-T_C Cuprates* (Princeton University Press, Princeton, 1997).

[12] E. Dagotto, Rev. Mod. Phys. **66**, 763 (1994).

[13] W. F. Brinkman and T. M. Rice, Phys. Rev. B **2**, 1324 (1970).

[14] B. I. Shraiman and E. D. Siggia, Phys. Rev. Lett. **60**, 740 (1988).

[15] S. A. Trugman, Phys. Rev. B **37**, 1597 (1988).

[16] S. Sachdev, Phys. Rev. B **39**, 12232 (1989).

[17] C. L. Kane, P. A. Lee, and N. Read, Phys. Rev. B **39**, 6880 (1989).

[18] G. Misguich and C. Lhuillier, *Frustrated Spin Systems*, edited by H. T. Diep (World Scientific, Singapore, 2004), Chap. 5.

[19] P. W. Anderson, Mater. Res. Bull. **8**, 153 (1973).

[20] P. W. Anderson, Science **235**, 1196 (1987).

[21] R. Moessner and K. S. Raman, *Introduction to Frustrated Magnetism*, edited by C. Lacroix, P. Mendels, and F. Mila (Springer, Berlin-Heidelberg, 2011), Chap. 17.

[22] S. A. Kivelson, D. S. Rokhsar, and J. P. Sethna, Phys. Rev. B **35**, 8865(R) (1987).

[23] D. S. Rokhsar and S. A. Kivelson, Phys. Rev. Lett. **61**, 2376 (1988).

[24] R. Moessner and S. L. Sondhi, Phys. Rev. Lett. **86**, 1881 (2001).

[25] X.-G. Wen, *Quantum Field Theory of Many-Body Systems* (Oxford University Press, Oxford, 2004).

[26] X. G. Wen and Q. Niu, Phys. Rev. B **41**, 9377 (1990).

[27] A. Kitaev and J. Preskill, Phys. Rev. Lett. **96**, 110404 (2006).

[28] M. Levin and X.-G. Wen, Phys. Rev. Lett. **96**, 110405 (2006).

[29] R. Moessner, S. L. Sondhi, and E. Fradkin, Phys. Rev. B **65**, 024504 (2001).

[30] R. Rajaraman, *Quantum [Un]speakables*, edited by R. A. Bertlmann and A. Zeilinger (Springer, Berlin-Heidelberg, 2002), Chap. 27.

[31] M. Oshikawa and T. Senthil, Phys. Rev. Lett. **96**, 060601 (2006).

[32] C. Nayak, S. H. Simon, A. Stern, M. Freedman, and S. Das Sarma, Rev. Mod. Phys. **80**, 1083 (2008).

[33] L. Balents, Nature **464**, 199 (2010).

[34] S. Yan, D. A. Huse, and S. R. White, Science **332**, 1173 (2011).

[35] T.-H. Han, J. S. Helton, S. Chu, D. G. Nocera, J. A. Rodriguez-Rivera, C. Broholm, and Y. S. Lee, Nature **492**, 406 (2012).

[36] M. J. P. Gingras and P. A. McClarty, Rep. Prog. Phys. **77**, 056501 (2014).

[37] M. P. Zaletel and A. Vishwanath, Phys. Rev. Lett. **114**, 077201 (2015).

[38] A. Y. Kitaev, Ann. Phys. **303**, 2 (2003).

[39] A. Y. Kitaev, Ann. Phys. **321**, 2 (2006).

[40] Z. Nussinov and J. van den Brink, Rev. Mod. Phys. **87**, 1 (2015).

[41] H.-D. Chen and Z. Nussinov, J. Phys. A: Math. Theor. **41**, 075001 (2008).

[42] X.-G. Wen, Phys. Rev. B **65**, 165113 (2002).

[43] H. Yao, S.-C. Zhang, and S. A. Kivelson, Phys. Rev. Lett. **102**, 217202 (2009).

[44] S. R. Hassan, P. V. Sriluckshmy, S. K. Goyal, R. Shankar, and D. Sénéchal, Phys. Rev. Lett. **110**, 037201 (2013).

[45] G. Baskaran, S. Mandal, and R. Shankar, Phys. Rev. Lett. **98**, 247201 (2007).

[46] S. Yang, S.-J. Gu, C.-P. Sun, and H.-Q. Lin, Phys. Rev. A **78**, 012304 (2008).

[47] J. Knolle, D. L. Kovrizhin, J. T. Chalker, and R. Moessner, Phys. Rev. Lett. **112**, 207203 (2014).

[48] L.-M. Duan, E. Demler, and M. D. Lukin, Phys. Rev. Lett. **91**, 090402 (2003).

[49] G. Jackeli and G. Khaliullin, Phys. Rev. Lett. **102**, 017205 (2009).

[50] A. Shitade, H. Katsura, J. Kuneš, X.-L. Qi, S.-C. Zhang, and N. Nagaosa, Phys. Rev. Lett. **102**, 256403 (2009).

[51] J. Chaloupka, G. Jackeli, and G. Khaliullin, Phys. Rev. Lett. **105**, 027204 (2010).

[52] J. Chaloupka, G. Jackeli, and G. Khaliullin, Phys. Rev. Lett. **110**, 097204 (2013).

[53] Y. Singh and P. Gegenwart, Phys. Rev. B **82**, 064412 (2010).

[54] X. Liu, T. Berlijn, W.-G. Yin, W. Ku, A. Tsvelik, Y.-J. Kim, H. Gretarsson, Y. Singh, P. Gegenwart, and J. P. Hill, Phys. Rev. B **83**, 220403(R) (2011).

[55] Y. Singh, S. Manni, J. Reuther, T. Berlijn, R. Thomale, W. Ku, S. Trebst, and P. Gegenwart, Phys. Rev. Lett. **108**, 127203 (2012).

[56] S. K. Choi, R. Coldea, A. N. Kolmogorov, T. Lancaster, I. I. Mazin, S. J. Blundell, P. G. Radaelli, Y. Singh, P. Gegenwart, K. R. Choi, S.-W. Cheong, P. J. Baker, C. Stock, and J. Taylor, Phys. Rev. Lett. **108**, 127204 (2012).

[57] F. Ye, S. Chi, H. Cao, B. C. Chakoumakos, J. A. Fernandez-Baca, R. Custelcean, T. F. Qi, O. B. Korneta, and G. Cao, Phys. Rev. B **85**, 180403(R) (2012).

[58] R. Comin, G. Levy, B. Ludbrook, Z.-H. Zhu, C. N. Veenstra, J. A. Rosen, Y. Singh, P. Gegenwart, D. Stricker, J. N. Hancock, D. van der Marel, I. S. Elfimov, and A. Damascelli, Phys. Rev. Lett. **109**, 266406 (2012).

[59] G. Baskaran, Z. Zou, and P. W. Anderson, Solid State Commun. **88**, 853 (1993).

[60] M. C. Gutzwiller, Phys. Rev. Lett. **10**, 159 (1963).

[61] T. A. Kaplan, P. Horsch, and P. Fulde, Phys. Rev. Lett. **49**, 889 (1982).

[62] G. Baskaran and P. W. Anderson, Phys. Rev. B **37**, 580(R) (1988).

[63] A. M. Essin and M. Hermele, Phys. Rev. B **87**, 104406 (2013).

[64] A. Mesaros and Y. Ran, Phys. Rev. B **87**, 155115 (2013).

[65] L.-Y. Hung and X.-G. Wen, Phys. Rev. B **87**, 165107 (2013).

[66] M. Hermele, T. Senthil, M. P. A. Fisher, P. A. Lee, N. Nagaosa, and X.-G. Wen, Phys. Rev. B **70**, 214437 (2004).

[67] F. J. Burnell and C. Nayak, Phys. Rev. B **84**, 125125 (2011).

[68] T. Hyart, A. R. Wright, G. Khaliullin, and B. Rosenow, Phys. Rev. B **85**, 140510(R) (2012).

[69] J.-W. Mei, Phys. Rev. Lett. **108**, 227207 (2012).

[70] Y.-Z. You, I. Kimchi, and A. Vishwanath, Phys. Rev. B **86**, 085145 (2012).

[71] S. Okamoto, Phys. Rev. B **87**, 064508 (2013).

[72] D. D. Scherer, M. M. Scherer, G. Khaliullin, C. Honerkamp, and B. Rosenow, Phys. Rev. B **90**, 045135 (2014).

[73] A. J. Willans, J. T. Chalker, and R. Moessner, Phys. Rev. Lett. **104**, 237203 (2010).

[74] A. J. Willans, J. T. Chalker, and R. Moessner, Phys. Rev. B **84**, 115146 (2011).

[75] E. H. Lieb, Phys. Rev. Lett. **73**, 2158 (1994).

[76] S. Dusuel, K. P. Schmidt, and J. Vidal, Phys. Rev. Lett. **100**, 177204 (2008).

[77] S. Kivelson, Phys. Rev. B **39**, 259 (1989).

[78] D. Poilblanc, Phys. Rev. Lett. **100**, 157206 (2008).

[79] L. Balents, M. P. A. Fisher, and C. Nayak, Phys. Rev. B **61**, 6307 (2000).

[80] P. W. Anderson, Phys. Rev. Lett. **64**, 1839 (1990).

[81] S. Schmitt-Rink, C. M. Varma, and A. E. Ruckenstein, Phys. Rev. Lett. **60**, 2793 (1988).

[82] S. A. Trugman, Phys. Rev. B **41**, 892 (1990).

[83] G. Martínez and P. Horsch, Phys. Rev. B **44**, 317 (1991).

[84] D. Poilblanc, T. Ziman, H. J. Schulz, and E. Dagotto, Phys. Rev. B **47**, 14267 (1993).

[85] M. Brunner, F. F. Assaad, and A. Muramatsu, Phys. Rev. B **62**, 15480 (2000).

[86] A. S. Mishchenko, N. V. Prokof'ev, and B. V. Svistunov, Phys. Rev. B **64**, 033101 (2001).

[87] F. Trousselet, P. Horsch, A. M. Oleś, and W.-L. You, Phys. Rev. B **90**, 024404 (2014).

[88] R. Comin and A. Damascelli, *Strongly Correlated Systems: Experimental Techniques*, edited by A. Avella and F. Mancini (Springer, Berlin-Heidelberg, 2015), Chap. 2.

[89] P. W. Anderson, Phys. Rev. Lett. **18**, 1049 (1967).

[90] Y. Nagaoka, Phys. Rev. **147**, 392 (1966).